ICE LOADS AND MOTIONS EXPERIENCED BY A FLOATING, MOORED PLATFORM IN MUSHY ICE RUBBLE

by

M. Matsuishi and R. Ettema

IIHR Report No. 295

Iowa Institute of I-Iydraulic Research
The University of Iowa
Iowa City, Iowa 52242 USA

November 1985

ABSTRACT

A 1.5-meter-diameter (at the load waterline) test platform was used to determine the ice loads and motions likely to be experienced by a moored floating platform, of conical hull form, in a layer of mushy ice rubble.

The test platform was connected to a mooring harness which simulated the mooring system of an existing platform, "Kulluk." In order to evaluate the effects of platform motions on ice loads, a parallel series of experiments were conducted with the test platform restrained, or fixed, from moving. The experiments were conducted using the IIHR ice towing tank.

It was found that the forces required to moor or restrain the conical test platform increased almost linearly with increasing thickness of ice-rubble layer. When impacted by ice rubble the moored platform drifted horizontally and changed its trim, but without undergoing cyclic motions. The test platform when moored experienced ice loads which were up to 26% less than it did when it was restrained from movinq.

The maximum ice loads that were experienced by the test platform, when either moored or restrained, did not vary significantly at the speed with which the layer of ice rubble impacted the test platform.

An important feature of ice-rubble impact with the test platform was the accumulation of ice rubble to form an "ice prow," at the leading perimeter of the test program. The ice load exerted against the test platform increased while an "ice prow" developed, becoming more or less steady when it had attained its esuilibrium extent.

ACKNOWLEDGEMENTS

This study was jointly conducted by Hitachi Zosen Corporation of Japan and The University of Iowa, Iowa Institute of Hydraulic Research (IIHR), U.S.A.

The authors wish to thank Messrs. S. Iwata, R. Hamer and J. Cramer for technical support provided during the experiments. Additionally, the authors would like to thank Dr. J.F. Kennedy, IIHR Director, for useful advice offered in the course of the study.

TABLE OF CONTENTS

LIST OF FIGURES

LIST OF TABLES

ICE LOADS AND MOTIONS EXPERIENCED BY A FLOATING, MOORED PLATFORM IN MUSHY ICE RUBBLE

I. INTRODUCTION

A moored, floating platform for use in ice-covered waters is likely to encounter and be impacted by fields of moving ice rubble, as is depicted in figure 1. The resulting ice loads exerted against a moored platform are, however, difficult to predict because their magnitudes are governed by both the pattern of ice-rubble accumulation around the platform and the motions that the platform may undergo during impact. In turn, the pattern of ice-rubble accumulation, and possible motions--displacements as well as accelerations--of the platform are influenced by the rubble-size composition, thickness and speed with which the field of ice rubble moves around the platform.

The primary aim of tie study described here was to determine the effects of the thickness and speed of a moving field of mushy ice rubble on the ice loads that the field may exert against a moored, floating platform. An additional aim of the study was to investigate the effect of platform motions on ice loads that it experiences during impact with a field of mushy ice.

In order to attain these aims, series of model tests were conducted with the test platform illustrated in figure 2. The test platform was shaped as an inverted cone with a diameter of 1.5 meters at its load waterline. The cone was flared to a cylindrical skirt which lined the bottom of the platform. The skirt is designed to protect the mooring cables for a floating platform from direct impact from the ice. A mooring harness which acted as a linear spring was used to simulate the system of mooring cables that would typically be used to moor a floating platform (e.g., see Gaida et al., 1981). The mooring harness enabled the moored test platform to surge, heave and pitch, without appreciable sway, yaw or roll.

Incidently, the test platform replicated, at an approximate scale of 1:45, an existing platform, "Kulluk," which is used for exploratory drilling activities in the Beaufort Sea. A recent article in ARCTIC NEWS RECORD (1984) briefly describes the problems that resulted when "Kulluk" became surrounded by rubble ice in the brash size range.

In order to illuminate the effects of platform motions on the ice loads that ice rubble could exert against the test platform, model tests were also conducted with the platform fixed so that it was restrained from surging, heaving and pitching. The comparison of the ice loads experienced by the test platform in the moored and fixed (fully restrained) conditions shed light on the influences of platform motions on the forces exerted by the ice rubble.

The present study is companion to an exploratory study by Matsuishi and Ettema (1985) on the dynamic behavior of a moored platform continuously impacted by floes of level, annual ice. The two studies were conducted concurrently. The sheets of urea ice that were used to model ice floes were fragmented to produce ice rubble which was of a relatively mushy consistency.

II. ICE LOADS EXERTED AGAINST A MOORED PLATFORM

A moored platform of conical hull form when located in a field of moving ice rubble experiences ice loads which can be resolved into horizontal, vertical and rotational components as shown in figure 3.

A Equations of Motion of a Floating, Moored Platform. The equations of motion for a floating, cable-moored platform can be written in the following general form:

$$\underset{(i)}{[m]\{\ddot{x}\}} + \underset{(ii)}{[c]\{\dot{x}\}} + \underset{(iii)}{[k]\{x\}} = \underset{(iv)}{\{F\}}\ , \qquad (1)$$

in which a term (i) relates to platform inertia; and terms (ii), (iii) and (iv) relate to damping, and mooring plus water-reaction restoring force/moment, and ice force/moment, respectively. Also, [m] = mass matrix, [c] = damping matrix, [k] = stiffness matrix, {x} = displacement vector and {F} = ice force/ moment vector,

$$\{F\} = \begin{Bmatrix} \int_A f_x \, dA \\ \int_A f_y \, dA \\ \int_A (f_x \ell_x - f_y \ell_y) \, dA \end{Bmatrix} \qquad (2)$$

in which f_x and f_y = ice pressure in the orthogonal x and y directions; ℓ_x and ℓ_Y = moment arms associated with the orthogonal lines of action of ice pressure against the hull; and, A = contact area between ice rubble and platform;

$$\{x\} = \begin{Bmatrix} x \\ y \\ \theta \end{Bmatrix} \tag{3}$$

Integration of the ice pressures f_x and f_y acting against the platform gives the total ice forces and pitch moment; for the horizontal, or surge. direction

$$F_x = \int_A f_x dA \; ; \tag{4}$$

for the vertical, or heave, direction

$$F_y = \int_A f_y dA \; ; \tag{5}$$

and for pitch

$$M_z = \int_A (f_x \ell_x - f_y \ell_y) dA \; . \tag{6}$$

As is described in section III, for the present study the ice forces F_x and F_y and the pitch moment M_z were not directly measured during experiments with the moored platform. Instead the mooring force $k_{11}y$ was measured (k_{11} = stiffness of mooring system in surge direction). Also measured for the moored platform were: surge displacement and acceleration, y and $\ddot{y}$; heave displacement and acceleration, x and $\ddot{x}$; pitch angle and acceleration, θ and $\ddot{\theta}$.

When, for the present study the test platform was fixed so that it could not move, inertia and damping forces and moments were zero. The ice forces F_x, F_y and the moment M_x were counter-acted by restraining forces in the surge and heave directions and by pitch moment, which were measured using a multi-axial load cell.

B. Prior Studies on Ice Loads Against Conical Structures. The literature on ice loads experienced by conical structures, especially floating ones, is not extensive although it is beginning to accumulate, in step with the recent burgeoning of activities related to navigation as well as exploration drilling through ice-covered waters. No published study has involved measurement of the ice or mooring forces (items (iii) and (iv) in (1) through (3)) as well as inertia forces or moments (terms (i)).

Ralston (1980) and Milano (1980, 1982) proposed analytical models for determining ice loads against fixed, conical structures. Frederking (1980), Frederking and Schwarz (1982) and Wessels (1984) presented results from model tests on ice loads exerted against a variety of conical structures some of which were able to surge, heave and pitch. All these studies have shown that lower ice loads occur for a conical form which deflects ice and fails in downwards flexure rather than one which deflects ice upwards and out of the water. This is one reason why the platform "Kulluk" has the form of a downwerd-deflecting cone, although details of the model tests and analyses performed for the design of "Kulluk" have not yet been published.

Frederking (1980), Frederking and Schwarz (1982), and Wessels (1984), Toyama and Yashima (1985) and more recently Matsuishi and Ettema (1985) offer some data and insight into the dynamic behavior of moored platforms of conical hull shape impacted by ice sheets. The collective body of data show that a conical platform which can surge, heave and pitch experiences, lesser ice forces does a conical platform which is restrained, or fixed, from moving. However, except for the study by Matsuishi and Ettema, these studies report only measured values of mooring or restraining forces but do not offer information on the magnitudes of platform motions.

There has yet to be conducted an extensive study of the loads imposed by ice rubble impacting against a moored platform of conical hull form. Some work has been done on the resistance encountered by cones and ship hulls towed through ice rubble (e.g., Mellor 1980, Keinonen 1980, Hellman 1984). Generally, however, the topic of ice loads imposed by ice rubble has not been the subject of much research. The present study is intended to probe the interaction dynamics of a floating conical platform in a field of ice rubble.

III. EXPERIMENTS

A. Experimental Set-up.

1. The IIHR Ice Towing Tank. The experiments were conducted using IIHR's 20-m-long, 5-m-wide, and 1.3-m-deep ice towing tank. A schematic layout of the cold room, in which the ice tank is housed, and its cooling system is given in figure 4. The cooling system is composed of two compressors which provide coolant to the two cooler units situated at each end of the cold room. The compressors are in turn cooled by water pumped from a 200 m^3 sump. If the sump exceeds a certain limiting temperature, a cooling tower situated out-doors is operated to cool the sump water.

Fans inside the four cooler units draw air from the cold room and, after the heat exchange has occurred, discharge it into eight ducts which extend the whole length of the cold room. This chilled air is forced through an array of 20-mm diameter holes along the base of each duct, thereby producing a flow of chilled air over the towing tank. The four ducts are alternately arrayed so as to provide an even distribution of cold air. Ever,, two hours, one pair of cooler units is defrosted by electrical heating. Depending on the ambient air temperature outside the cold room, the total cooling capacity of the system varies between 15 and 20 kW, which enables an ice sheet to grow at a rate of about 1.5 to 2.0 mm per hour.

A push-blade was installed on the 5-m wide, 2.4-m long motorized carriage, shown in figure 5, for driving the modelled fields of rubble ice against the model platform. The depth of the push-blade was kept equal to the thickness of the ice rubble layer so that the ice rubble layer did not increase its thickness, at the push blade, during the test. The carriage runs along rails on the tank's walls. The level of each rail was adjusted to a tolerance of ± 1.5 mm along its length. An angle beam on one side of the basin gives the lateral guidance to the carriage and carries the rack of the rack-and-pinion drive mechanism. The D.C. motor on the carriage has a maximum torque of 31 Nm and a speed range of 58 to 1750 RPM. A 1:15 gear box increases the torque to 465 Nm and gives a reduced speed range of 3.9 to 117 KPM. The effective radius of the pinion is 0.06 m; consequently the carriage has a maximum driving force of 7750 N and a velocity range of 0.024 m/sec to

0.74 m/sec. Higher velocities, up to 2.2 m/sec, can be achieved if a 1:5 gear box is coupled to the D.C. motor.

In order to measure the velocity of the carriage, a wheel carrying a circular array of holes is mounted on the drive shaft of the D.C. motor. The passage of each hole, as the shaft rotates, is sensed by a photo detector which emits a light through the hole. The number of pulses counted during a time interval is proportional to the velocity of the carriage. The length of the time interval is 0.371 seconds so that 1000 pulses correspond to a velocity of 0.333 m/sec. After each interval of 0.371 sec, the number of pulses is latched to a display and to a digital-analog converter which holds the voltage during the following interval until the next measurement is available. The mean velocity of the preceding interval is therefore, displayed and can be sampled.

2. The Test Platform. The test platform simulated approximately, at 1:45-scale, the moored platform "Kulluk." The principal dimensions of the test platform and "Kulluk" are listed in table 1. Figure 6 shows the form and principal dimensions of the test platform. In form, the platform was an inverted cone which flared down to a flat-bottom cylinder. The transition from conical to cylindrical section was rounded so that ice rubble would move smoothly around the hull without becoming lodged in the region of the transition from cone to cylinder forms.

Moored platforms are acted upon by mooring-cable tensions and foundation reaction which is equal to buoyancy less weight of the platform. The equivalent spring stiffnesses of the test platform were:

a) stiffness of mooring cables

$$k_s = k_{11} = 1.7 \text{ kN/m;} \tag{7}$$

b) stiffness of the foundation reaction

$$k_h = k_{33} = 17.3 \text{ kN/m, for heave;} \tag{8}$$

$$k_P = k_{55} = 35.1 \text{ Nm/degree, for pitch rotation.} \tag{9}$$

Note that the subscripts ij (e.g., 11,33,55) are per convention for the tensorial form of the equations of motion (e.g., see Sarpkaya and Issacson 1981).

The ratios of water depth to typical lengths of mooring cables are in the range of 0.02 to 0.05 (see Gaida et al. 1983), which results in a much smaller vertical component of the mooring forces compared to a horizontal component. As the equivalent spring stiffness of mooring cables, (7), is an order of magnitude smaller than the equivalent spring stiffness of the foundation, (8), the contribution of mooring cables to vertical force and pitching moment can be disregarded. However, the maximum drift of a drilling platform is restricted to within 5% of water depth, in order to protect drilling equipment. Additionally, the cables are pretensioned so as to increase the overall stiffness of the mooring system. The cable mooring system can, therefore, be idealized as being a linear horizontal spring.

3. **Instrumentation.** The test platform was connected to an instrument beam by way of the linear mooring harness and a load cell as shown in figures 7 and 8. The motions of a cable-moored, floating platform were simulated using a mooring harness which was comprised of a pair of elastic leaf springs, a spline bearing, stroke bearings and universal bearings, as shown in figure 8. The horizontal mooring force was measured using a 490-newton NISHO DENKI LMC-3502-50 load cell which connected the instrument harness to the instrument beam. Yawing and swaying of the moored platform were restricted by the locations of two vertical rods at its fore and aft as shown in figure 7. The 10-mm diameter rods were constrained to slide in 10.5-mm wide slots as shown in figure 9. The moored, test platform could surge, heave and pitch.

The heave and pitch motions of the moored platform were measured by recording, with two linear voltage displacement transducers (LVDT's), the elevation of the platform at two positions.

Vertical and horizontal accelerations of the moored platform were measured with three 2G (19.6 m/s^2) KYOWA ASQ - 2BL accelerometers.

For a parallel series of experiments the test platform was fixed to the instrument beam by way of a load cell as is shown in figure 10. This condition of retraint was used to simulate the impact of ice rubble with a fixed conical structure and, by comparison of results with the moored test platform, to elucidate the influence of platform motions on ice-related forces.

The horizontal and vertical restraining forces and pitching moment of the fixed platform were measured using a 196-newton and 98-newton-meter NISHO DENKI LMC-4107-20 load cell connecting the platform and the instrument beam.

The locations of the measuring sensors and the positive directions of recorded data are shown in figure 11.

The output voltages from the load cells, LVDT's, accelerometers and the carriage velocimeter were scanned using a digital voltmeter. The digitized data were serially transmitted through a telephone link to the IIHR HP-1000 E computer system and were then stored on disk. The band width of the data acquisition link was 120 Hz, although each channel was sampled at a rate of 5 or 10 Hz.

4. Calibration of transducers. The zero level and sensitivity of each transducer (force, moment, displacement and acceleration) was determined before each test.

Each output voltage, V, of the load cells and accelerometers was measured for a calibration strain, ε_c, created by an amplifier. The sensitivity of each transducer, S, was calculated as

$$S = C(V/\varepsilon_c) \tag{10}$$

in which C is a predetermined ratio of strain to force or acceleration experienced by transducer.

The sensitivity of LVDT's, 13.03 mm/Volt and 12.92 mm/Volt, were evaluated by measuring the voltage change for a given displacement of each transducer rod.

The sensitivity of the circuit for the carriage velocity was determined by correlating its output voltage with the mean velocity of the carriage (determined by use of a stop watch and a length scale).

5. The Platform's Natural Periods of Oscillation. Free-oscillation tests were carried out to determine the natural periods and logarithmic decrements of surge and pitch for the test platform. The recorded data are shown in table 2. The platform's natural period of heave was estimated from

$$T = 2\pi/\omega = 2\pi / \sqrt{\rho_w g A_w / (M+\Delta M)} \qquad (11)$$

in which A_w = the platform's water-plane area = $\pi D_{LW}^2/4$; D_{LW} = the platform diameter at the load waterline; M = the platform's mass; ΔM = added mass, assumed to be 1.2 M (from Faltinsen 1975, Van Oortmerssen 1976); and $\rho_w g$ = specific weight of water.

6. Openwater Tests. Openwater tests were conducted to check that the push-blade which was used to drive the layer of ice rubble did not cause additional hydrodynamic forces to be exerted against the test platform. It was found that the additional hydrodynamic forces exerted against the platform in openwater were negligibly small for the range of speeds that were tested. The push-blade was perforated by many holes so that it could not push a significant surge of water ahead of the carriage.

B. Ice-Rubble Simulation.

1. Ice-Rubble Fields. The simulated fields of rubble ice were 5-m wide, or 3.3 times the diameter of the platform at the load waterline. The field was sufficiently wide such that the side-walls of the ice tank did not significantly affect the test results.

2. Ice Rubble. Ice sheets were grown from a 0.7-percent, by weight, urea solution according to the following procedure. With the cooler system operating at full capacity, the urea solution was cooled to a temperature of about 0.1°C above the solution's freezing temperature (-0.30°C) and the air in the room was chilled to about -12°C. Water circulation system provided necessary mixing of the solution to prevent the formation of the unwanted ice cover. Before being wet-seeded, the surface of the urea solution was screened to remove the ice which had formed during the solution cooling process. Then, the water circulation and the blowers of the cooling units were shut off and the cold room was fogged with a fine spray of water droplets. The spray was produced using a pressurized air spray gun and a pressurized tank. The water droplets froze in the air and settled onto the surface of the water which had by then reached the freezing temperature of the solution (-0.30°C). The wet-seeding process prevented the unwanted formation of relatively large ice crystals and enabled a multitude of small crystals to grow simultaneously over

the surface of the urea solution. Eventually, after growing through a transition layer, the ice grew with the columnar structure of thermal ice.

Each ice sheet was grown to about \$5-percent of its final thickness, 30 mm. The room temperature was then raised so that the air temperature at an elevation of about 10 mm above the ice sheets was about 2 to 4°C, and ice sheet was warmed and weakened. The principal properties of the ice sheets are listed in table 3.

The ice rubble was prepared by dicing a 30-mm thick urea ice sheet (1.35 m prototype thickness) grown prior to each test series. The urea ice fragments were mustered in the model-ice tank and groomed into a layer having a uniform thickness of either 0.16, 0.32, 0.48 or 0.80 times the draft of the test platform. The surface of the simulated ice-rubble field was not refrozen.

C. Test Procedure. A total of 26 tests were conducted, of which 18 were with the test platform moored (figure 7), and 8 with the test platform fixed from moving (figure 10). The test program is summarized in figure 12. For each test series, the thickness of the layer of ice rubble was kept constant. The layer was driven with a constant speed in the range of 0.02 to 0.20 m/s (0.26 to 2.6 kts in prototype scale) as indicated in figure 12, and shown in tables A-1 and A-2. After each test, the layer of ice rubble was regroomed to its original condition. For some thicknesses of ice-rubble layer, three tests were conducted to examine the reproducability of test results.

The porosity of each layer of ice rubble was measured by removing a portion of each layer with a sieve-like canister of known volume and weight. The porosity of the rubble ice layer before each test was typically 0.52. The average diameter of the ice fragments was slightly less than 50 mm. The size range of the fragments was fairly broad; varying from individual crystals to blocks of ice.

The relationships between model and prototype values of rubble ice speeds are given in figure 13, while the relationships between forces and moments of model platform and those of prototype are shown in figure 14.

The submerged depth of the push-blade was equal to the initial thickness

of each layer of ice rubble. In this manner, ice rubble protruding beneath the push-blade was swept hack behind the blade, and in effect, the push-blade simulated an ice mass which, driven by wind or other ice masses, pushes a layer of ice rubble, as is suggested in figure 15.

IV. RESULTS

The pressures exerted by ice rubble impacting against the test platform attained maximum values when an ice ridge or "ice prow" (a term suggested and used by Ashton et al. 1973 and Mellor 1980) developed around the leading portion of the platform's waterline perimeter. The development of a prow of ice rubble accumulated against the platform is illustrated in figure 16.

Because the accumulation of ice rubble around the test platform significantly affected the ice loads that it experienced, a discussion about the influences of rubble thickness and speed on ice loads is best prefaced by a brief description of the manner whereby ice rubble moved and accumulate around the test platform.

A. Observations on the Movement and Accumulation of Ice Rubble around the Test Platform. As a layer of ice rubble was pushed toward and around the test platform, ice rubble accumulated along the leading perimeter of the platform and, thereby, formed a relatively stationary zone, or prow of ice rubble. The advancing field of ice rubble was forced to pass around the platform with its prow of ice rubble. The boundaries of the prow delineated shear surfaces between stationary ice and the moving field of ice rubble. Figure 16 shows schematically the manner whereby ice rubble moved and accumulated around the test platform.

While the prow of ice-rubble was forming, and had not yet reached its equilibrium size, the ice load exerted against the platform increased monotonically, as is indicated in figure 17. Once the prow had attained its equilibrium size the ice loads became more-or-less steady.

Commensurate with increasing ice load were changes in the platform's displacement and the force required to moor the platform. With increasing ice load, the moored platform drifted horizontally and altered its trim. However,

during continuous impact with ice rubble, the moored platform did not experience cyclic motions.

Measured forces, moments and motions of the test platform are summarized in Appendix 1. Time histories of mooring force, as well as heave displacement and pitch angle are given in Appendix 2 for the moored, test platform. Also given in Appendix 2 are the time histories of the horizontal (surge) and vertical (heave) restraining forces that were recorded from the test platform when it was fixed from moving.

The thickness of the prow of accumulated ice rubble was measured after each test. As is plotted in figure 18, it is evident that the thickness of the ice-rubble prow increased with increasing layer thickness. It appears from figure 18 that the maximum thickness of the prow asymptotes to about twice the draft of the platform; draft = 0.187 m Measured thicknesses of ice rubble accumulation at various locations around the test platform are given in Appendix 3.

Measurements of the porosity of the ice prow of ice rubble showed that the prow had, on average, typically a porosity of about 11% less than did the initial layer of ice rubble.

B. The Effect of Thickness of Ice-Rubble Layer on Ice Loads and Platform Motions. The maximum mooring force (in the surge direction), $k_s y$, and heave displacement, x, experienced by the test platform when moored increased with increasing thickness of ice rubble layer as shown in figures 19 and 20, respectively. The relationship between mooring force and layer thickness is shown in figure 19, in which it is apparent that the relationship is almost linear.

Pitch angle, θ, increased slightly with increasing thickness of layer for the layer thicknesses up to 90 mm (4.05 m in prototype scale) as shown in figure 21. Thereafter pitch angle decreased and the direction reversed direction. The scatter of recorded pitch angle was also greatest for the thickest layer of ice rubble.

The equations for pitch moment, (6), can be used to help explain the change of pitching direction and scatter of record for thicker rubble ice layer;

$$M_z = \int_A (f_x \ell_x - f_y \ell_y) dA \ . \qquad (6)$$

Ice pressures against the platform f_x and f_y, are highly dependent on the submergence, accumulation and compaction of ice rubble around the platform. Consequently, the spatial distribution of ice pressure against the platform may vary, especially over the bottom of the platform. Because pitching moment, M is particularly sensitive to the spatial distribution of ice pressure against the platform, and, as is indicated in (6), its rotational direction may change in accordance with the distribution of ice rubble accumulated around and beneath the platform. It seems that, for the thickest layer of ice rubble, the distribution of ice ruhble and, commensurately, ice pressures were such that the direction of platform pitch differed to that for the thinner layers.

When the test platform was fixed so that it was restrained from moving, the restraining forces (surge and heave) and pitch moment increased linearly with increasing thickness of ice rubble layer. The relationships between the maximum values of F_Y, F_X and M and layer thickness are shown in figures 22, 23, and 24, respectively.

C. The Effect of Speed of Ice-Rubble Movement on Ice Loads and Platform Motions. The maximum values of mooring forces and heave displacements that were experienced by the moored test platform remained constant over the range of impact speeds tested (0.02 to 0.20 m/s in model scale, 0.26 to 2.6 kts in prototype scale). These results are portrayed in figures 25 and 26 for mooring force in the surge direction, $k_s y$, and heave displacement, x, respectively.

Presented in figure 27 are values of the pitch angle that were assumed by the test platform when it was in full contact with a layer of moving ice rubble. It is evident that more data is needed to lucidly explain the influence of layer speed on platform pitch angle.

By influencing the size of the ice prow formed ahead of the platform, and, relatedly, by influencing the distribution of ice rubble accumulated beneath the platform, it is apparent that the platform's angle of pitch was affected by the speed with which a layer of ice rubble moved around the test

platform. The speed effect is difficult to unravel from the effect of layer thickness.

D. The Effect of Platform Motions on Ice Loads. If the inertia and damping terms are neglected in (1) and (2), it is possible to compare the quasi-steady loads experienced by the moored test platform (figures 19 and 20) to the loads experienced by the platform when it was fixed or restrained from moving (figures 22 and 23). Table 4 is a summary of the comparison for a moderately high speed of rubble ice impact, 0.08 m/s (1.04 kts in prototype scale). Appendix 1 contains a more detailed list of the data.

The horizontal (mooring) and vertical restoring (buoyancy) forces that were experienced by the moored platform were less than the horizontal and vertical restraining forces experienced by the fixed platform. The difference between the horizontal ice loads (mooring force and surge-restraining force) decreased with increasing layer thickness of ice rubble. For the thinnest layer (16% of platform draft), the ice load exerted against the moored platform was 26% less than that exerted against the fixed platform. However, for the thickest layer (80% of platform draft), the ice load that was exerted against the moored platform was only 2% less than that exerted against the fixed platform.

Other than saying that the platform's facility to move led to a reduction in the vertical component of ice loads, compared to the loads exerted when the platform was fixed, the influence of platform motion on (ice-related) vertical forces for varying impact speeds and layer thicknesses is difficult to discern clearly. For the thinnest layer, the vertical ice load exerted against the moored platform was 19% less than that exerted against the fixed platform. For intermediate layer thicknesses (32 to 48% of platform draft), the vertical ice load exerted against the moored platform was about 38% less than that exerted against the fixed platform. The difference decreased to about 26% for the thickest layer.

V. CONCLUSIONS

The following principal conclusions were drawn from the study:

1. When impacted by ice rubble, the moored test platform drifted horizontally and altered its trim, but did not undergo cyclic motions.

2. The mooring force experienced by the moored test platform increased monotonically as a "prow" of ice rubble developed around the leading perimeter of the platform. Once the "prow" had reached an equilibrium size, the ice loads remained steady.

3. The horizontal (surge) restraining force and pitch-restraining moment experienced by the test platform, when restrained from moving, increased monotonically and attained a maximum steady value in the same manner as for the test platform when it was moored. The vertical (heave) restraining forces increased with small fluctuations and attained maximum value in a similar manner as did the horizontal restraining force.

4. The maximum values of mooring forces and heave displacements that were experienced by the moored test platform, and the maximum restraining forces and moments that were experienced by the test platform when restrained from moving, were almost linearly proportional to the thickness of the ice rubble layer.

5. The maximum values of pitching angles that were experienced by the moored test platform increased slightly with increasing thickness of ice-rubble layer. However, for the thickest layer of ice rubble (150 mm) the pitching angle changed direction and the scatter of data was great.

6. The maximum values of the mooring force and heave displacements that were experienced by the moored test platform were generally constant over the range of impact speeds, 0.02 to 0.20 m/s.

7. The maximum values of the pitch angles of the moored test platform impacted by the intermediate thickness (48% of platform draft) of ice

rubble were constant over the whole range of impact speeds. However, for both the thinnest and thickest layers (16 and 80% of platform draft) the maximum pitch angles increased with increasing speed of ice impact.

8. The mooring and heave restoring forces experienced by the moored test platform were 26% and 19%, respectively, smaller than the restraining forces experienced by the fixed platform for a moderately high speed of ice rubble impact, 0.08 m/s. However, as layer thickness increased, the difference between the mooring and surge-restraining forces decreased. In other words, the horizontal ice load exerted against the moored platform approached that exerted against the fixed platform, as layer thickness increased.

REFERENCES

ARCTIC NEWS-RECORD (1984/85), "Fighting Ice to extend Beaufort Season," Fall-Winter, MUNCK International A/S, Norway, p. 6-8.

Ashton, G.D., Den Nartog, S.L. and Hanamoto, B. (1973), "Icebreaking by Tow on the Mississippi River," U.S. Army CRREL Special Report No. 192.

Faltinsen, O.M. (1975), "Motion of Large Structure in Waves at Zero Froude Number," Int. Symp. on Dynamics of Marine Vehicles and Structures in Waves, p. 99-114.

Frederking, R. (1980), "Dynamic Ice Forces on an Inclined Structure," Physics and Mechanics of Ice, P. Tryde (Ed.), IUTAM Symposium, Copenhagen, Denmark.

Frederking, R. and Schwarz, J. (1982), "Model Test of Ice Forces on Fixed and Oscillating Cones," Cold Regions Science and Technology, Vol. 6, p. 61-72, Elsevier, Amsterdam.

Gaida, K.P., Barnes, J.R., and Wright, B.D. (1983), "Kulluk-an Arctic Exploratory Drilling Unit," OTC 4481, OTC, p. 337-346.

Hellman, J.H. (1984), "Basic Investigations on Mush Ice," IAHR Ice Symposium, Vol. 3, pp. 37-55, Hamburg.

Keinonen, A. (1979), "An Analytical Method for Calculating the Pure Ridge Resistance Encountered by Ships in First Year Ice Ridges," Helsinki University of Technology, Ship Hydrodynamics Laboratory, Otaniemi, Finland, Report No. 17, p. 1-114.

Matsuishi, M. and Ettema, R., (1985), "The Dynamic Behavior of a Floating Platform Continuously Impacted by Ice Floes," IIHR Report in preparation, The University of Iowa, Iowa City, Iowa.

Mellor, M. (1980), "Ship Resistance in Thick Brash Ice," Cold Regions Science and Technology, Vol. 3, pp. 305-321, Elsevier, Amsterdam.

Milano, V. (1980), "A Reanalysis of Ship Resistance when in Continuous Motion through Solid Ice," Intermaritech 80, Hamburg, p. 456-475.

Milano, V. (1982), "Correlation of Analytical Prediction of Ship Resistance in Ice with Model and Full Scale Test Results," Intermaritec 82, Hamburg, p. 350-372.

Ralston, T. (1980), "Plastic Limit Analysis of Sheet Ice Loads on Conical Structures," Physics and Mechanics of Ice, Per Tryde (Ed.), IUTAM Symp., Copenhagen, p. 289-308.

Sarpkaya, T. and Issacson, M. (1981), "Mechanics of Waves Forces on Offshore Structures," Van Nostrand Reinhold Company, New York.

Van Oortmerssen, G. (1976), "The Motion of a Ship in Shallow Water," Ocean Engineering, Vol. 3, p. 221-255.

Wessels, E. (1984), "Model Test Investigation of Ice Forces on Fixed and Floating Conical Structures," IAHR Ice Symposium, Vol. 3, pp. 203-219, Hamburg.

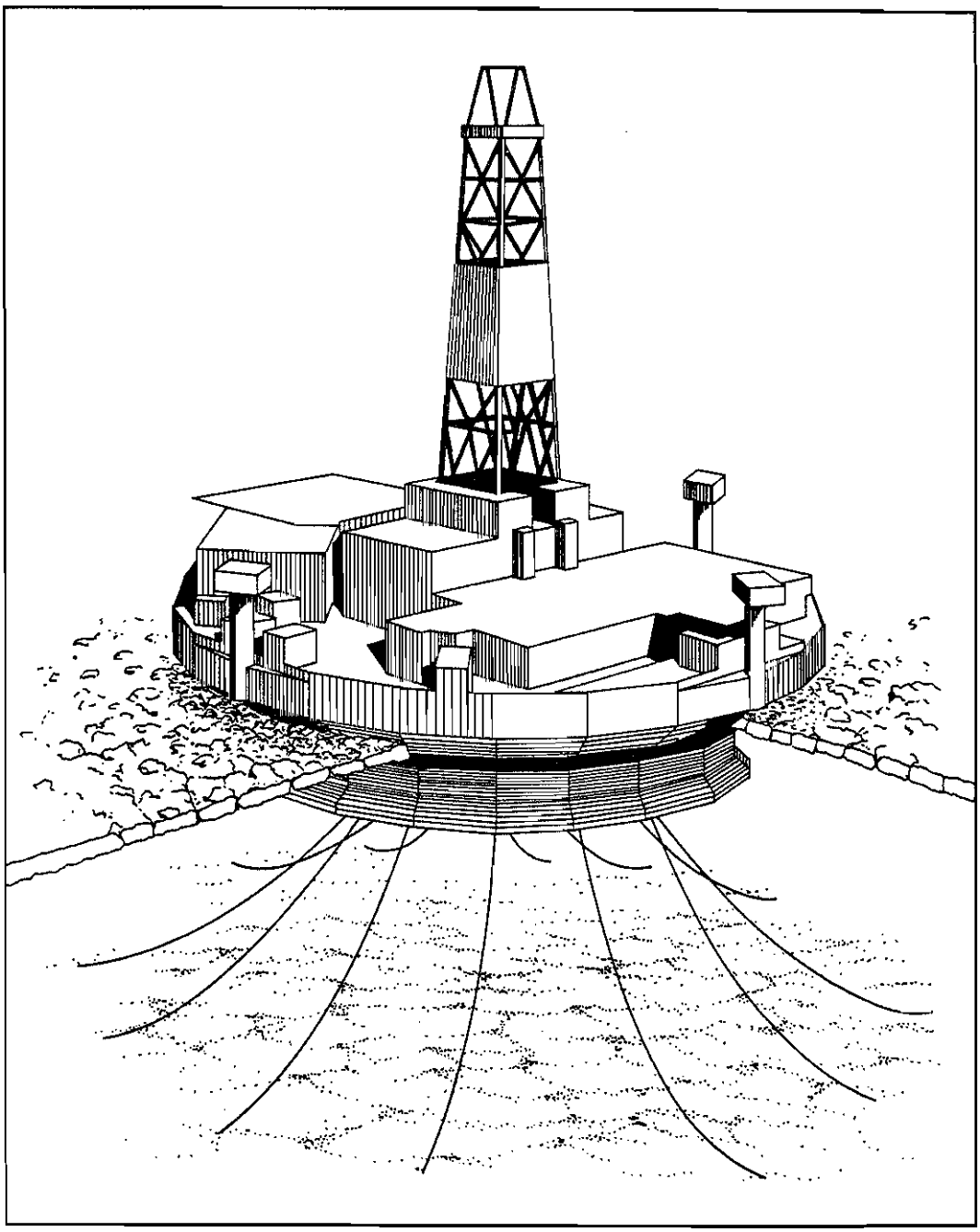

Figure 1. Layout of a floating, moored platform in ice-covered waters.

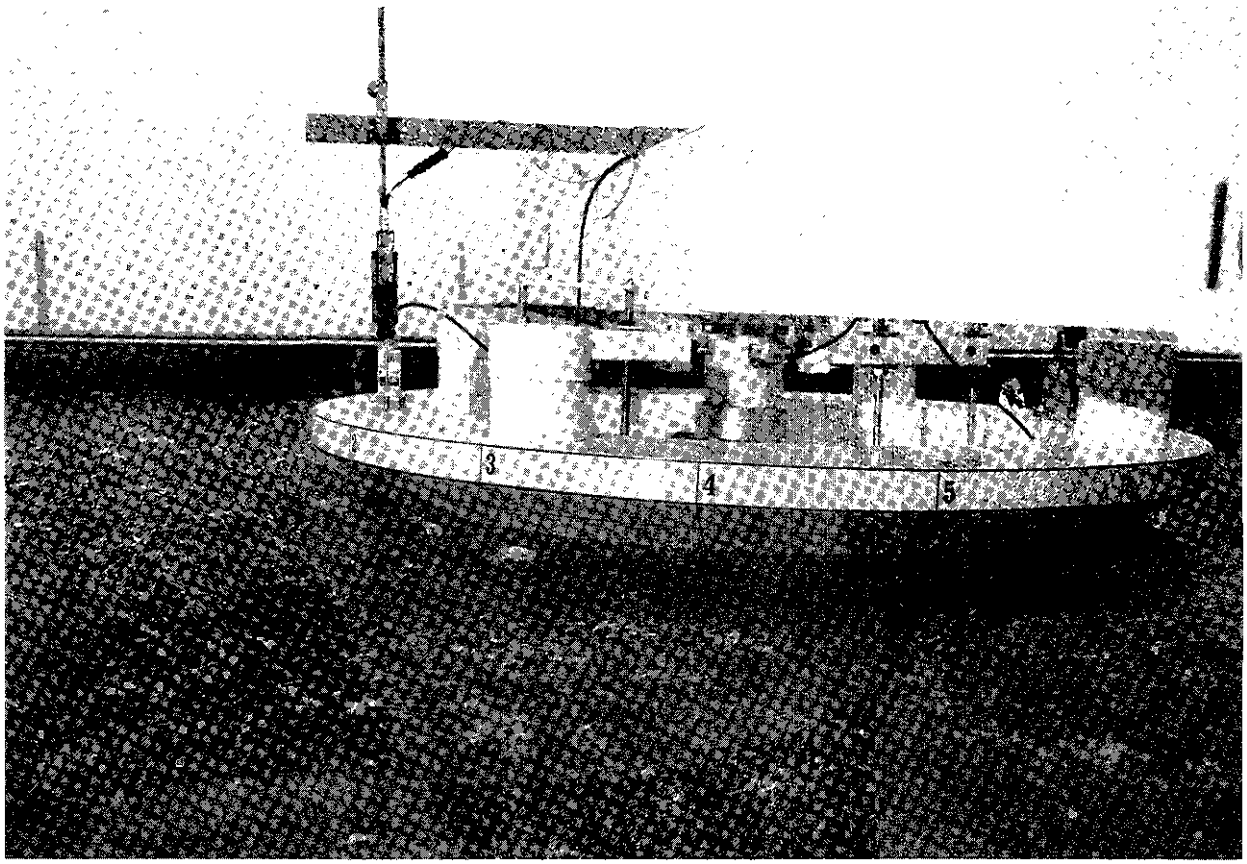

Figure 2. The test platform in a simulated field of mushy ice.

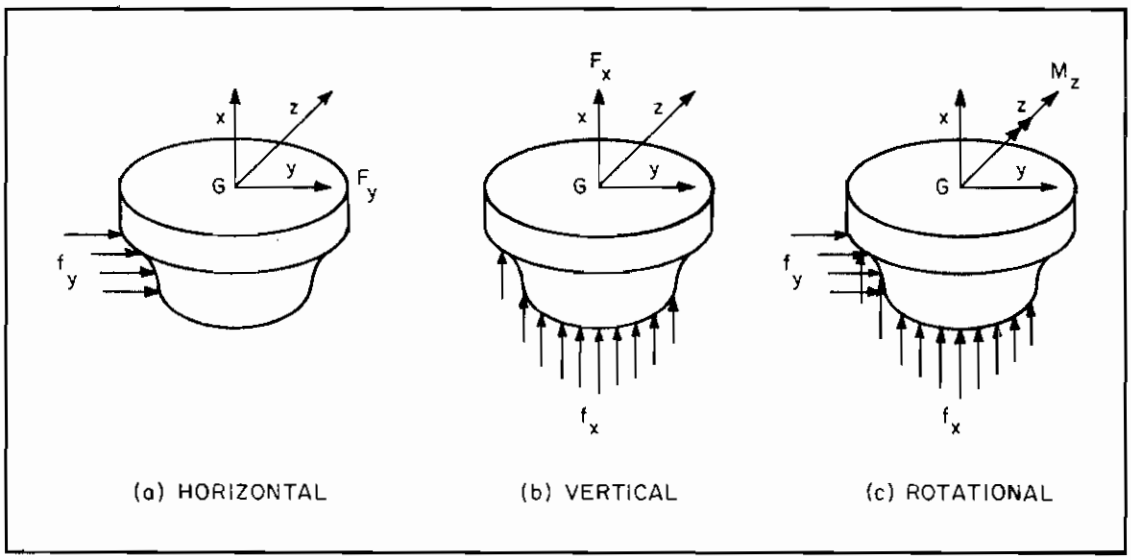

Figure 3. Ice forces and moment associated with rubble-ice pressure.

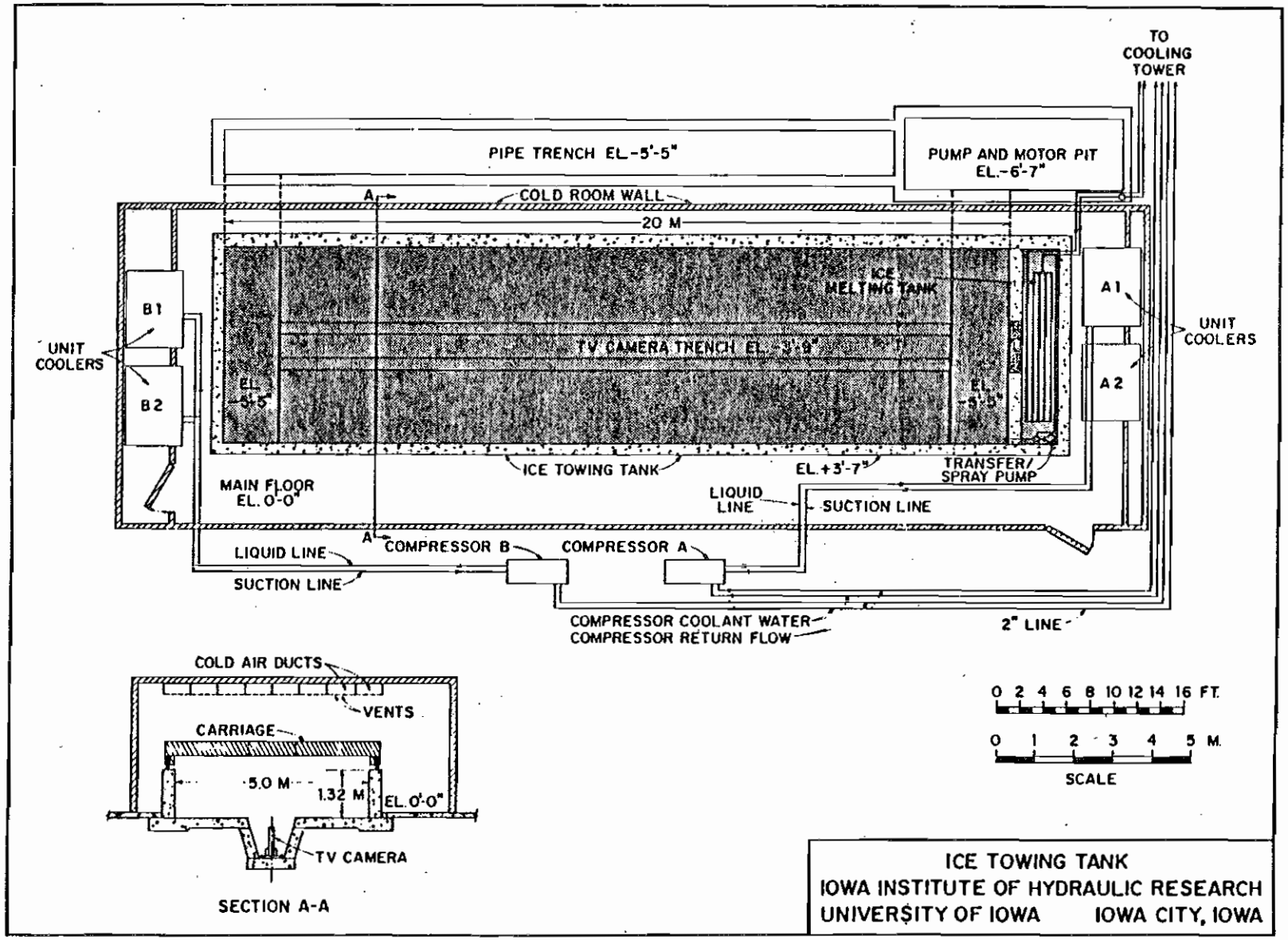

Figure 4. The IIHR ice towing tank.

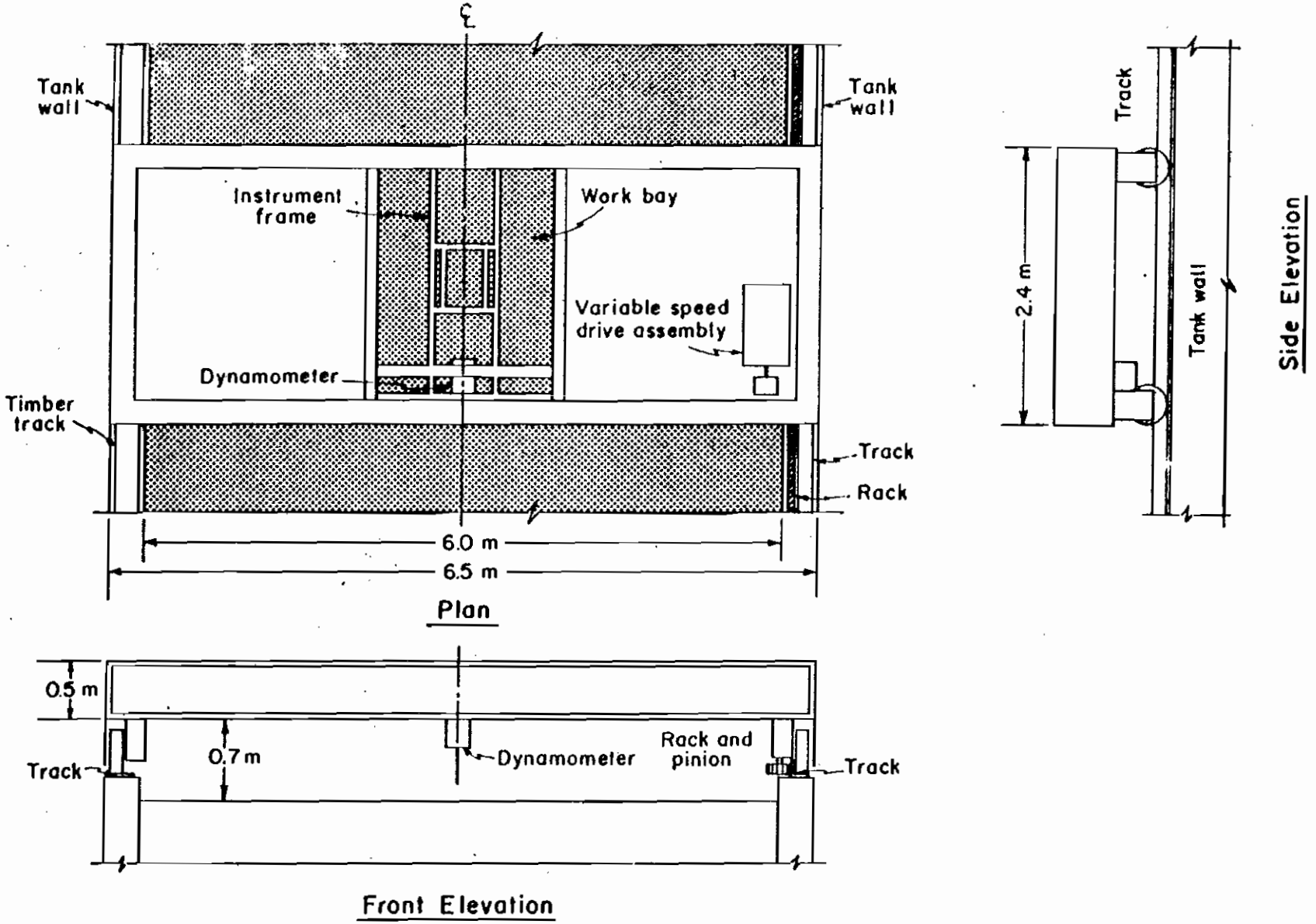

Figure 5. The towing carriage.

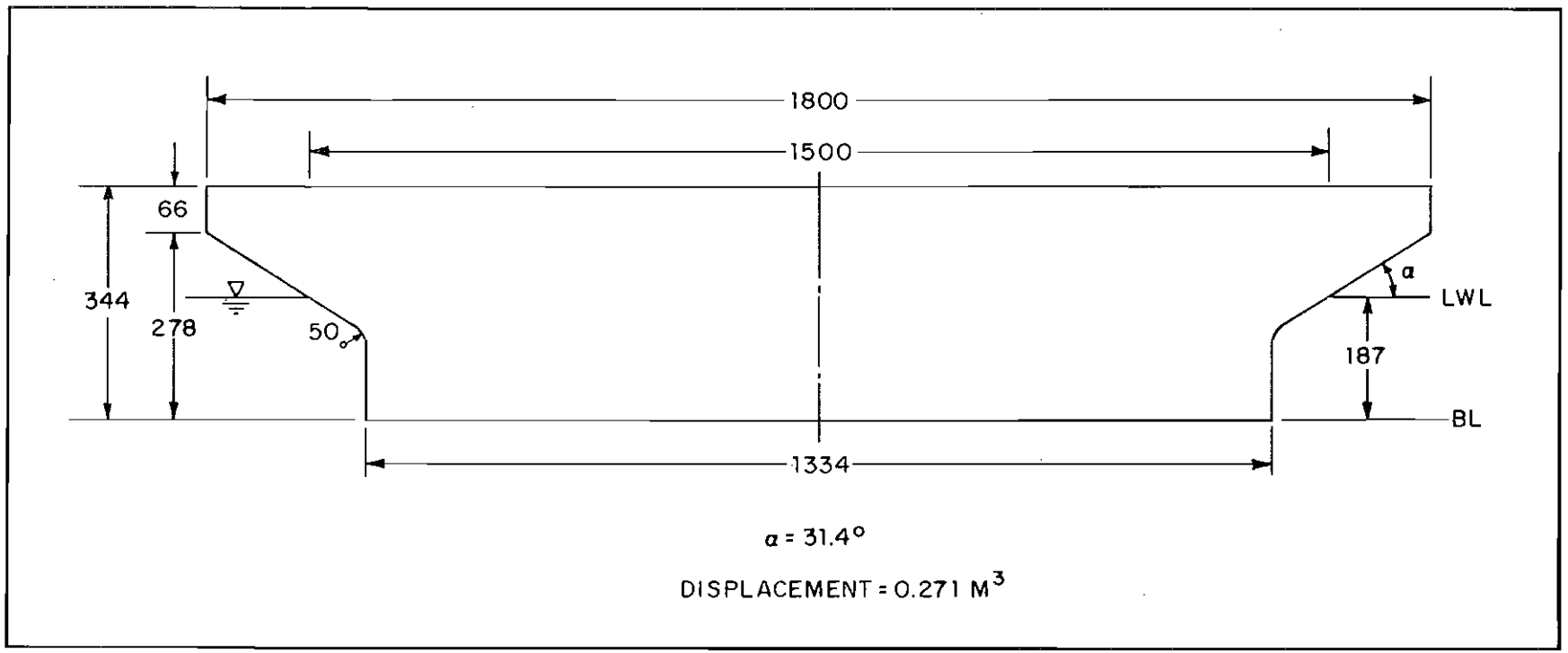

Figure 6. Form and principal dimensions of the test platform; lengths are in millimeters

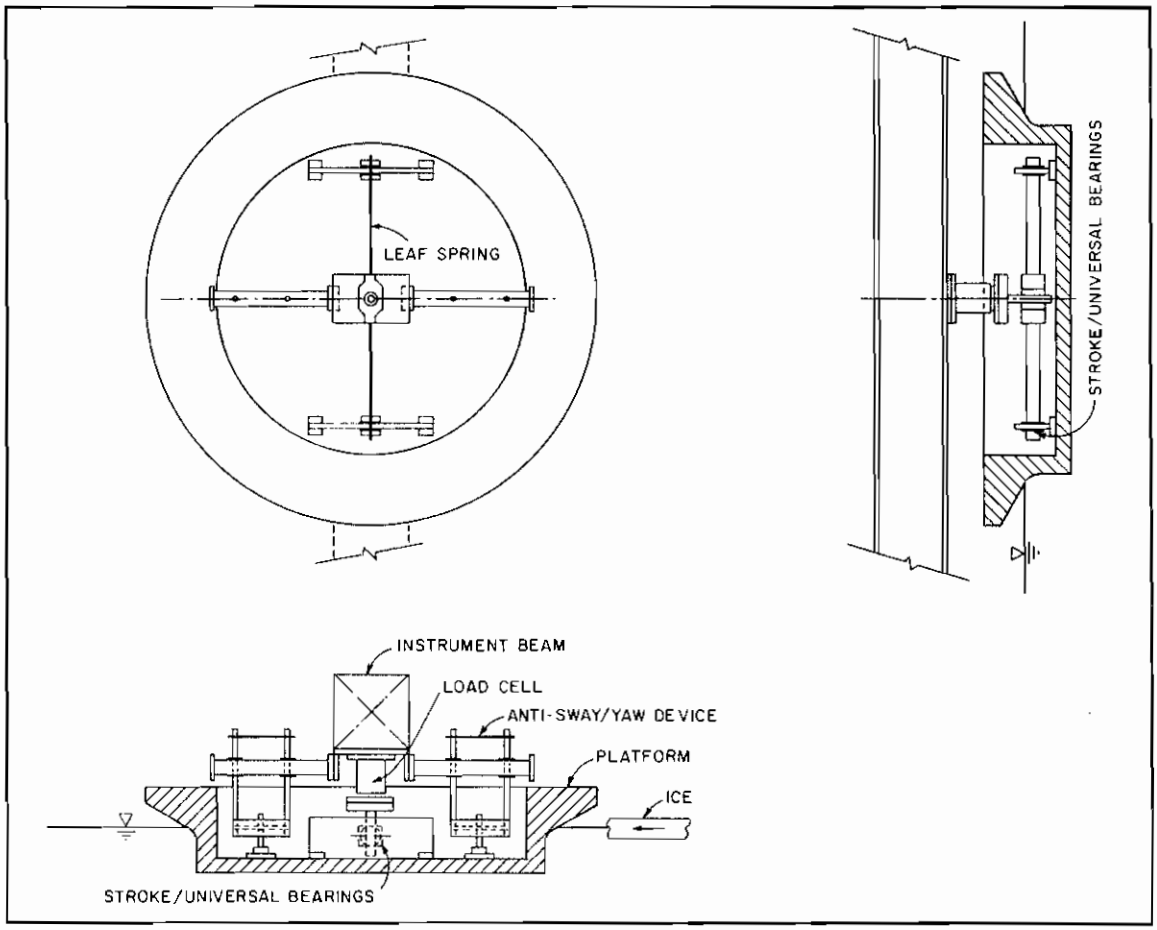

Figure 7. Instrumentation of moored platform.

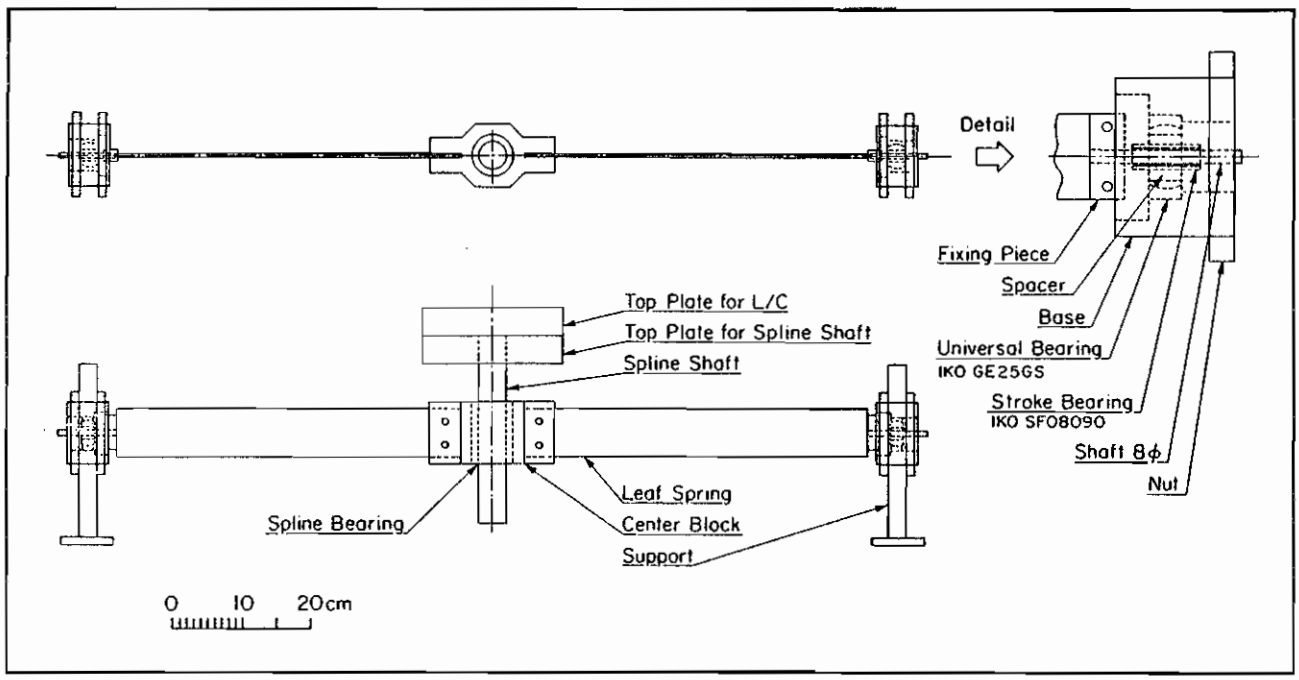

Figure 8. Details of the mooring harness.

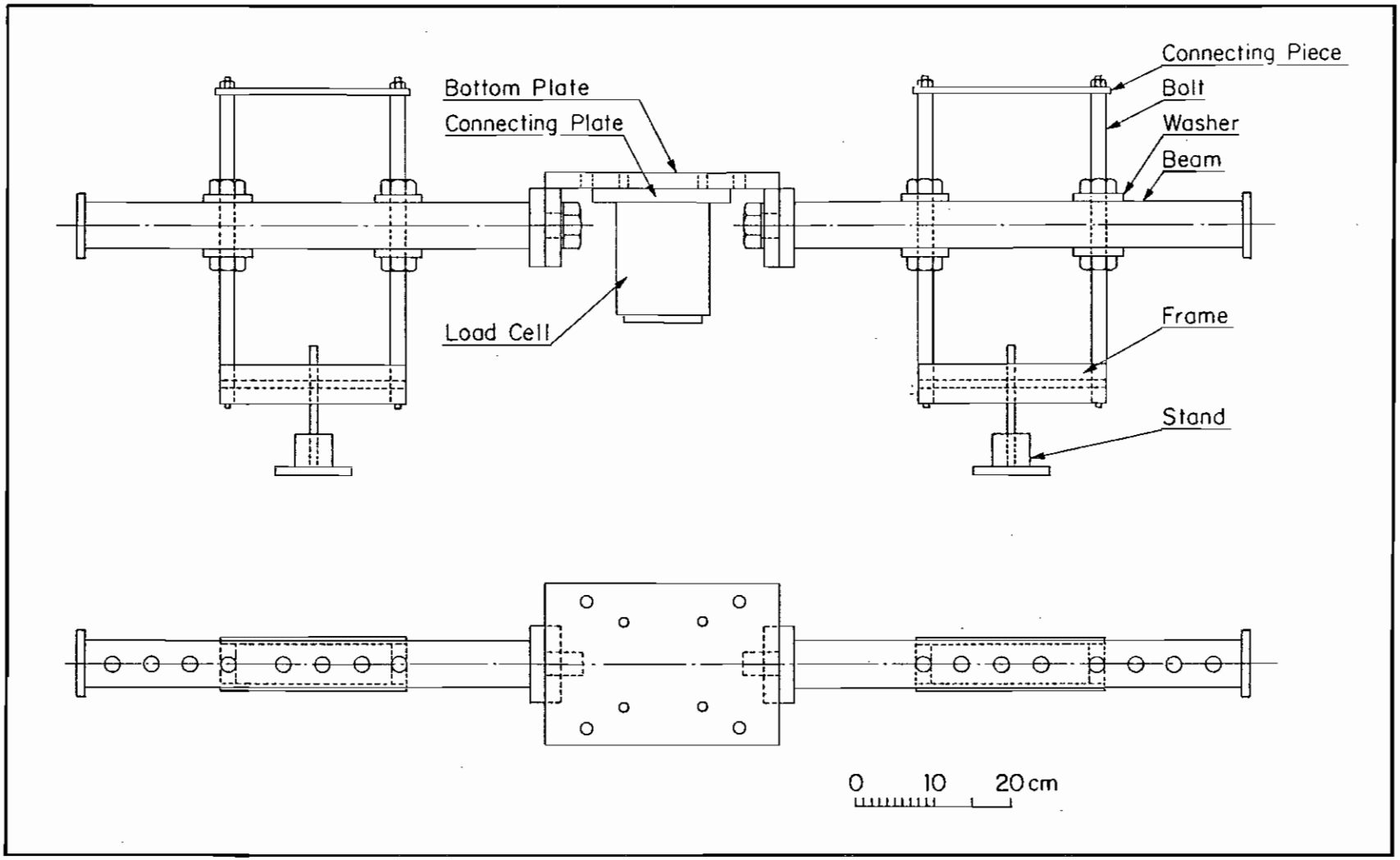

Figure 9. Details of sway and yaw restraining device.

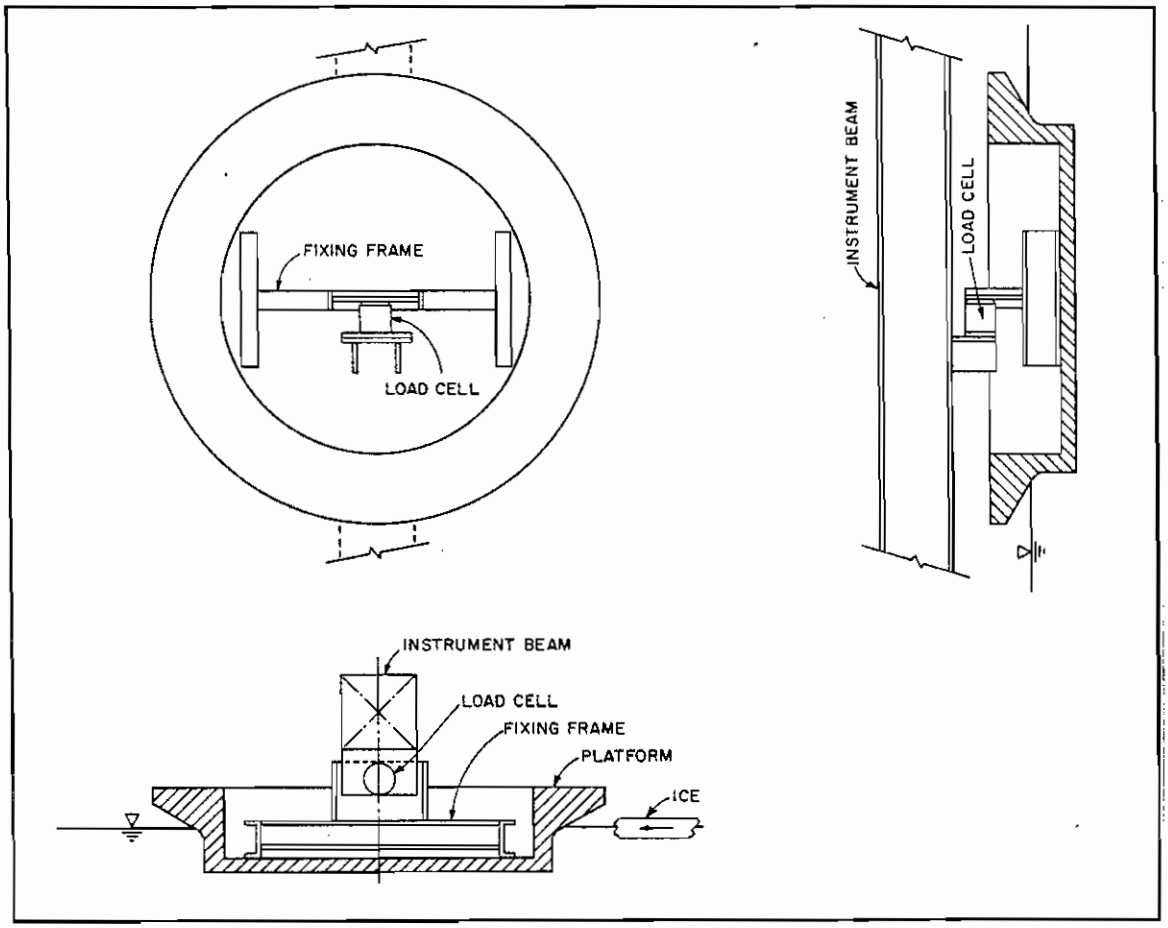

Figure 10. Instrumentation of fixed platform.

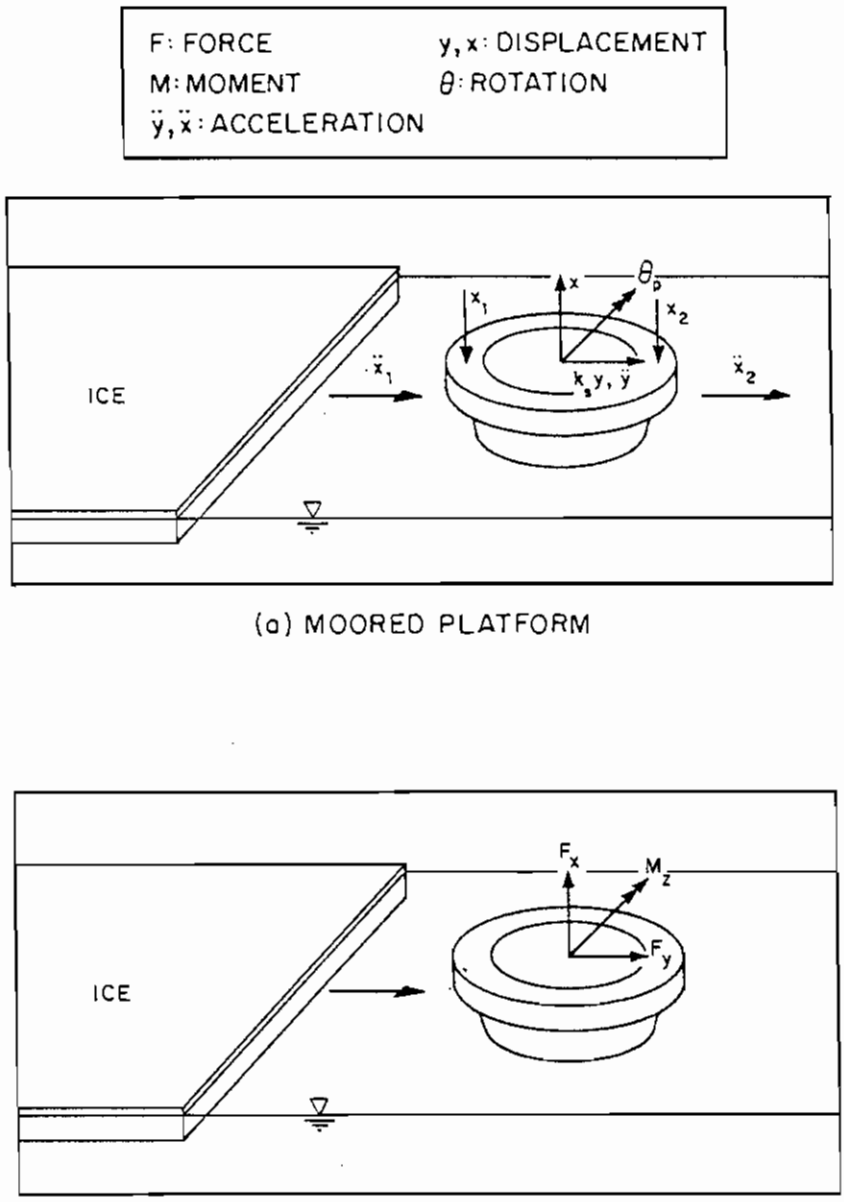

Figure 11. Locations of measurements and positive directions.

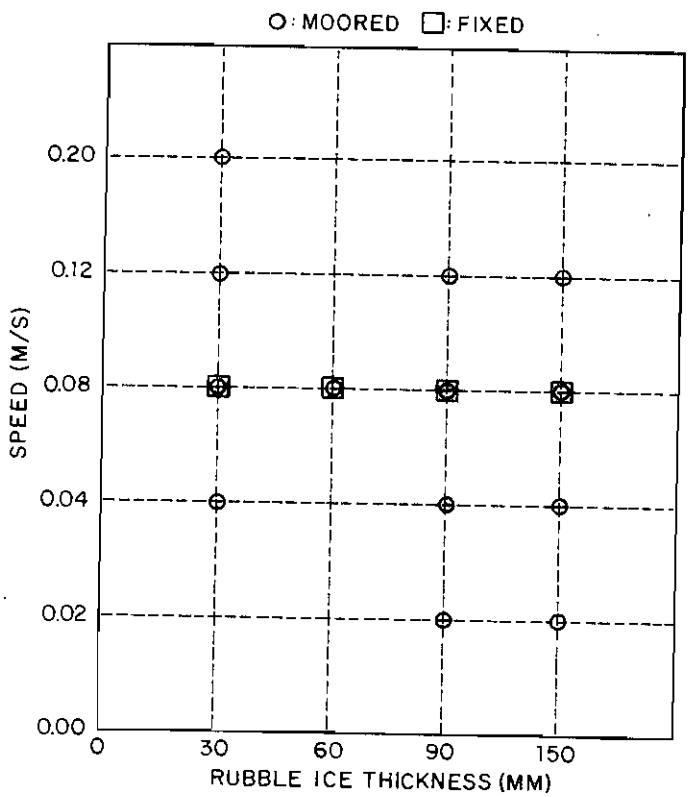

Figure 12. Program of experiments.

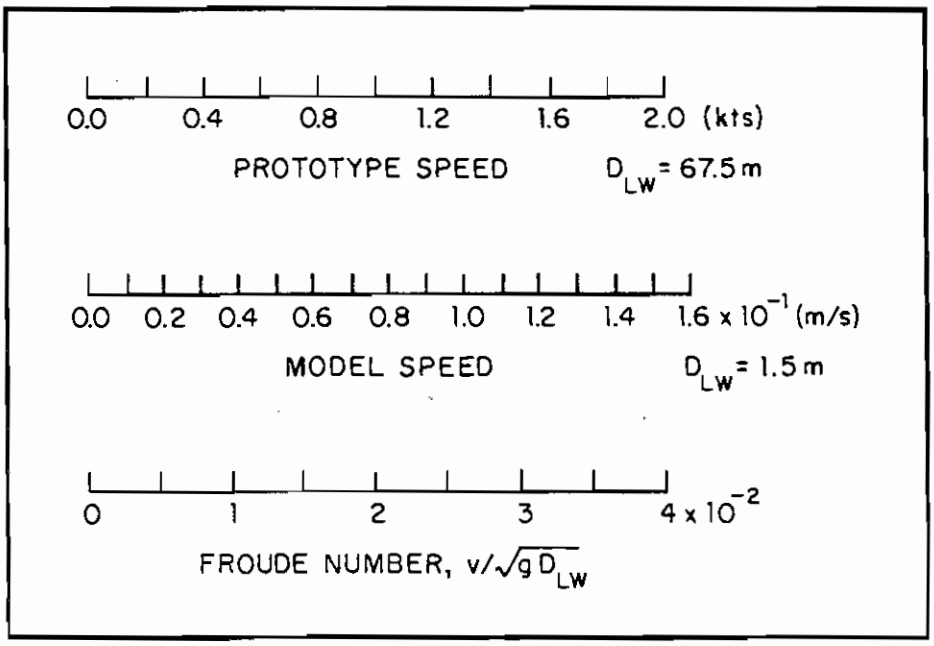

Figure 13. Relationships between model and prototype ice impact speed.

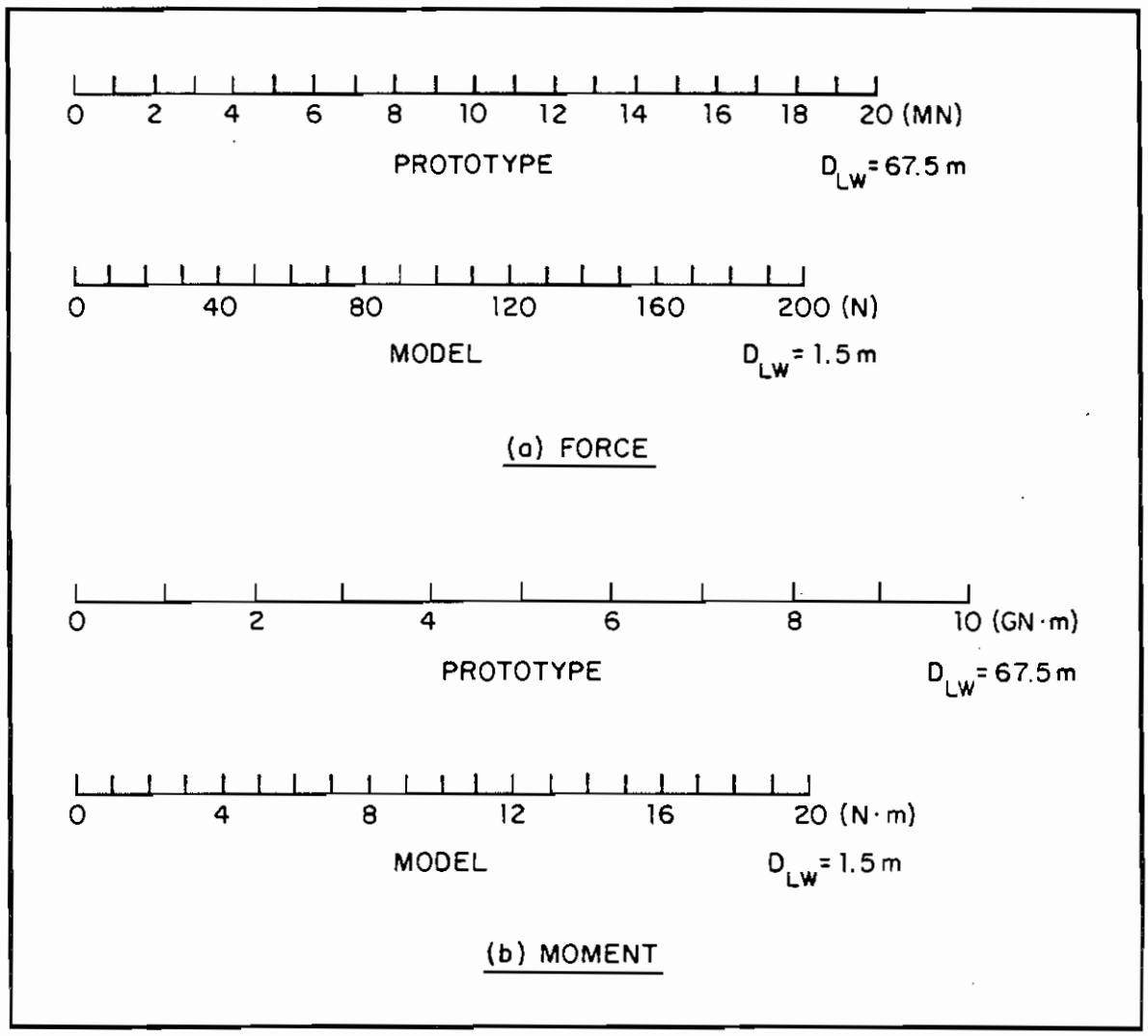

Figure 14. Relationships between model and prototype forces.

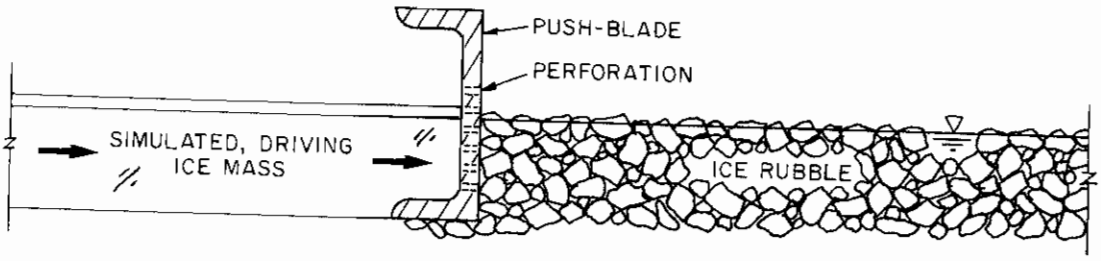

Figure 15. Push-blade arrangement.

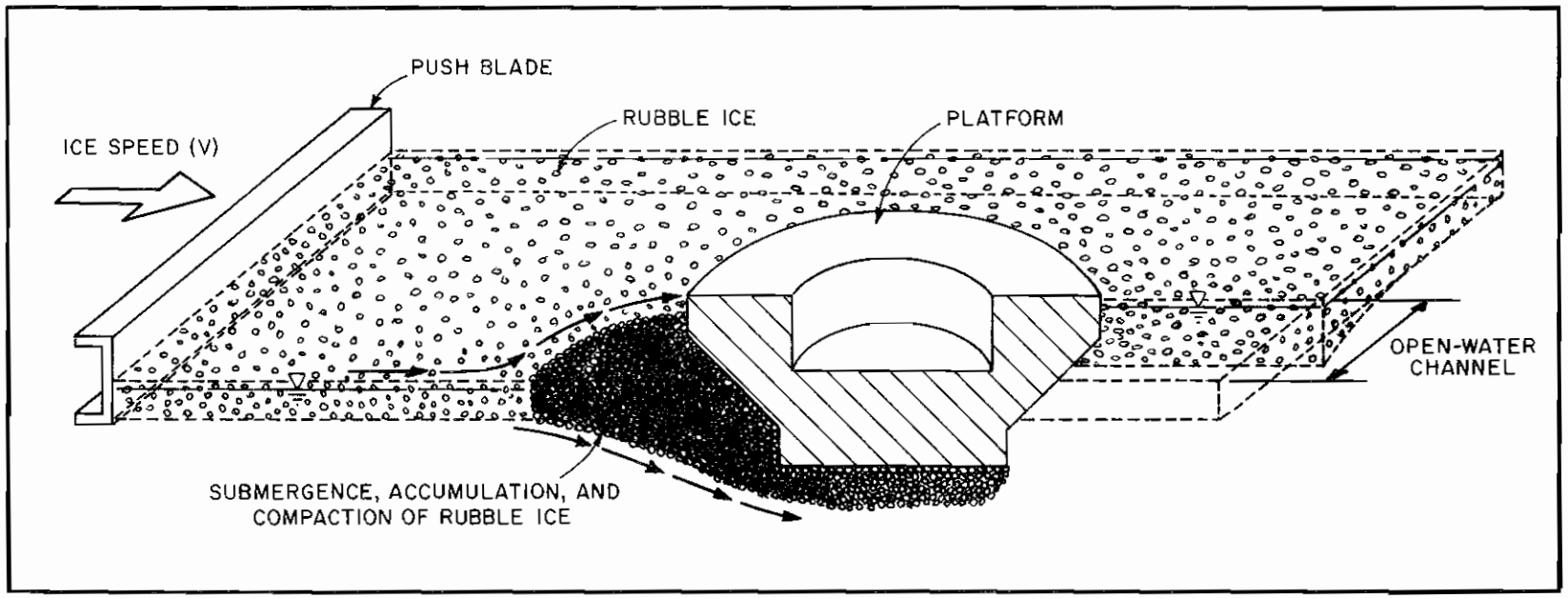

Figure 16. Ice-rubble movement and accumulation around the test platform.

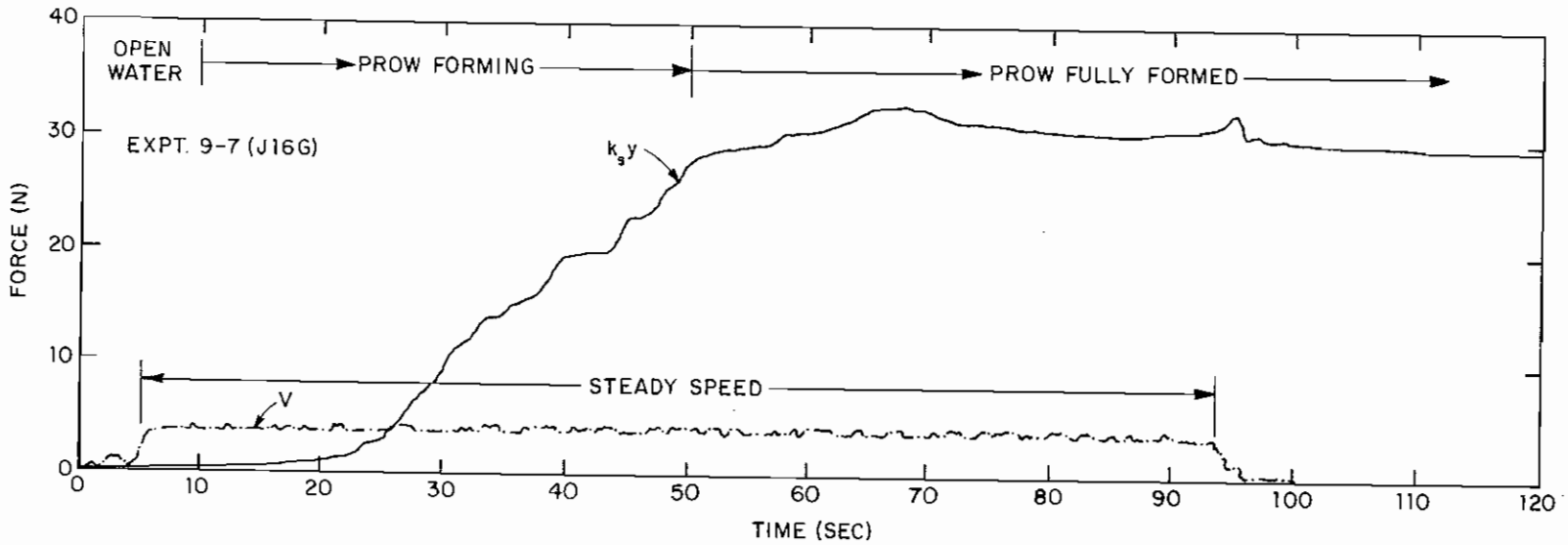

Figure 17. Time-history of mooring force increase while an "ice prow" developed at the leading perimeter of the moored test platform.

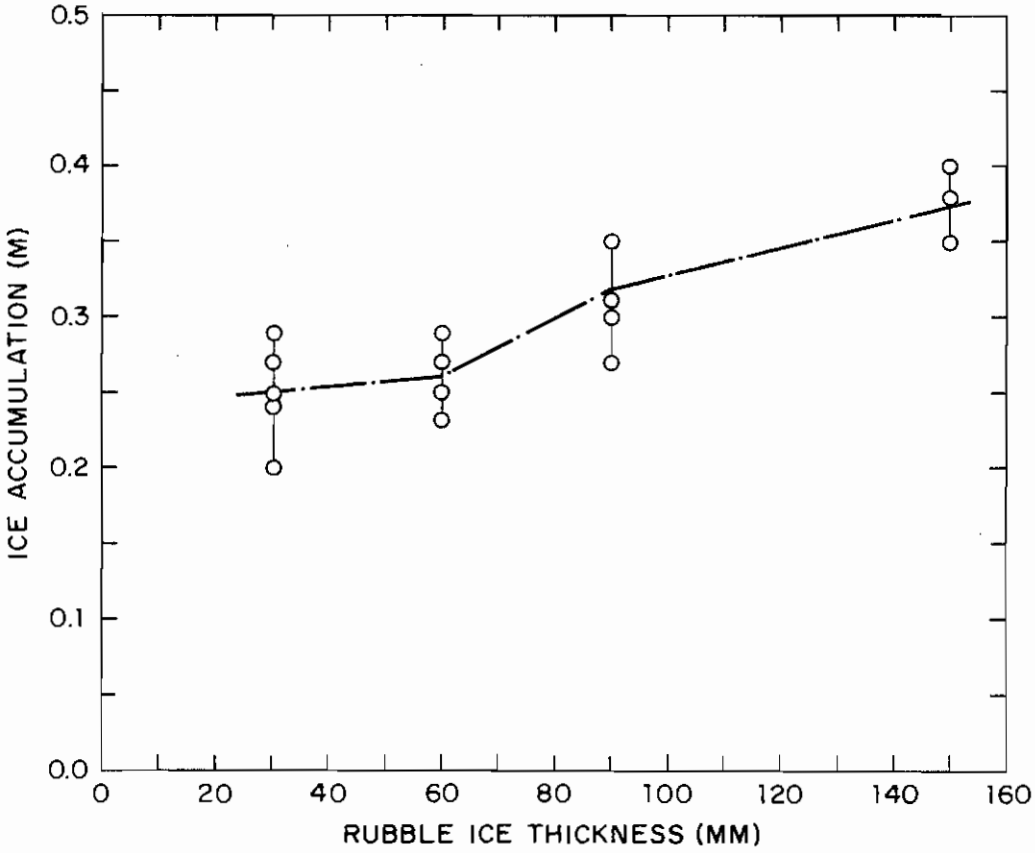

Figure 18. Thickness of ice-rubble accumulation as a "prow."

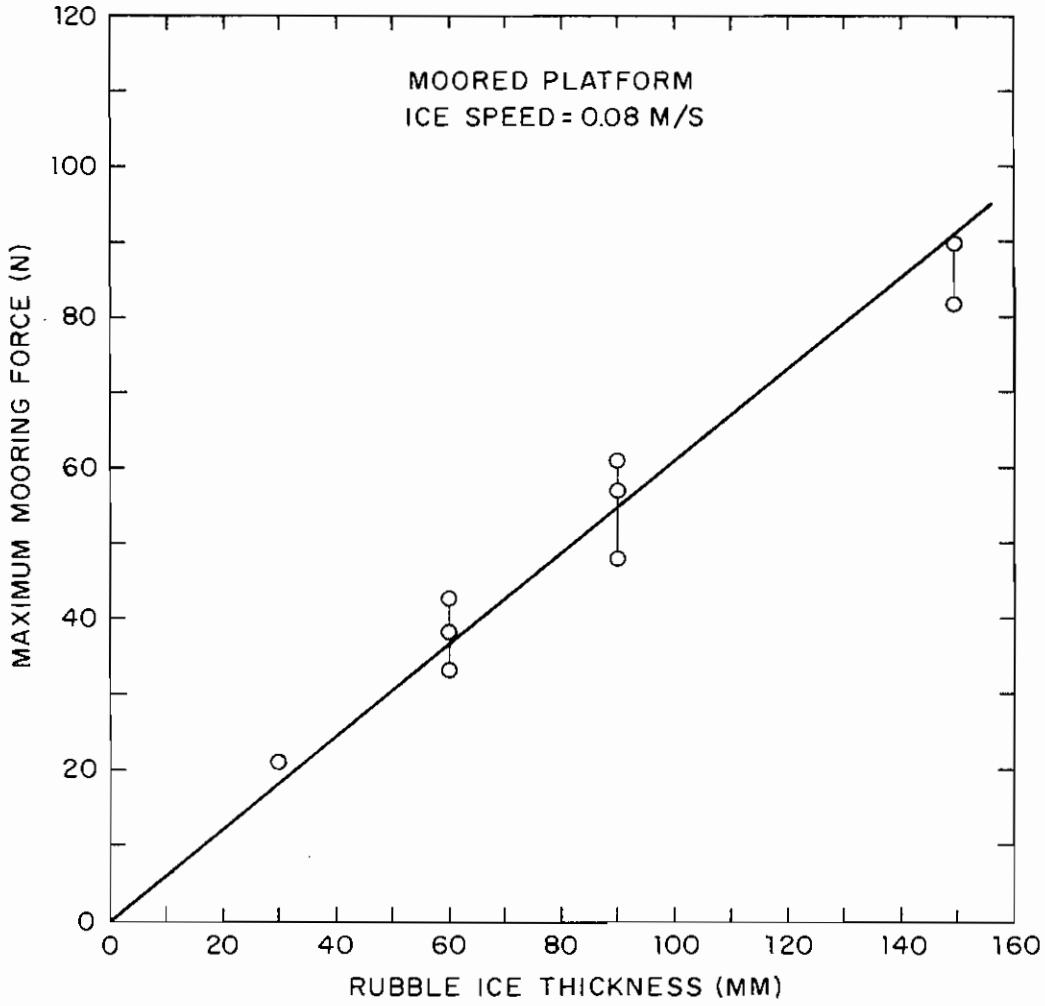

Figure 19. The effect of ice-rubble thickness on mooring force.

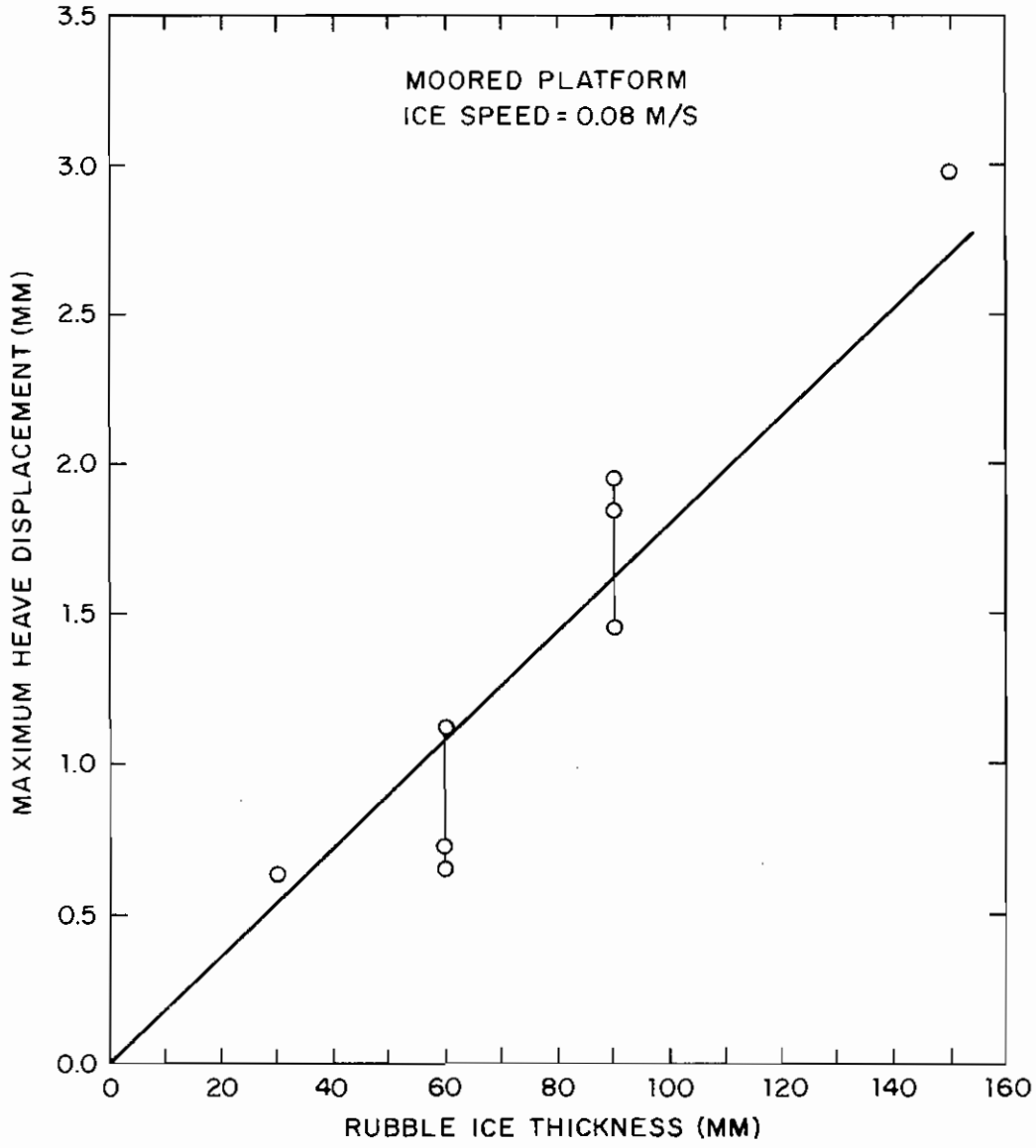

Figure 20. The effect of ice-rubble thickness on heave displacement.

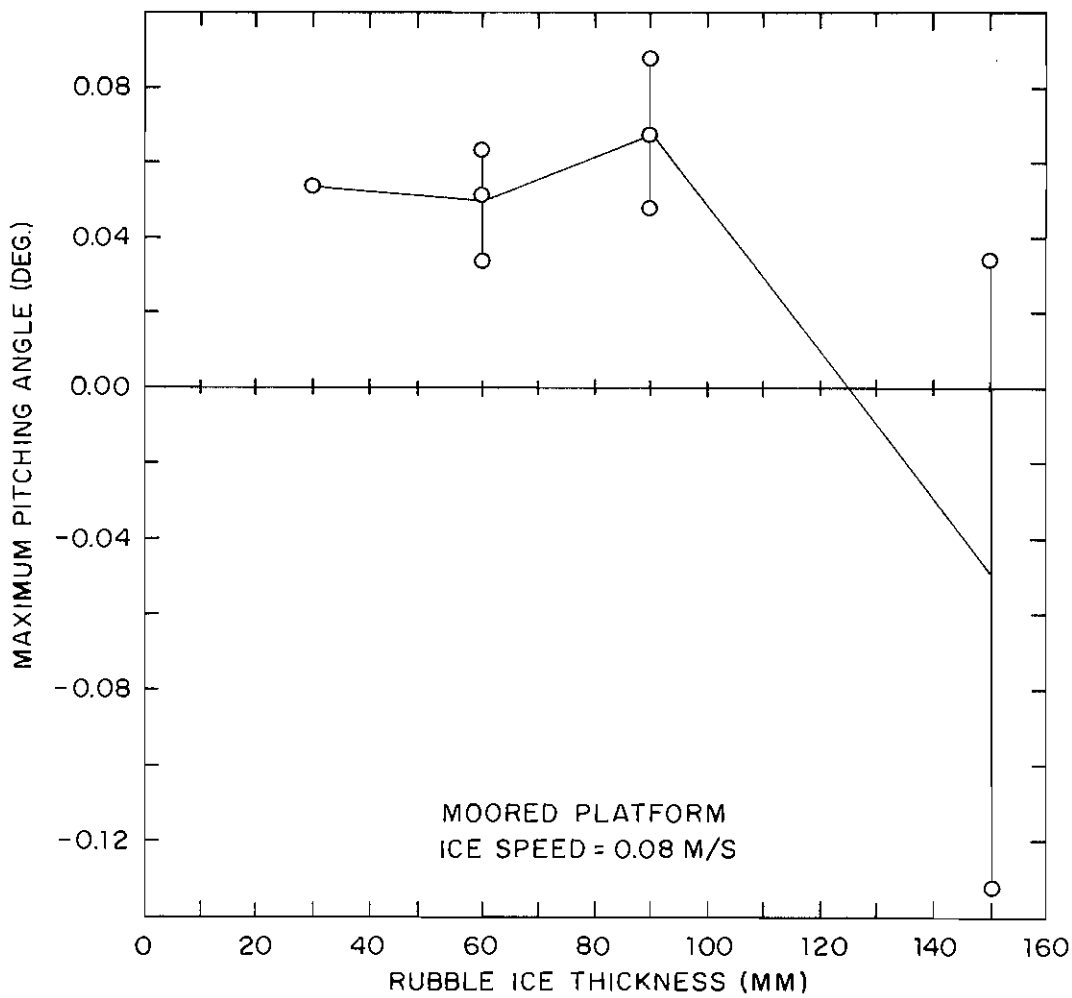

Figure 21. The effect of ice-rubble thickness on maximum pitching angle.

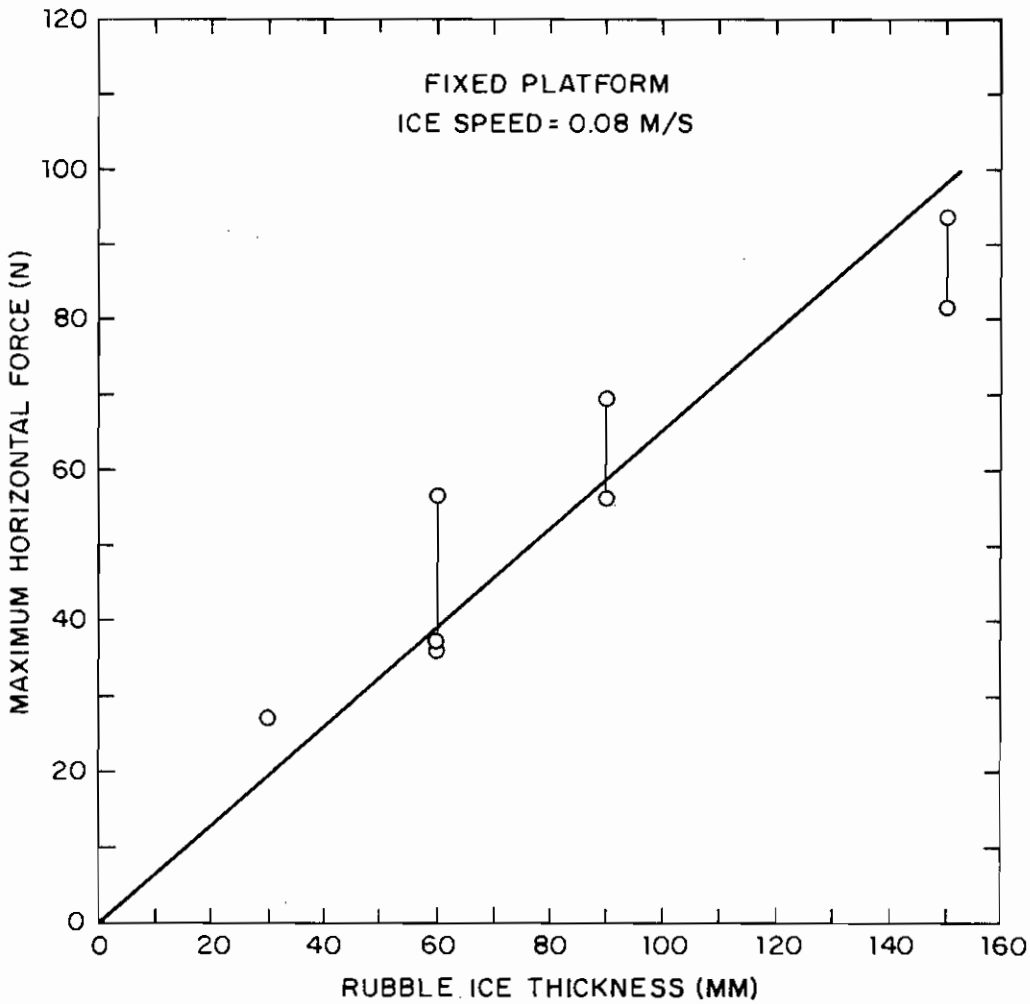

Figure 22. The effect of ice-rubble thickness on horizontal (surge) restraining force.

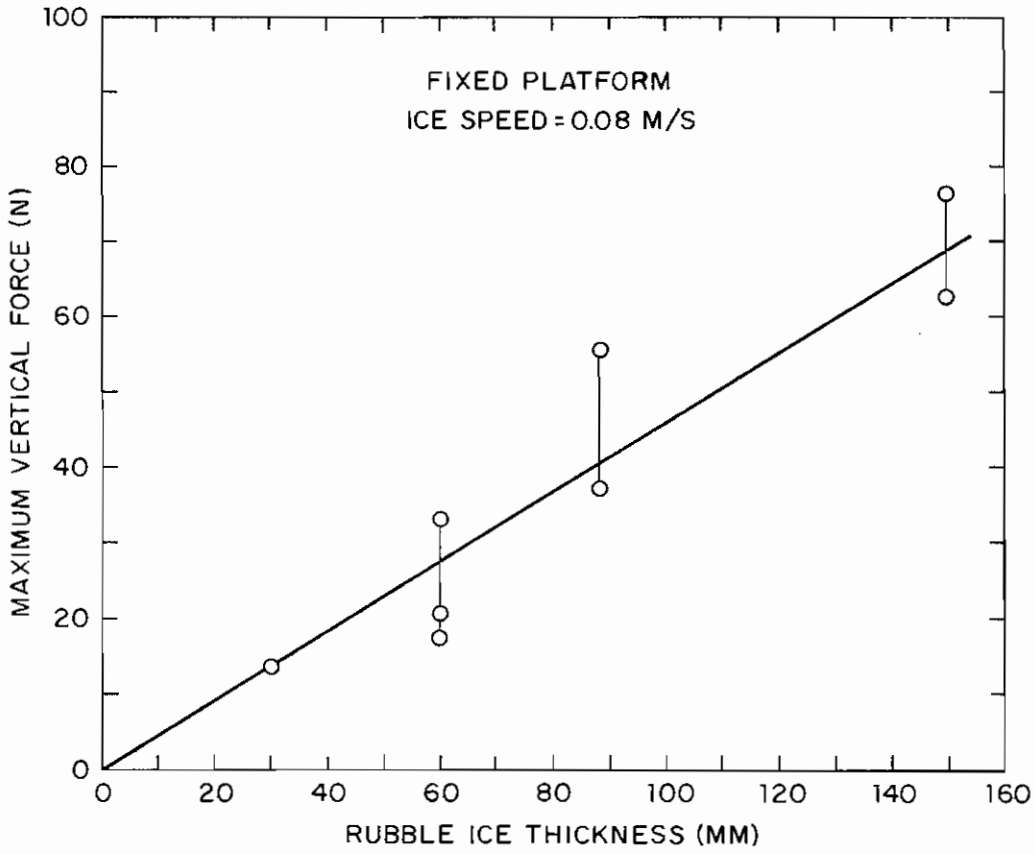

Figure 23. The effect of ice-rubble thickness on vertical (heave) restraining force.

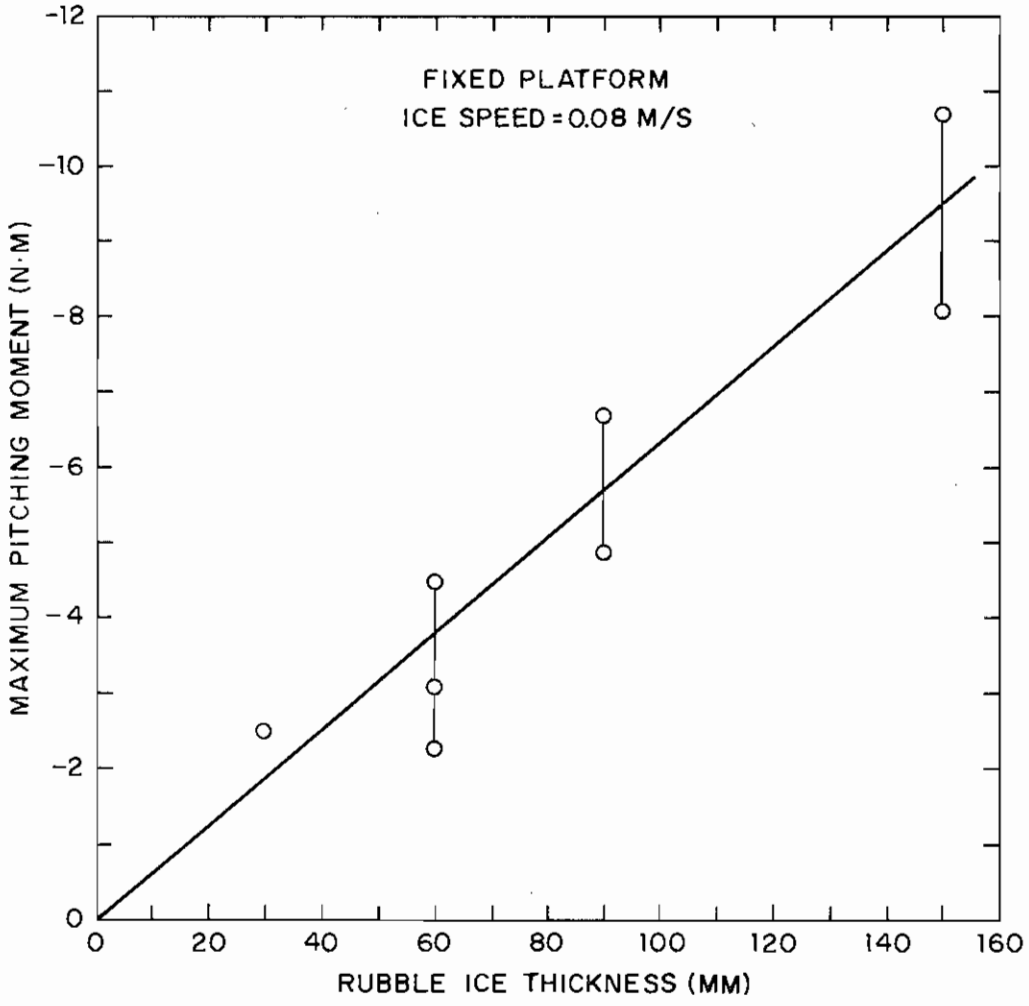

Figure 24. The effect of ice-rubble thickness on pitching moment.

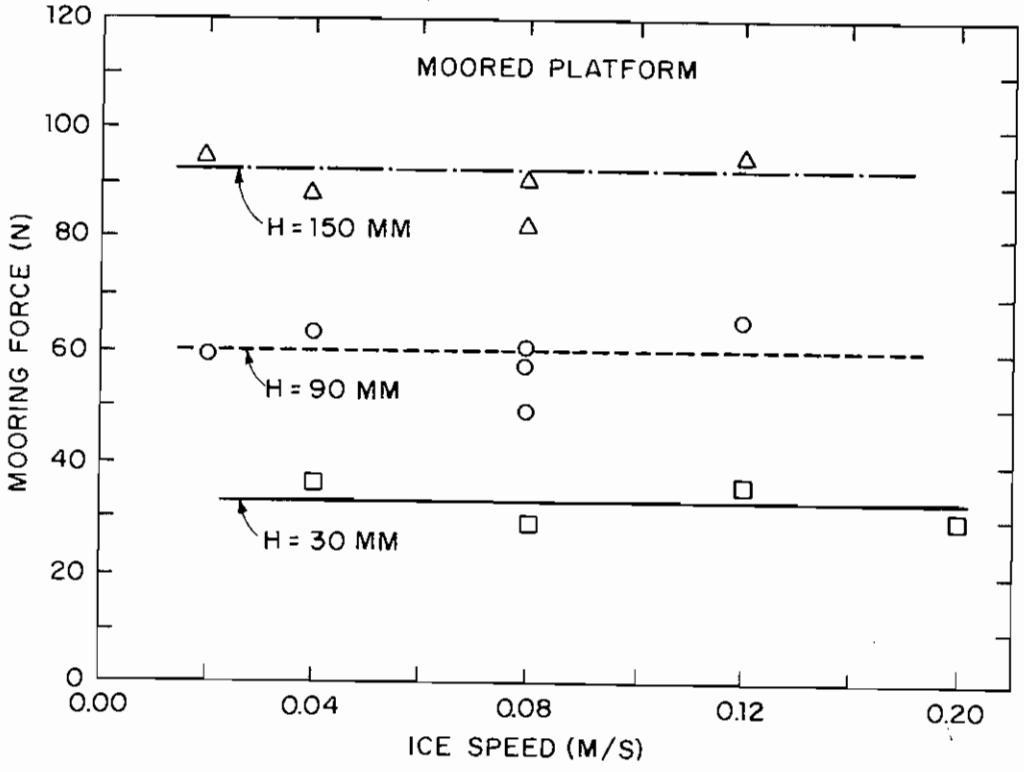

Figure 25. The effect of ice-rubble speed on mooring force.

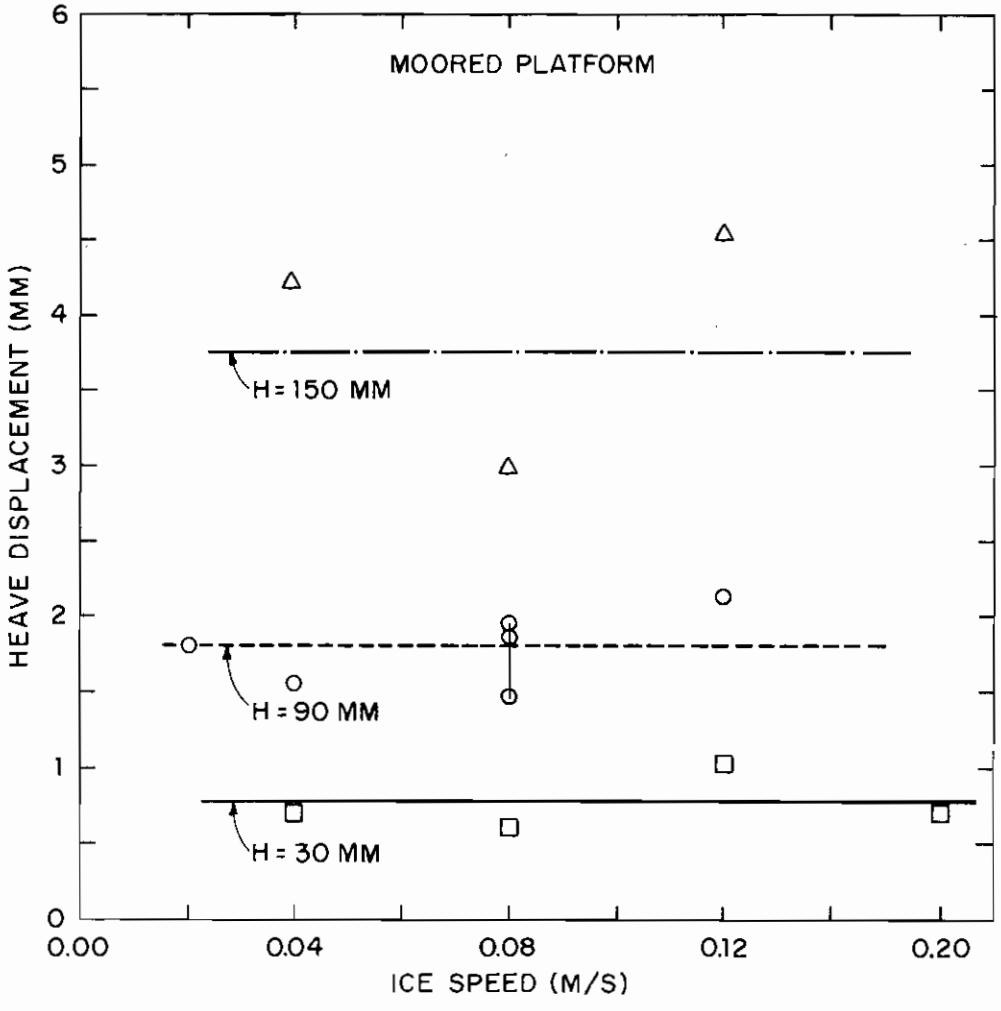

Figure 26. The effect of ice-rubble speed on heave displacement.

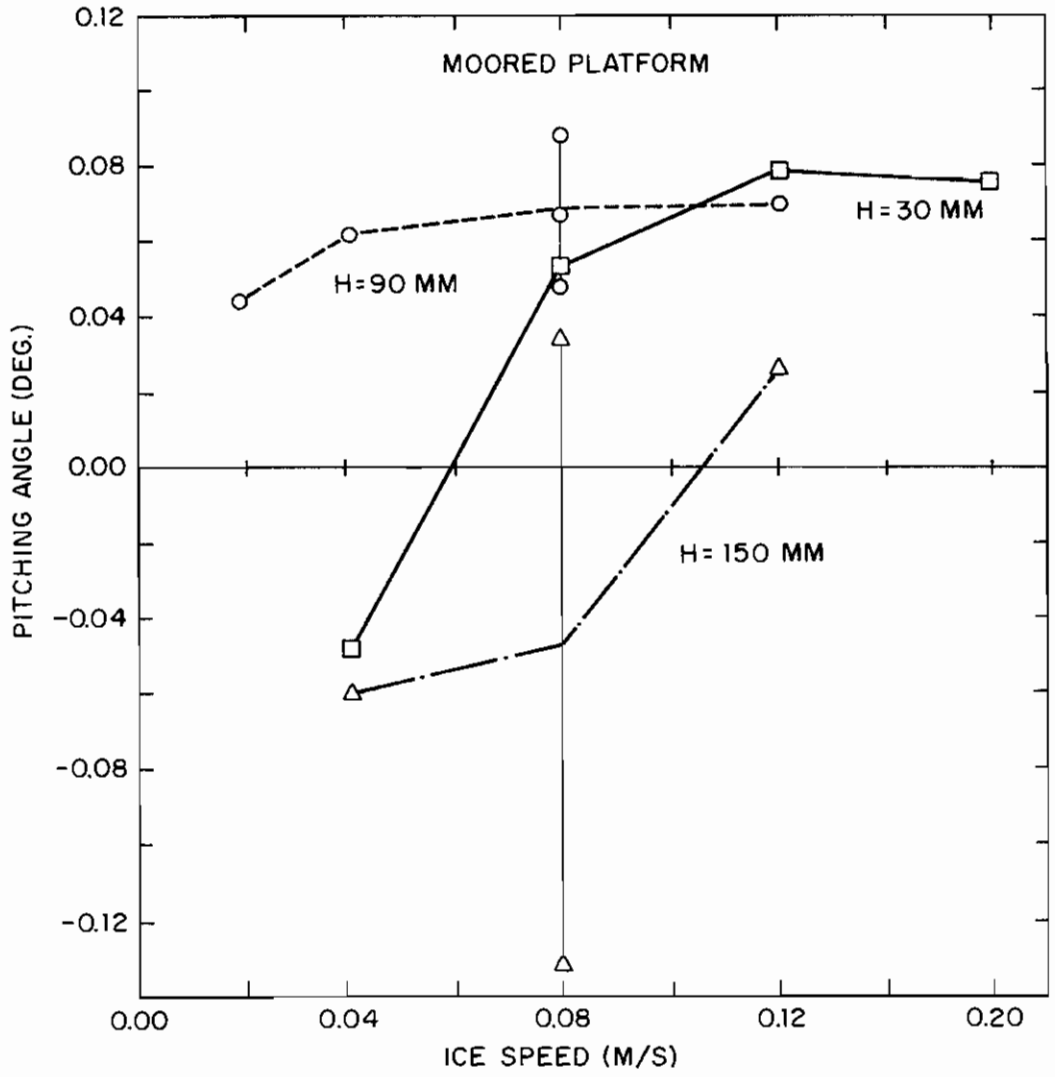

Figure 27. The effect of ice-rubble speed on maximum pitching angle.

Table 1. Principal Dimensions of the Test Platform and "Kulluk."

		Test Platform (1/45 scale)	"Kulluk"
Diameter at deck level, D_D	(m)	1.8	81.0
Diameter at load waterline, D_{LW}	(m)	1.5	67.5
Diameter at base line, D_B	(m)	1.334	60.0
Depth, D	(m)	0.334	15.5
Draft, d	(m)	0.187	8.4
Displacement, ∇	(m^3)	0.271	24700
Cone angle, α	(degree)	31.4	31.4

Table 2. Natural periods and logarithmic decrements of model platform

	SURGE	HEAVE	PITCH
Natural Period, T (seconds)	3.00	1.41	1.17
Logarithmic Decrement, δ	0.29	--	0.55

Table 3. Ice-sheet data

Thickness, t(m)	0.029-0.032
Flexural strength, σ_f (kPa)	16.6 - 24.4
Elastic modulus, E(MPa)	8.2 - 14.8

Table 4. Comparison of ice loadings experienced by the platform when moored and when fixed

Layer Thickness H (m)	Layer Speed V (m/s)	Ratio for moored: fixed condition of platform restraint	
		Surge Force	Heave Force
0.03	0.08	0.74	0.81
0.06	0.08	0.87	0.61
0.09	0.08	0.88	0.65
0.15	0.08	0.98	0.74

APPENDIX 1. Tables of Measured and Analyzed Data

Expt. No.	File No.	H (mm)	V (m/s)	F_y (N)	δ_H (mm)	θ (deg)
5-7	J03G	30	0.04	37.1	0.70	-0.047
5-4	J03D	30	0.08	20.9	0.63	0.054
5-8	J03H	30	0.12	36.0	1.04	0.080
5-9	J03I	30	0.20	29.4	0.70	0.076
9-5	J16E	60	0.08	42.5	1.12	0.052
9-7	J16G	60	0.08	33.0	0.65	0.034
10-3	J18C	60	0.08	37.9	0.72	0.063
7-5	J11E	90	0.02	59.6	1.82	0.044
7-3	J11C	90	0.04	63.9	1.55	0.062
5-5	J03E	90	0.08	60.8	1.84	0.048
9-6	J16F	90	0.08	57.0	1.95	0.067
10-4	J18D	90	0.08	47.9	1.45	0.088
7-4	J11D	90	0.12	66.1	2.12	0.070
7-8	J11H	150	0.02	95.6	Not	Measured
7-6	J11F	150	0.04	88.5	4.2	-0.060
5-6	J03F	150	0.08	89.8	2.99	-0.132
10-5	J18E	150	0.08	81.7	2.99	0.034
7-7	J11G	150	0.12	96.1	4.54	0.027

Table A-1. Summary of Data for the Moored Test Platform

Expt. No.	File No.	H (mm)	V (m/s)	F_x (N)	F_y (N)	M_z (Nm)
8-3	J14C	30	0.08	13.5	27.1	-2.5
8-4	J14D	60	0.08	33.0	56.8	-4.5
11-5	J21E	60	0.08	20.6	37.2	-3.1
11-7	J21G	60	0.08	17.3	36.3	-2.3
8-5	J14E	90	0.08	55.4	69.7	-6.7
11-6	J21F	90	0.08	37.1	56.3	-4.9
8-6	J14F	150	0.08	76.2	93.5	-10.7
11-8	J21H	150	0.08	62.7	81.5	-8.1

Table A-2. Summary of Data for the Fixed Test Platform

APPENDIX 2: Time Histories of Measured Quantities

Note:

(1) Ordinate is in voltage.

(2) Calibration coefficient for the ice speed (V) is (0.417 volts - 0.0025) m/s.

(3) Heave displacement is downward positive.

(4) Pitching angle is positive when fore part of platform moves downward and aft upward.

Table A-3. Calibration Coefficients

Exp. No.	F_x (N/V)	F_y (N/V)	M_z (N-m/V)	X_1 (m m/V)	X_2 (m m/V)	A_1, A_2, A_3 ($m/s^2/V$)
1-1 1-9	21.4	21.4	21.4	13.03	12.92	-
2-1 2-6	9.8	9.8	9.8	13.03	12.92	-
3-1 3-14	19-6	19.6	19.6	13.03	12.92	-
4-1 4-5	19.6	19.6	19.6	13.03	12.92	-
5-1 5-9	19.6	19.6	19.6	13.03	12.92	0.490
6-1	19.6	19.6	19.6	13.03	12.92	0.196
7-1 7-8	19.6	19.6	19.6	13.03	12.92	0.196
8-1 8-6	19.6	19.6	19.6	13.03	12.92	0.196
9-1 9-7	19.6	19.6	19.6	13.03	12.92	0.196
10-1 10-5	19.6	19.6	19.6	13.03	12.92	0.196
11-1 11-8	19.6	19.6	19.6	13.03	12.92	0.196

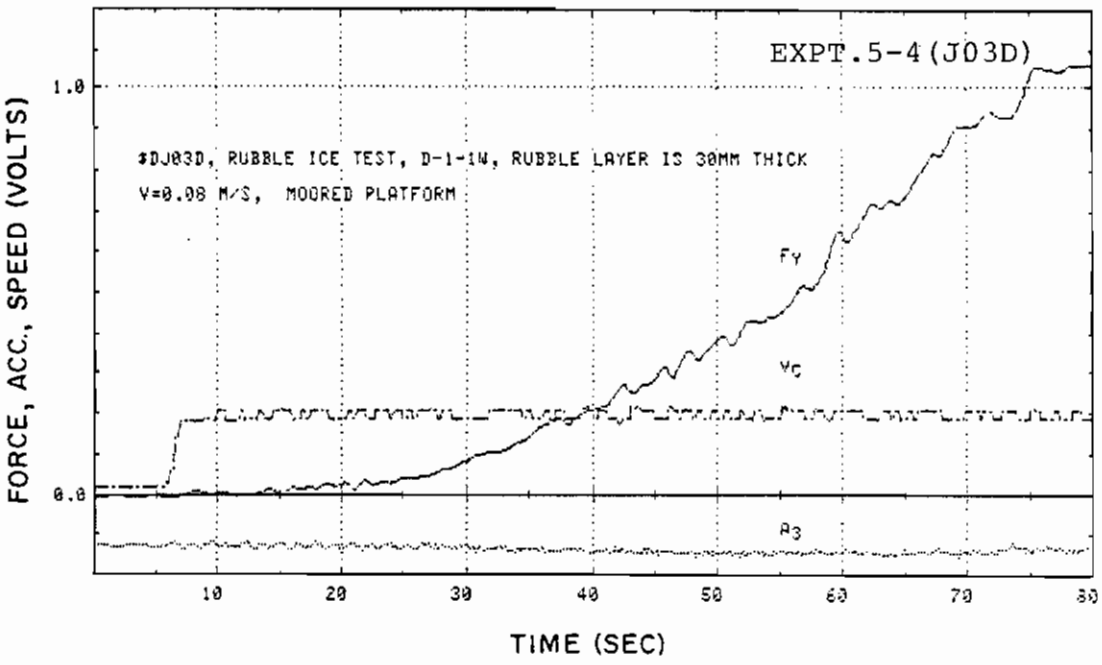

Fig. A-2-1

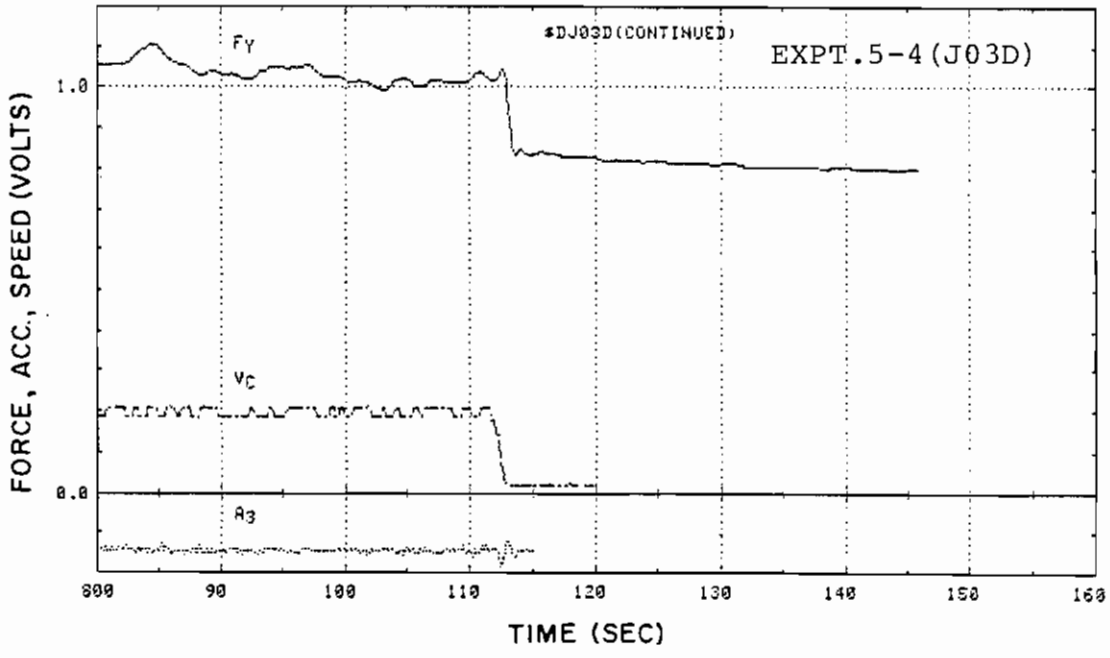

Fig. A-2-2

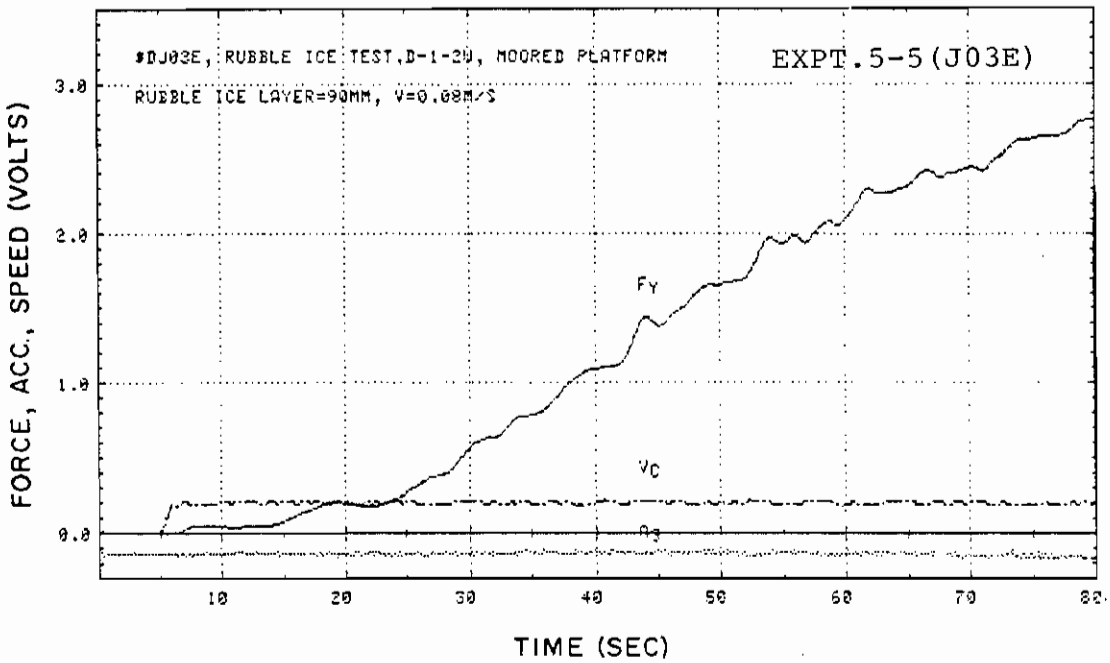

Fig. A-2-3

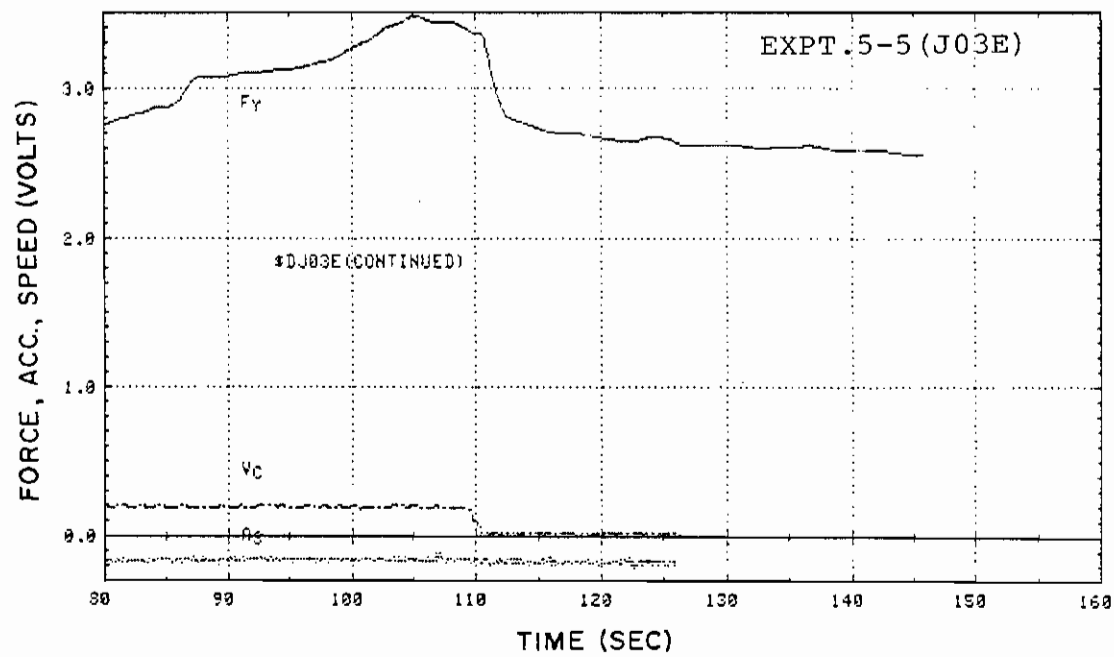

Fig. A-2-4

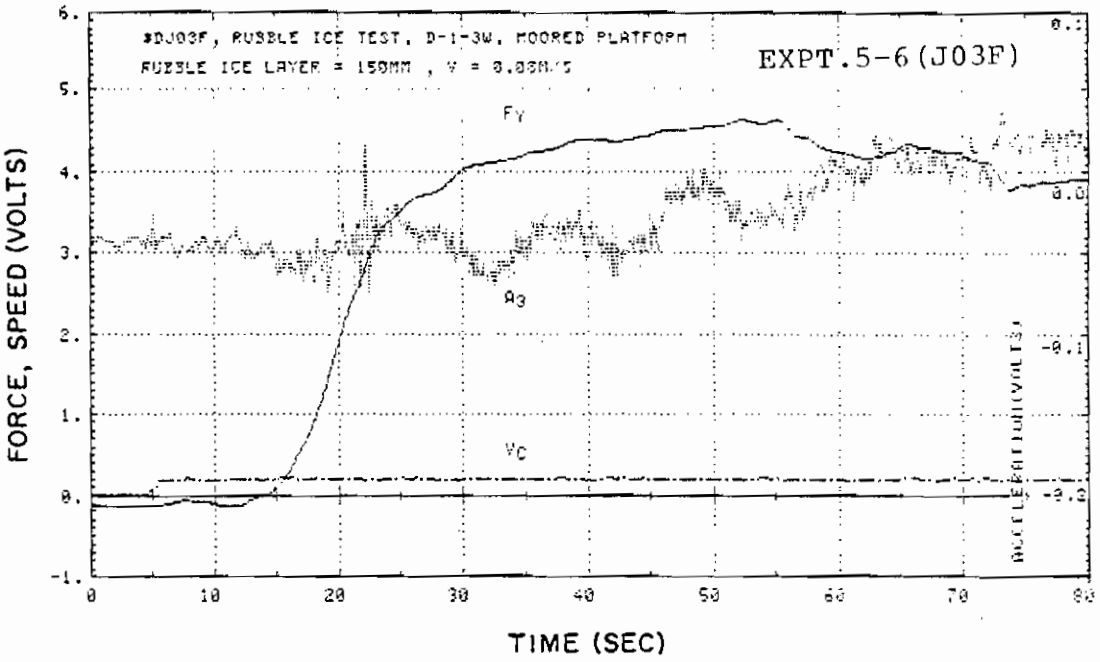

Fig. A-2-5

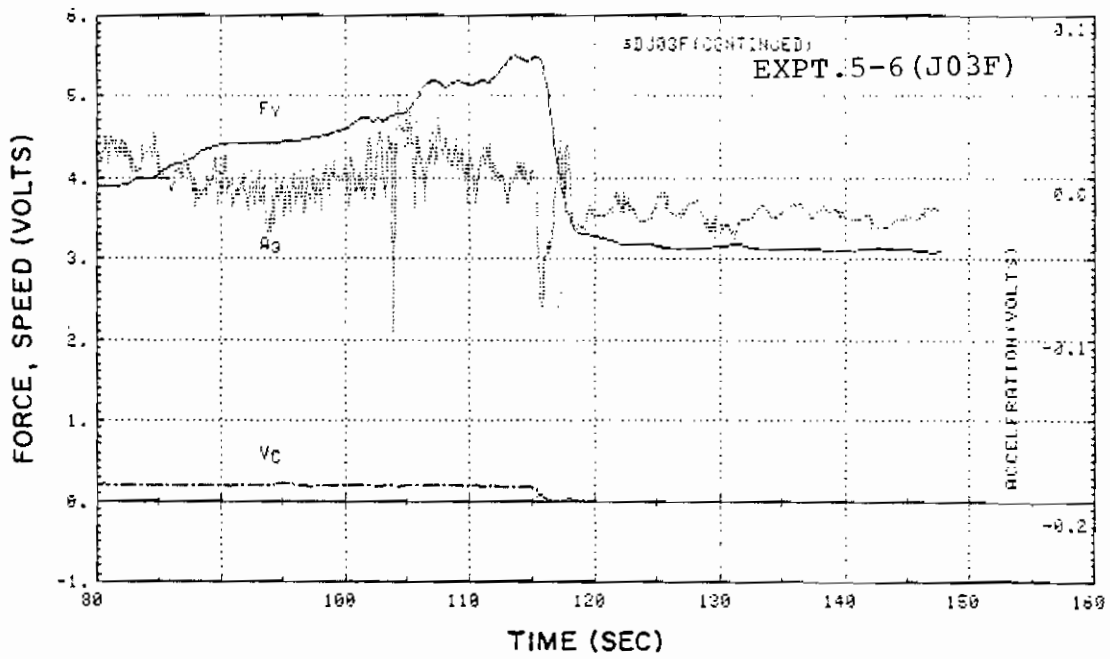

Fig. A-2-6

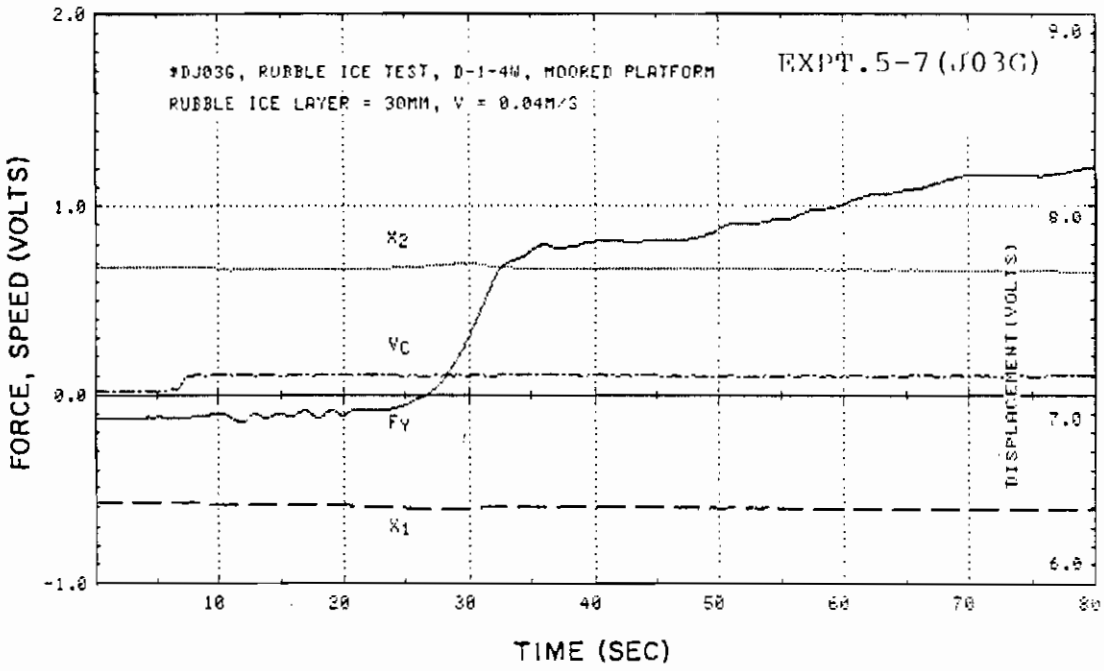

Fig. A-2-7

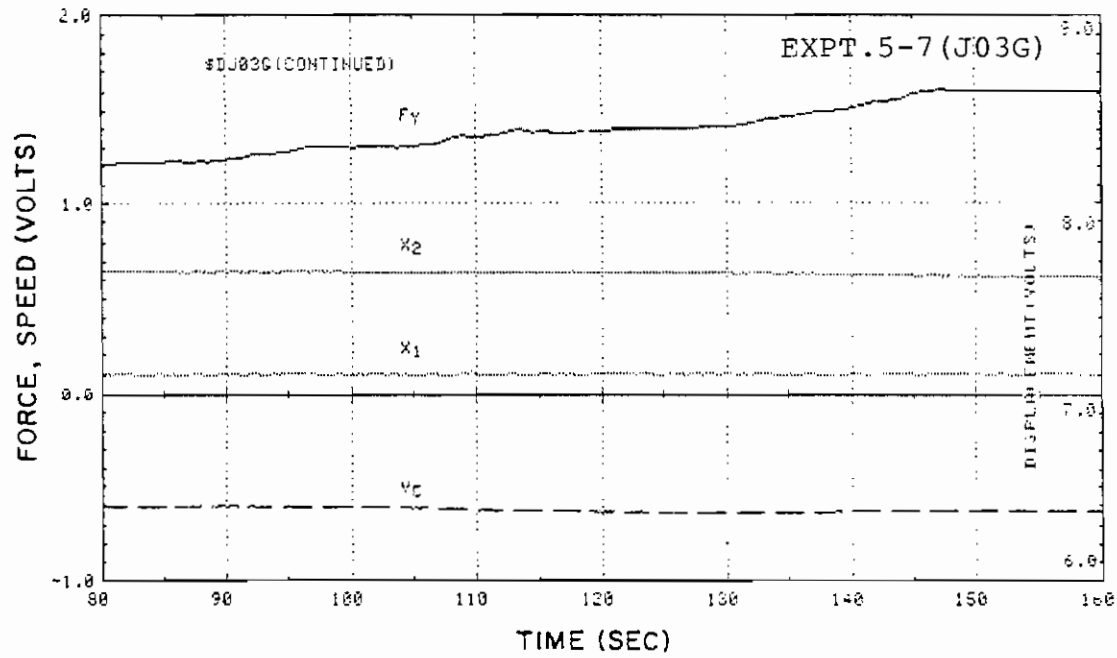

Fig. A-2-8

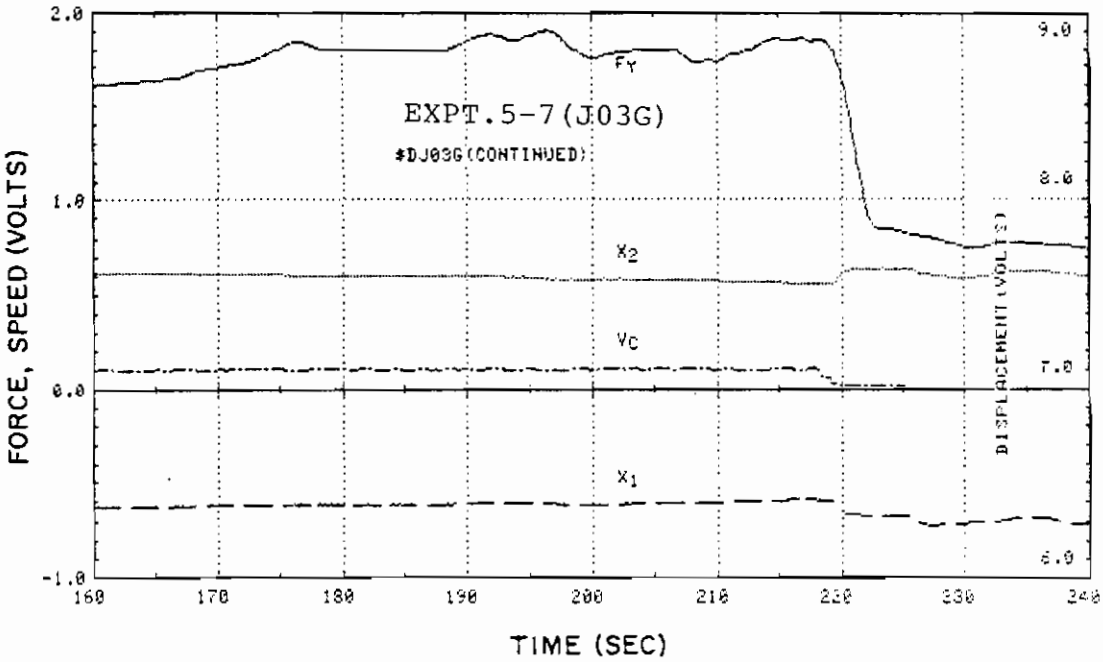

Fig. A-2-9

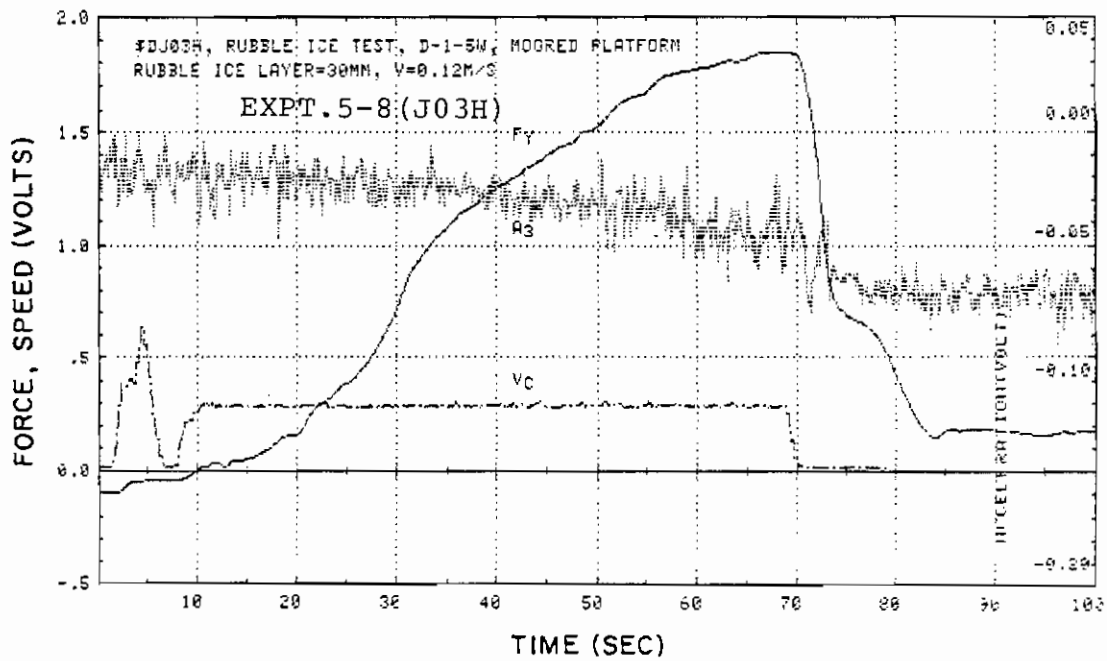

Fig. A-2-10

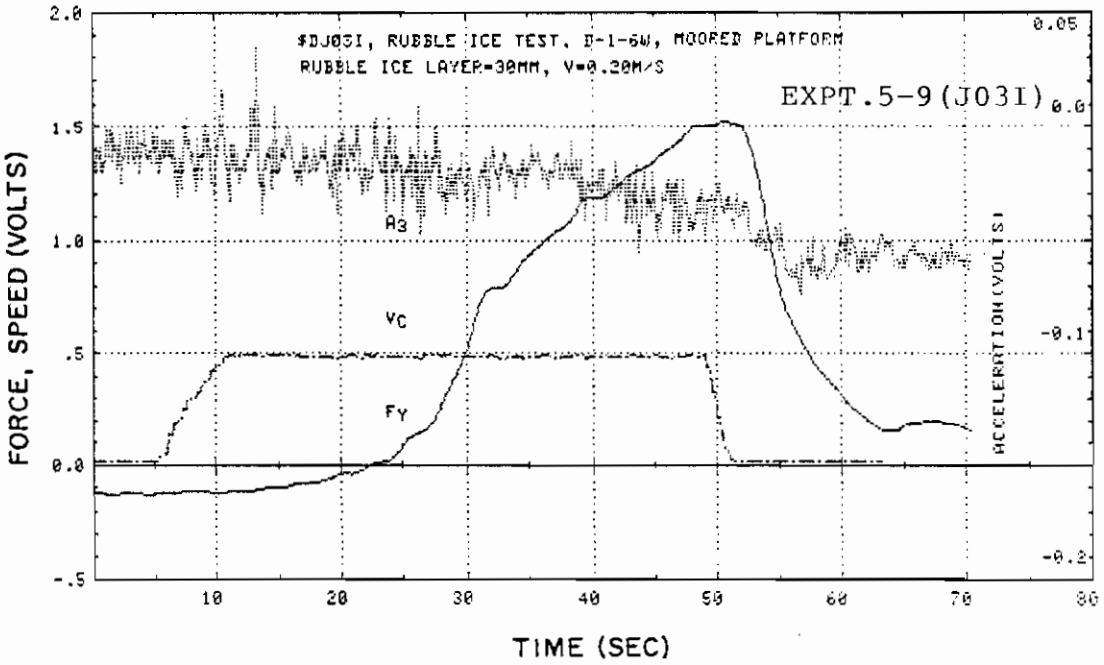
$DJ03I, RUBBLE ICE TEST, D-1-6W, MOORED PLATFORM
RUBBLE ICE LAYER=30MM, V=0.20M/S
EXPT.5-9(J03I)
A3
Vc
Fy
FORCE, SPEED (VOLTS)
ACCELERATION (VOLTS)
TIME (SEC)
2.0
1.5
1.0
.5
0.0
-.5
0.05
0.0
-0.1
-0.2
10
20
30
40
50
60
70
80

Fig. A-2-11

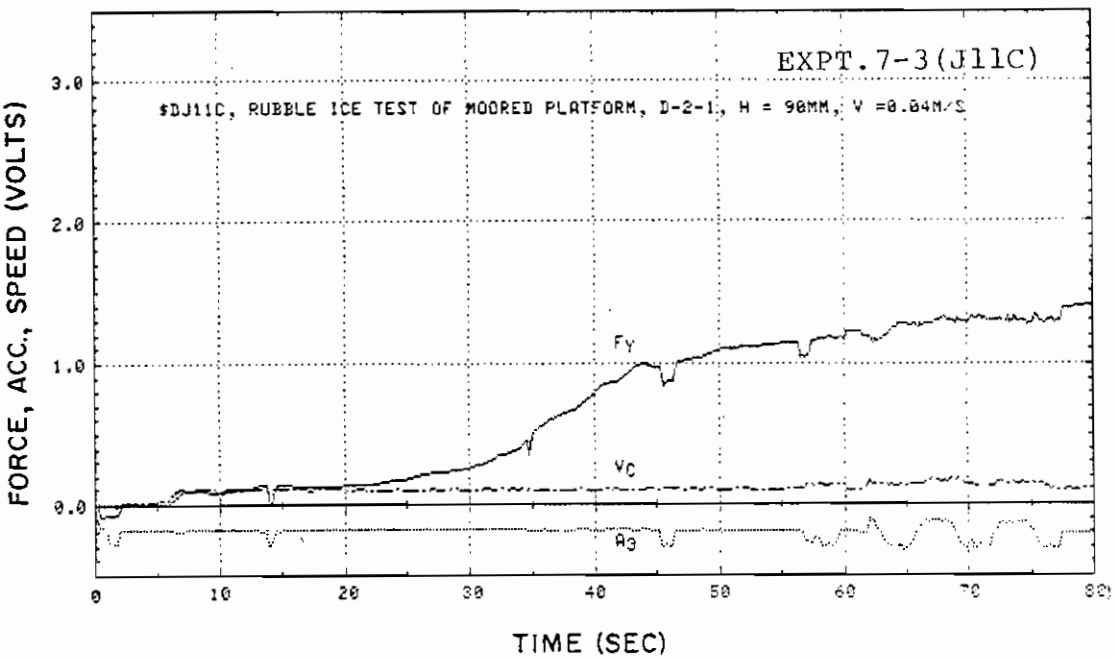

Fig. A-2-12

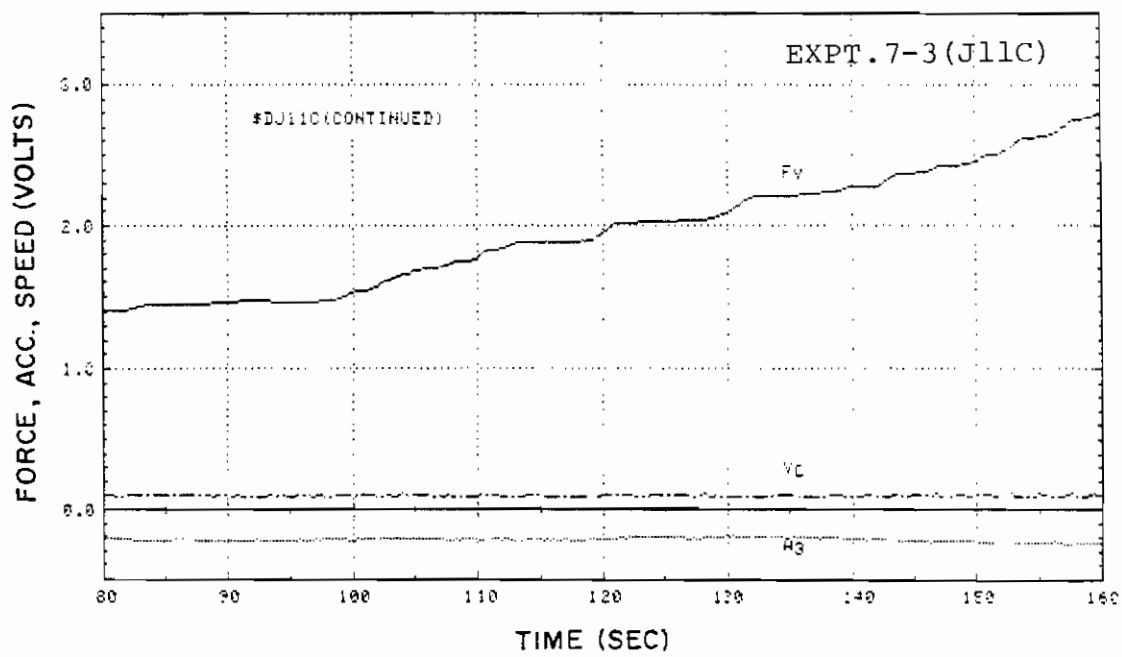

Fig. A-2-13

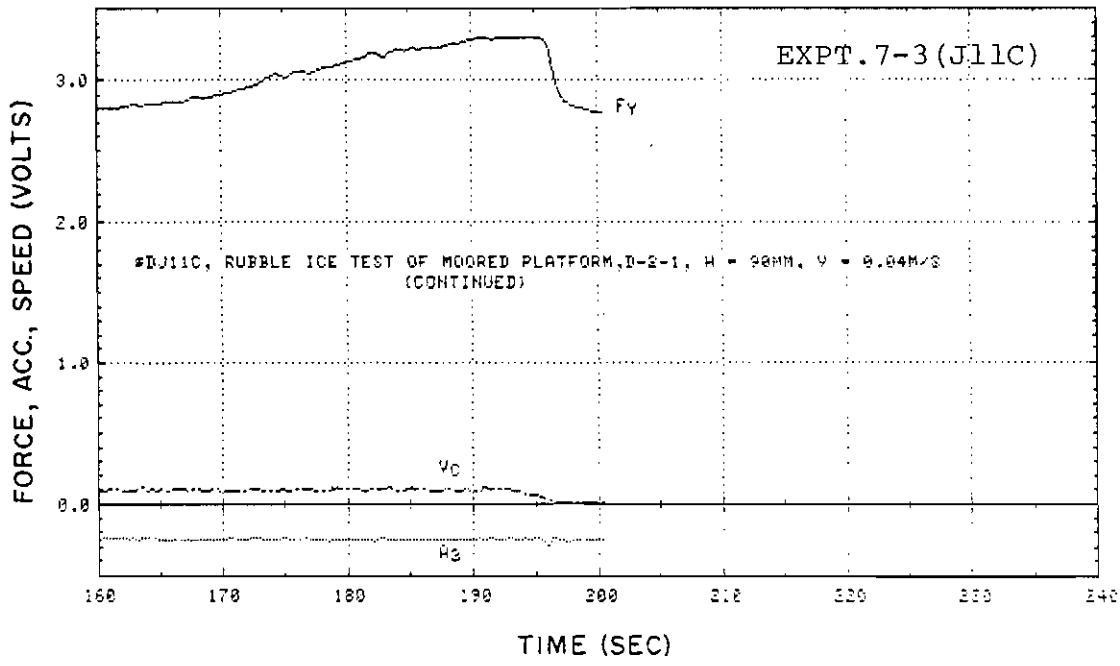
EXPT.7-3(J11C)
FY
#DJ11C, RUBBLE ICE TEST OF MOORED PLATFORM,D-2-1, H = 90MM, V = 0.04M/S
(CONTINUED)
VC
AB
3.0
2.0
1.0
0.0
FORCE, ACC., SPEED (VOLTS)
160
170
180
190
200
210
220
230
240
TIME (SEC)

Fig. A-2-14

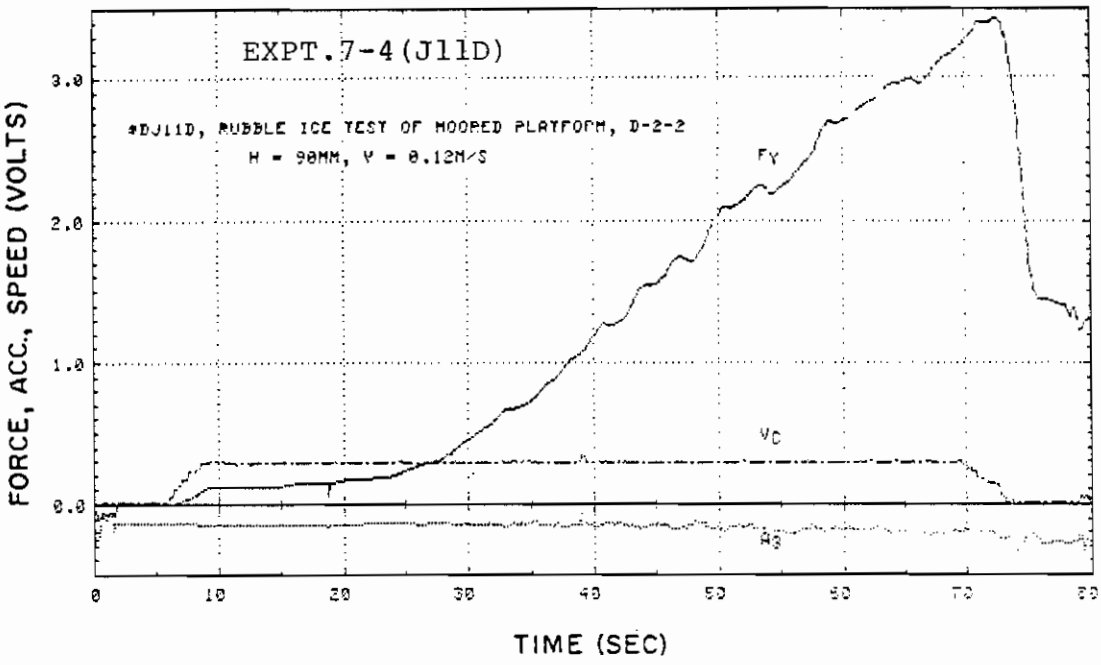

Fig. A-2-15

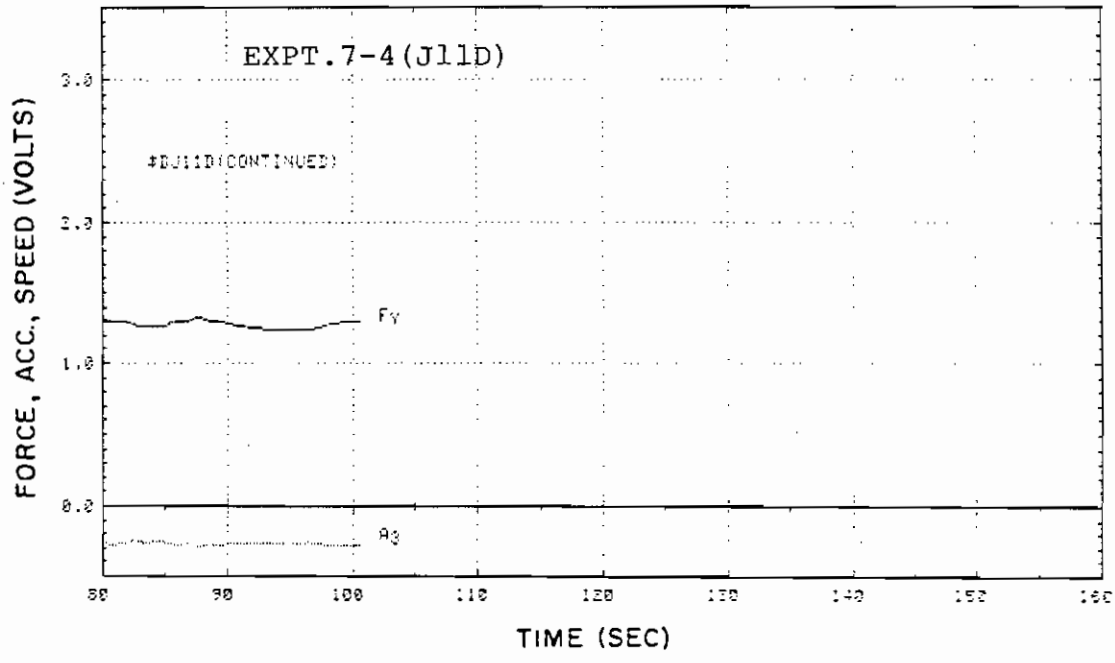

Fig. A-2-16

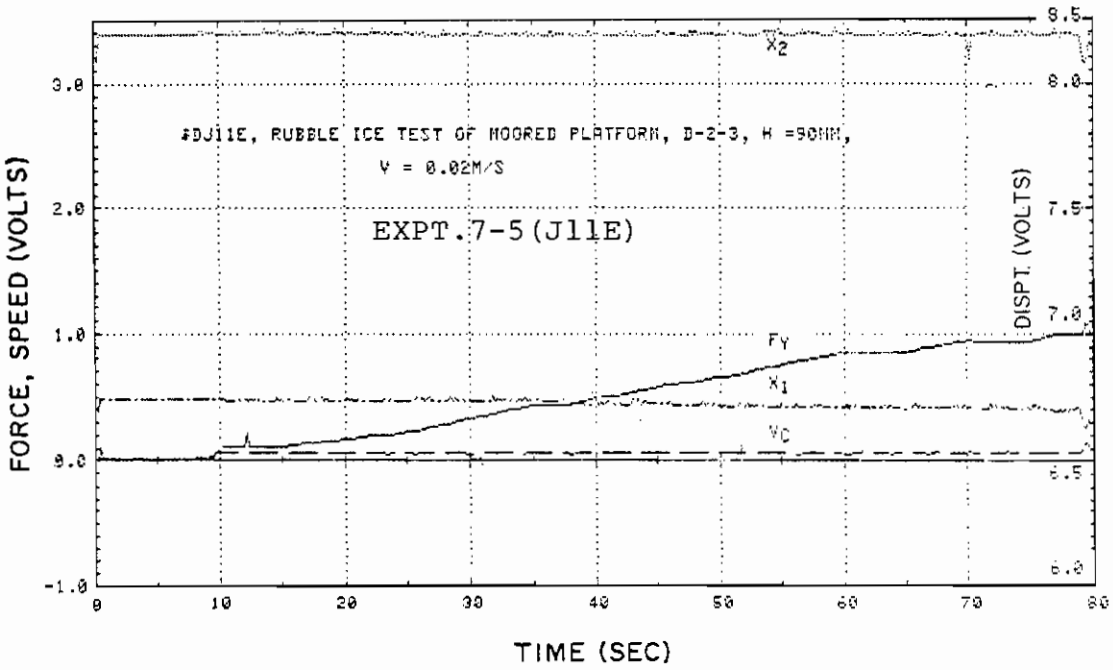

Fig. A-2-17

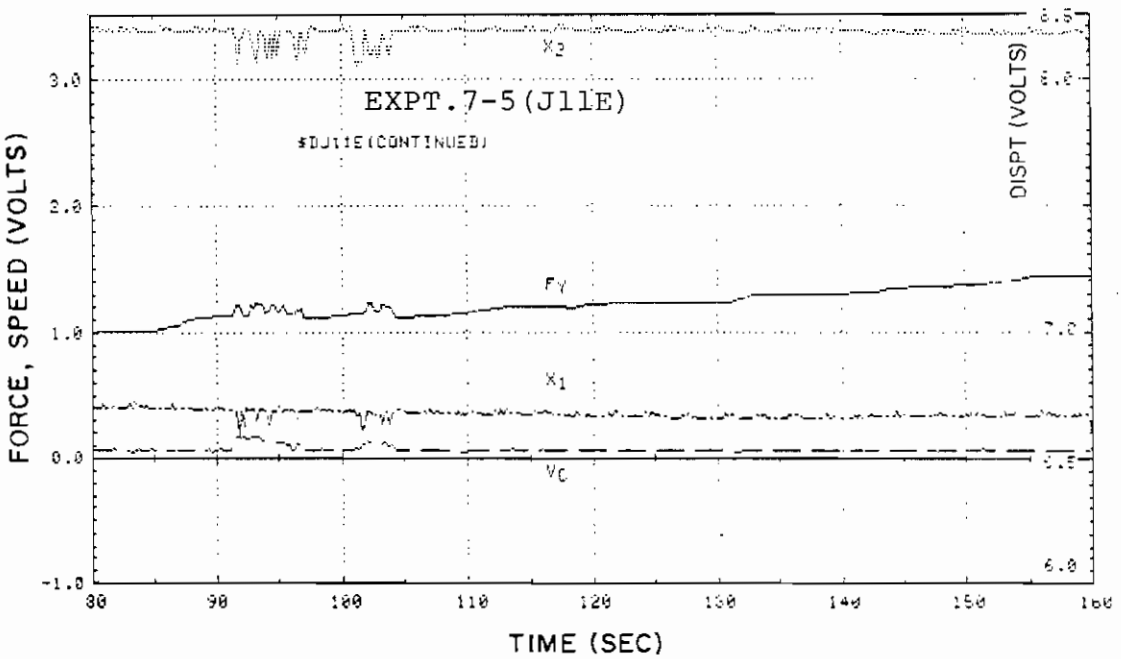

Fig. A-2-18

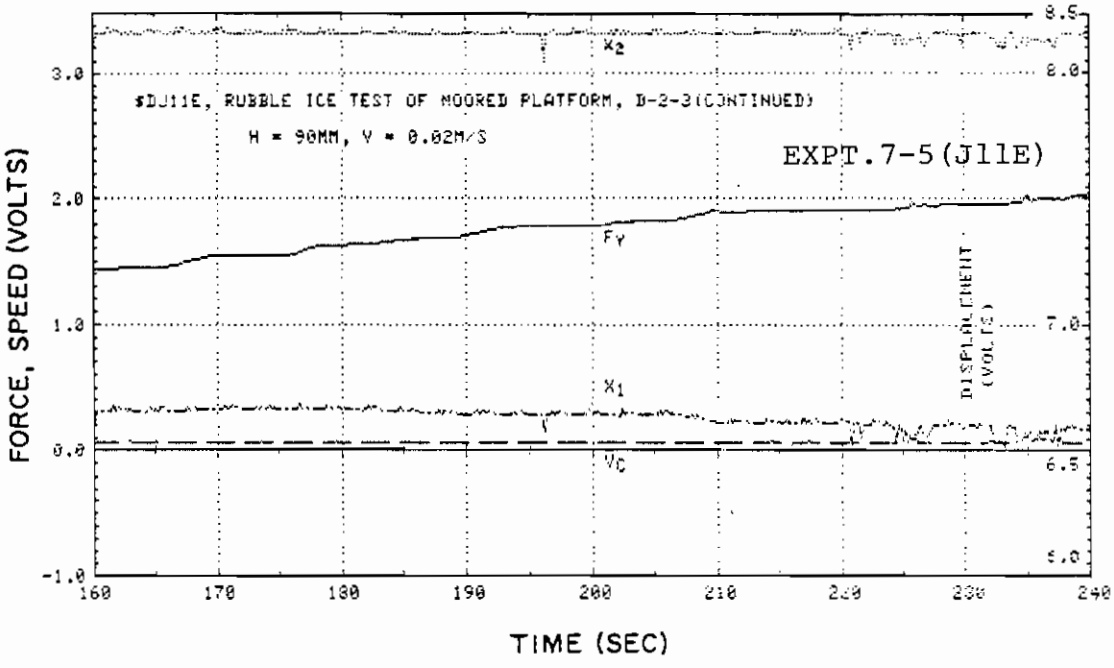
$DJ11E, RUBBLE ICE TEST OF MOORED PLATFORM, B-2-3(CONTINUED)
H = 90MM, V = 0.02M/S
EXPT.7-5(J11E)
X2
Fy
X1
Vc
FORCE, SPEED (VOLTS)
TIME (SEC)
DISPLACEMENT (VOLTS)
3.0
2.0
1.0
0.0
-1.0
8.5
8.0
7.0
6.5
6.0
160
170
180
190
200
210
220
230
240

Fig. A-2-19

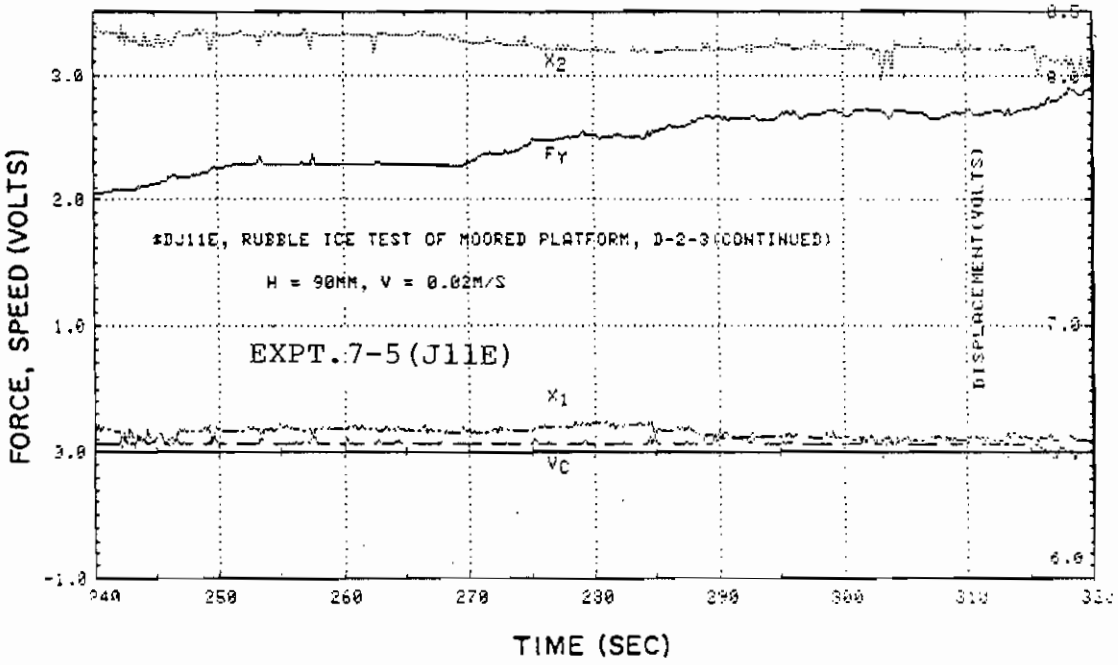

Fig. A-2-20

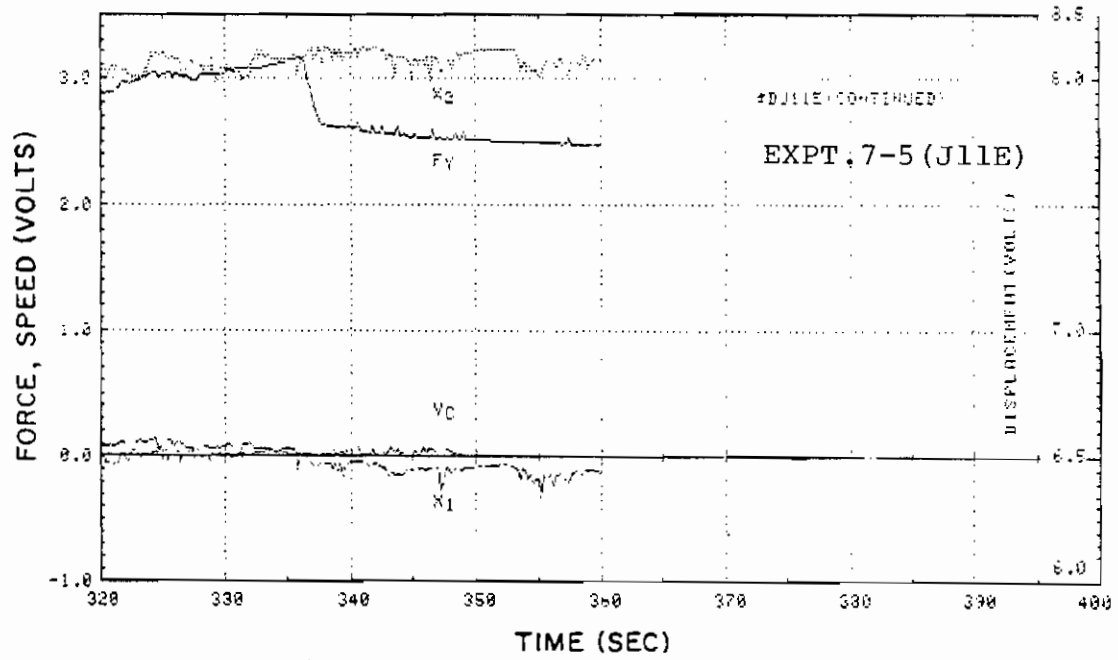

Fig. A-2-21

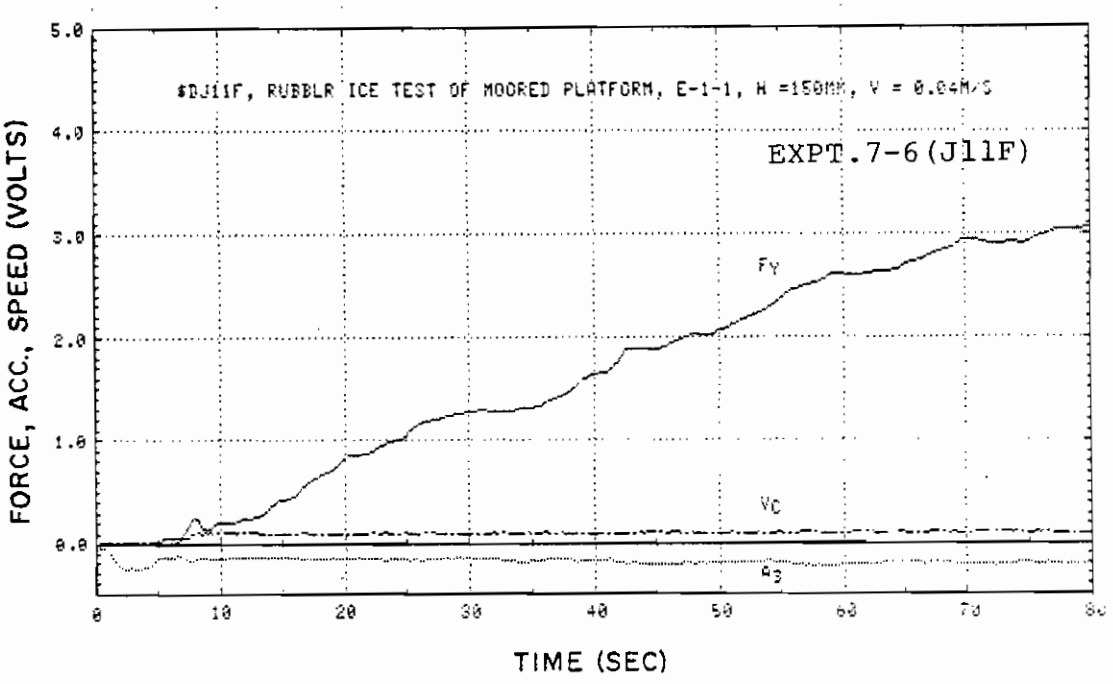

Fig. A-2-22

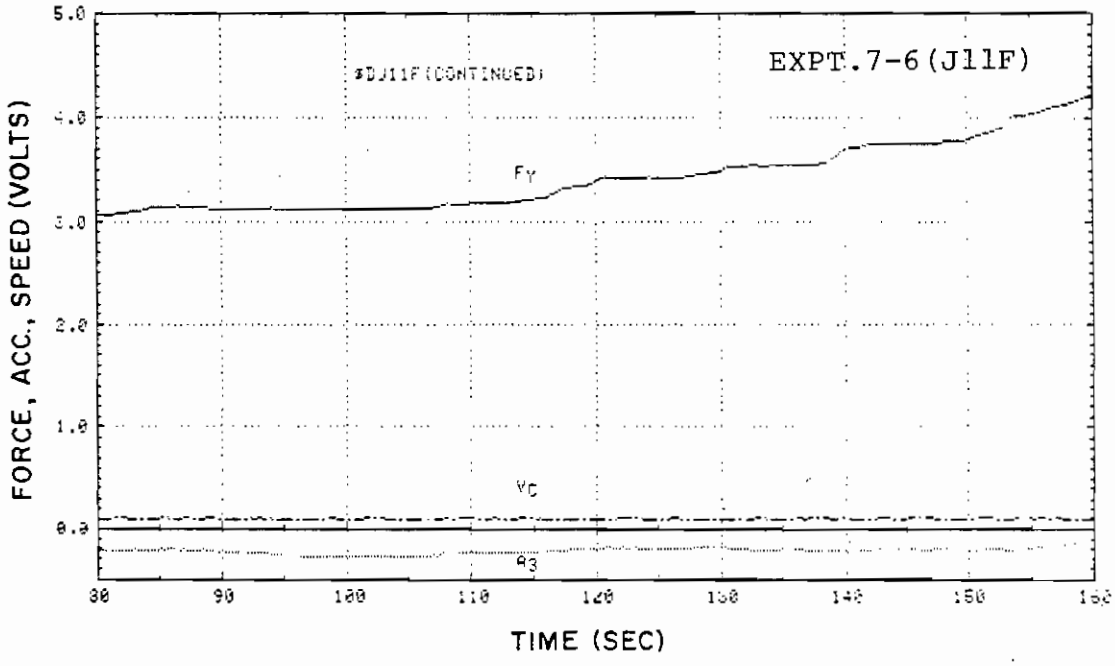

Fig. A-2-23

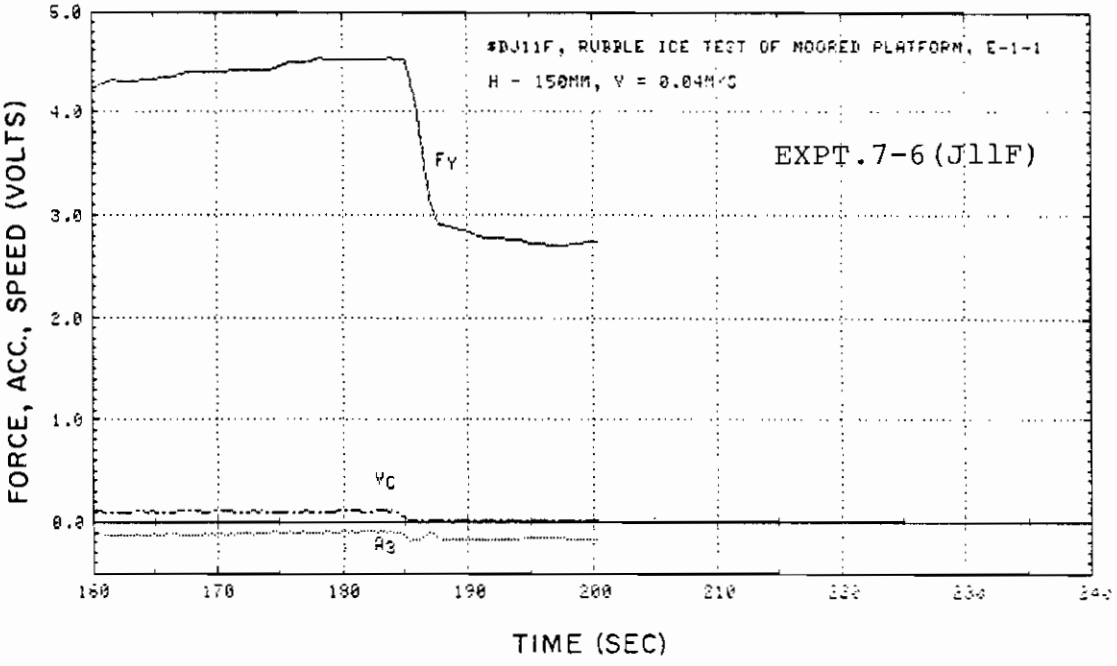

Fig. A-2-24

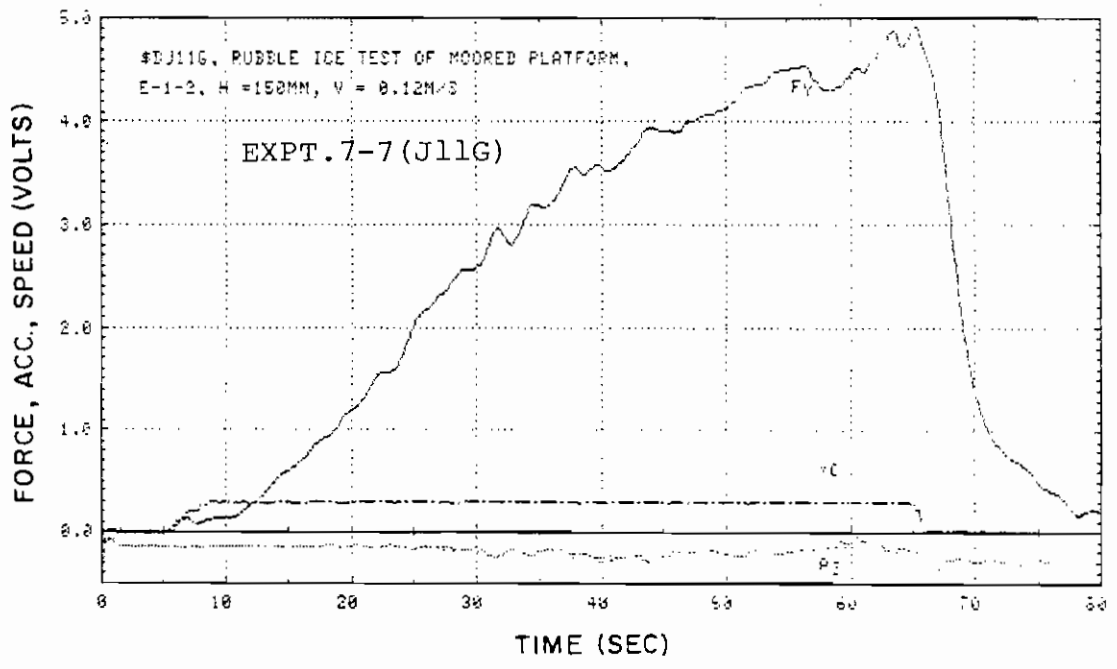

Fig. A-2-25

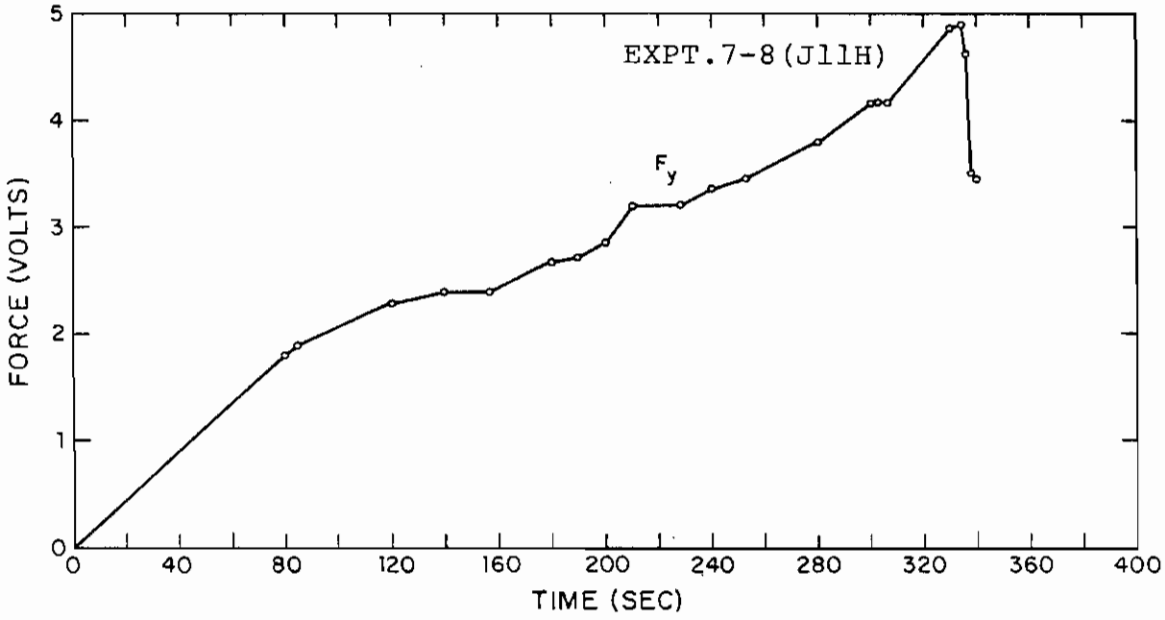
EXPT.7-8(J11H)
F_y
FORCE (VOLTS)
TIME (SEC)
0
1
2
3
4
5
0
40
80
120
160
200
240
280
320
360
400

Fig. A-2-26

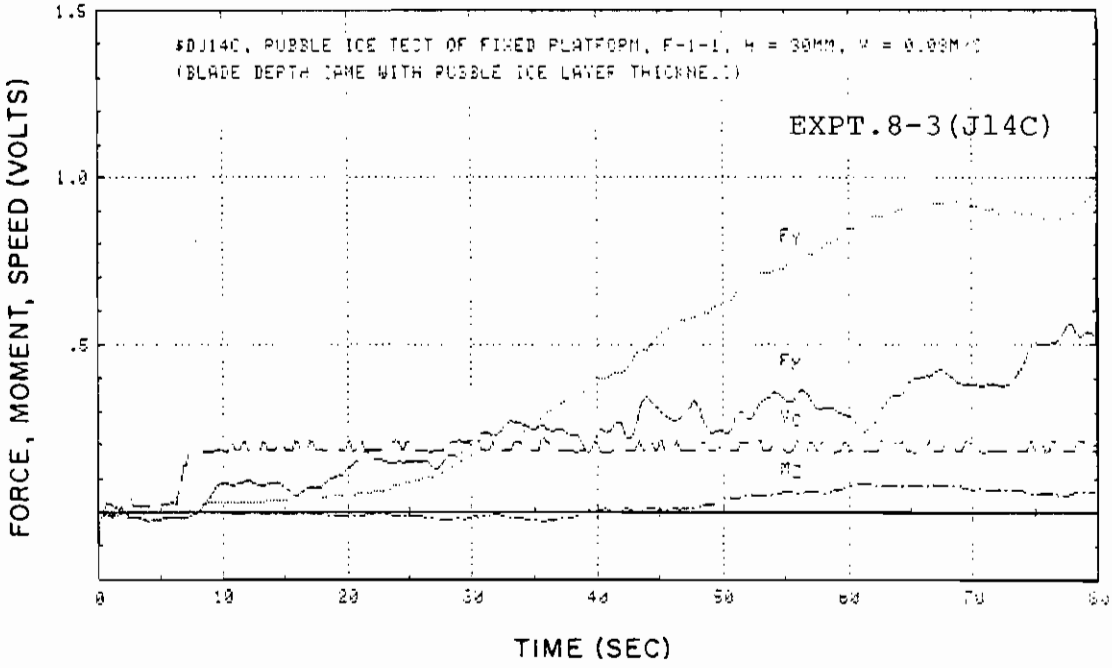

Fig. A-2-27

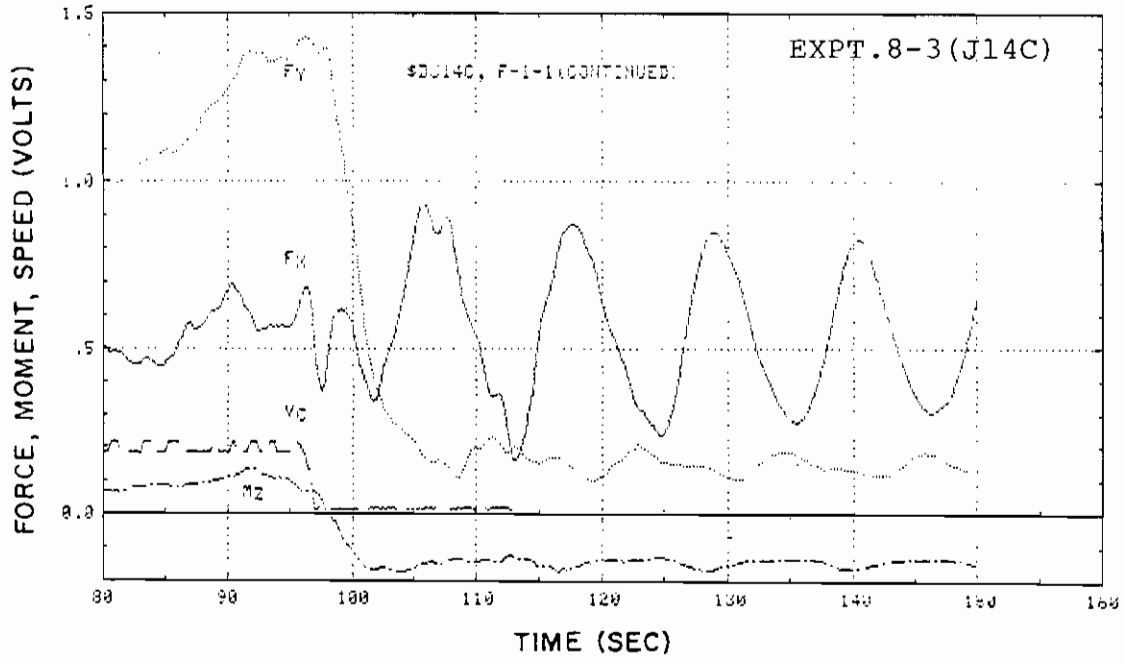

Fig. A-2-28

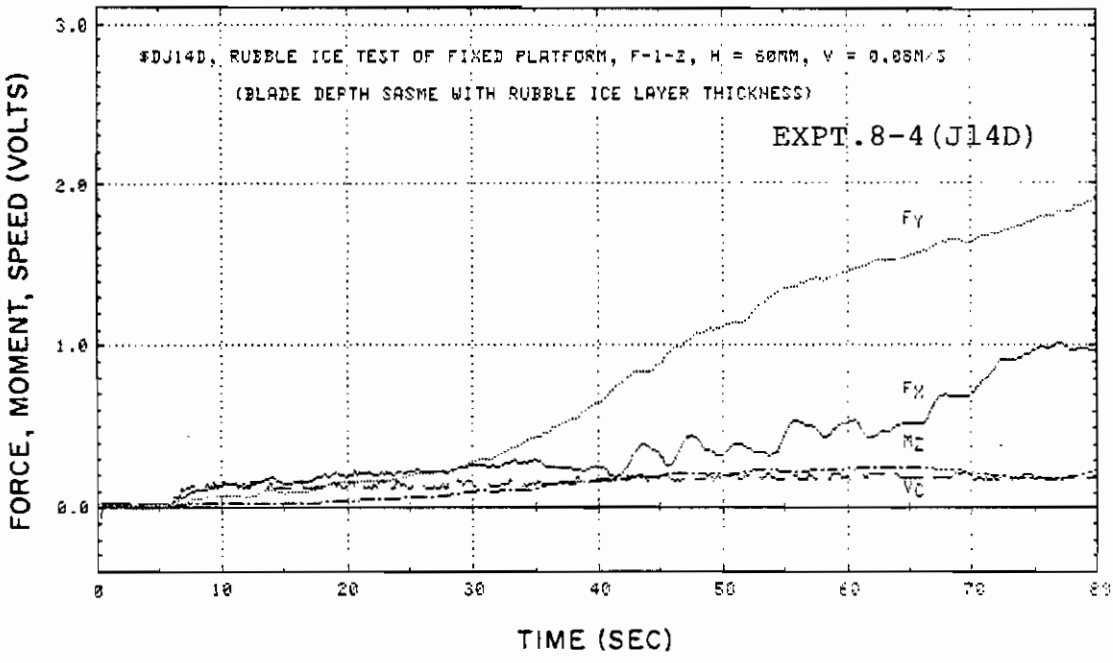

Fig. A-2-29

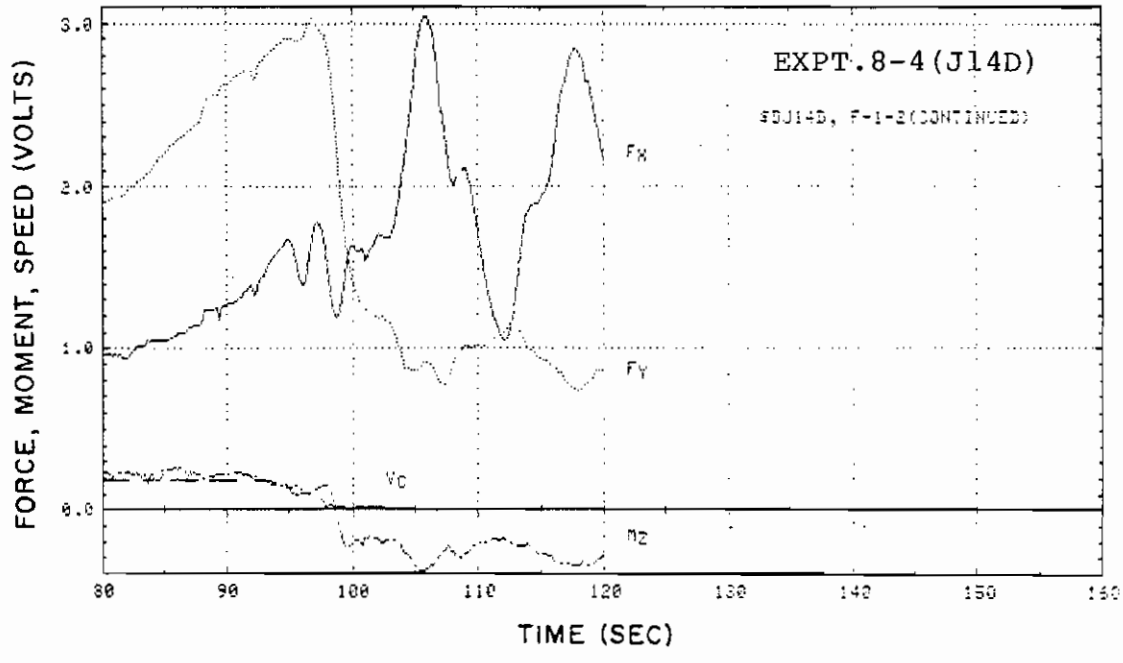

Fig. A-2-30

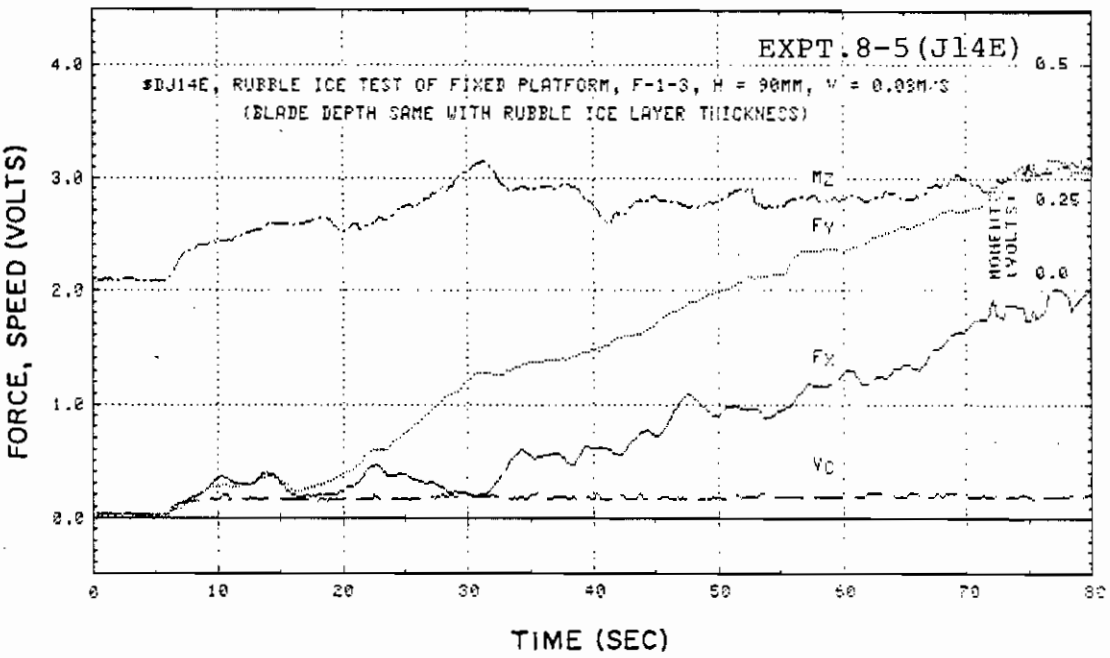

Fig. A-2-31

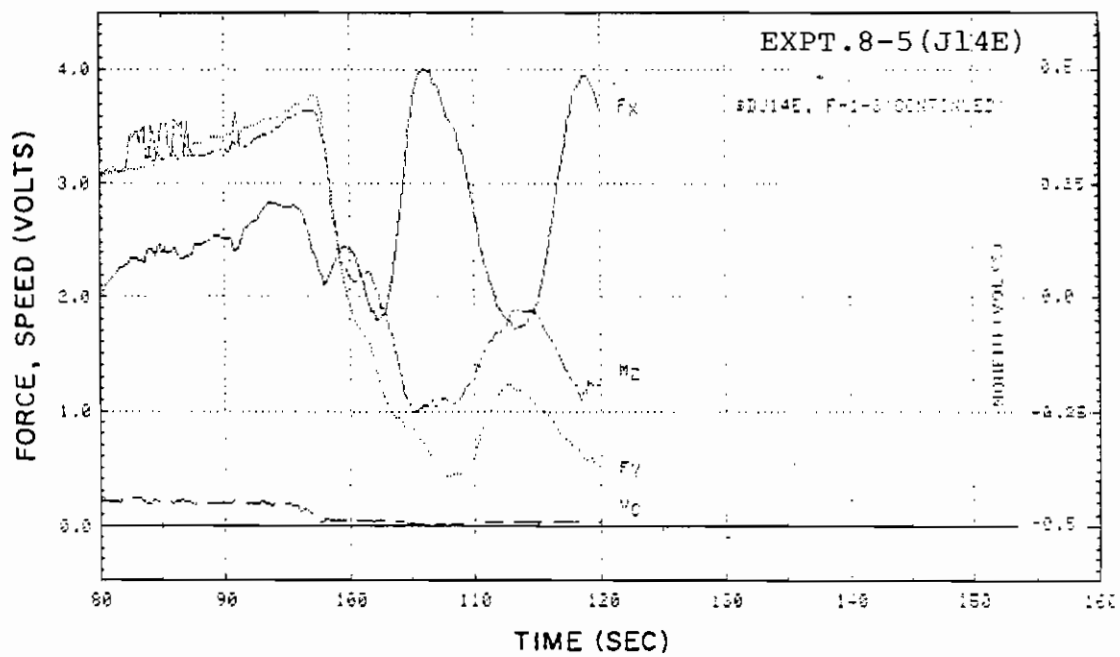

Fig. A-2-32

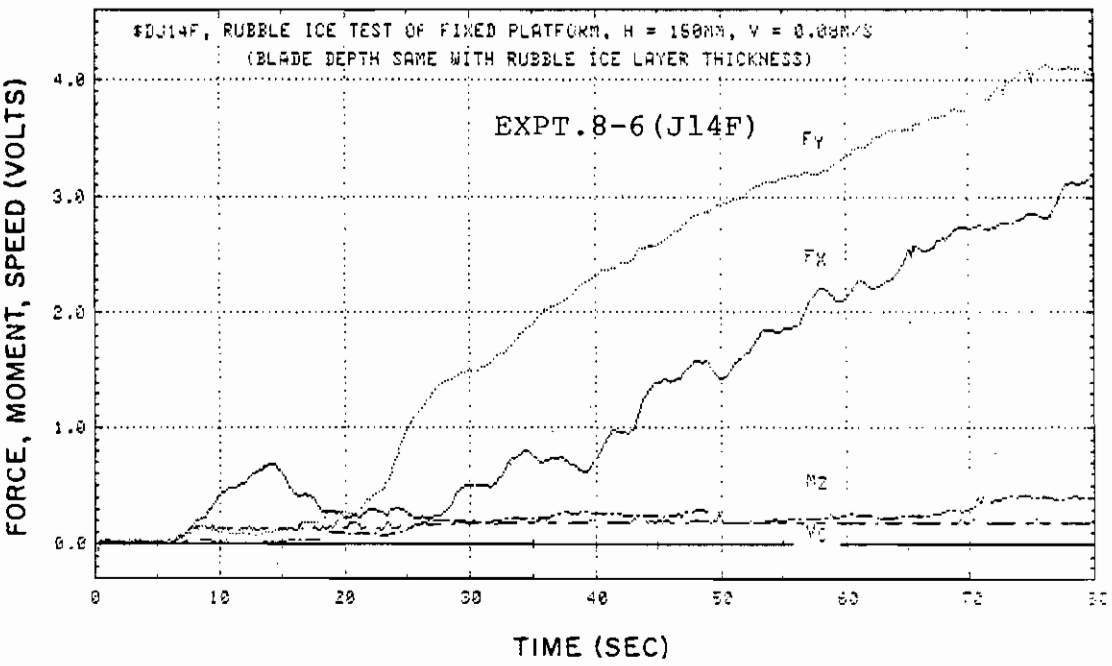

Fig. A-2-33

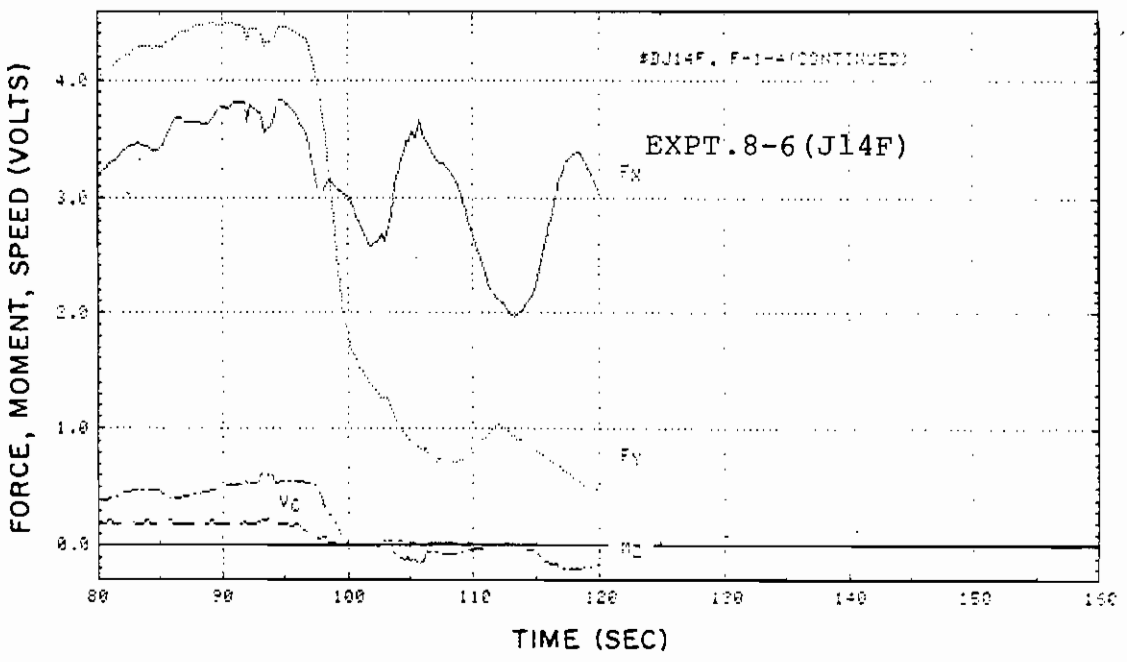

Fig. A-2-34

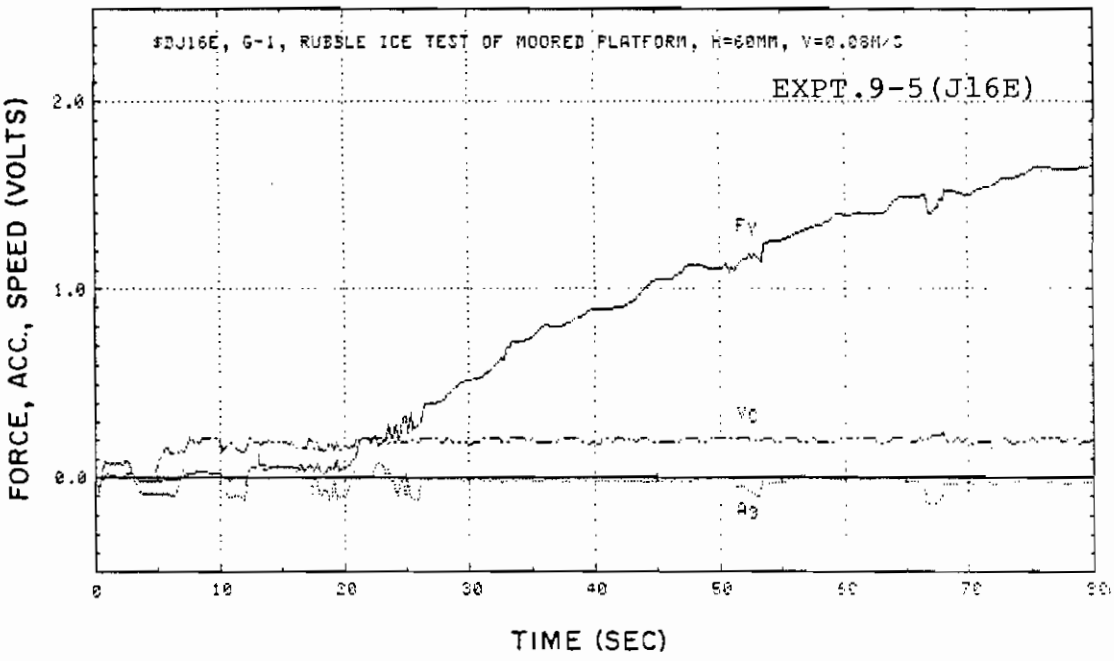

Fig. A-2-35

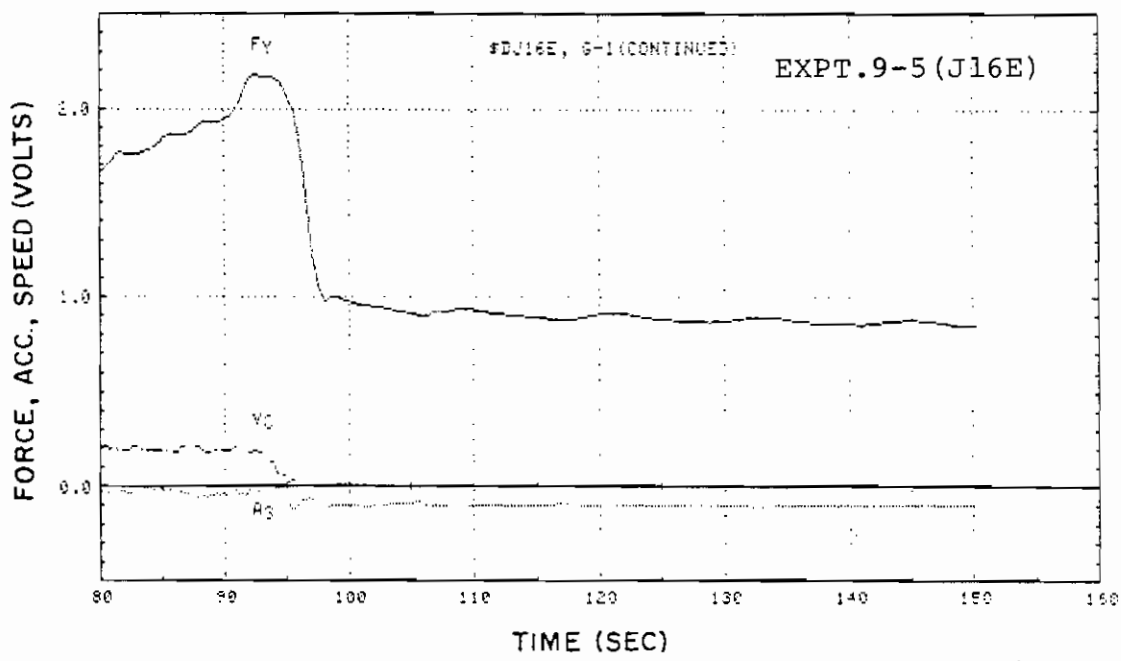

Fig. A-2-36

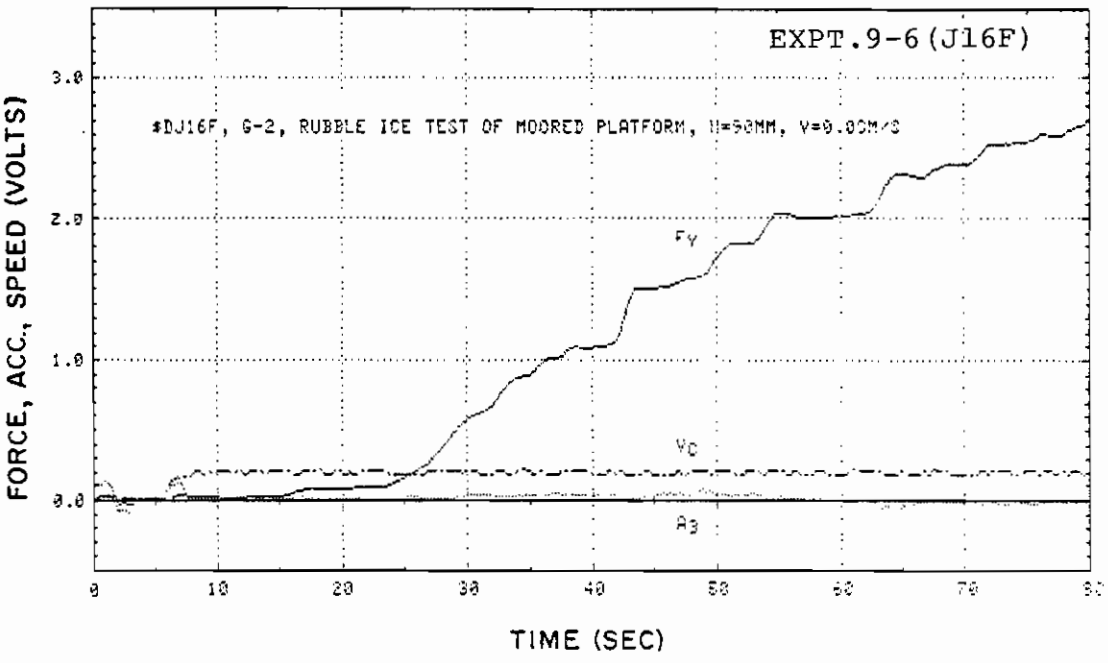

Fig. A-2-37

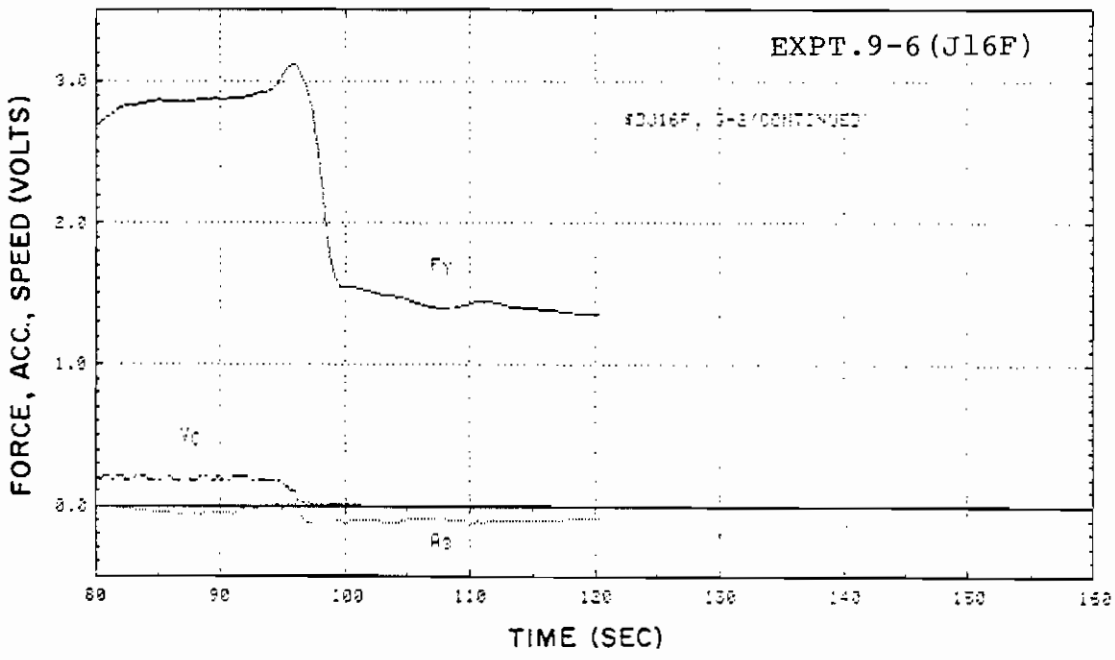

Fig. A-2-38

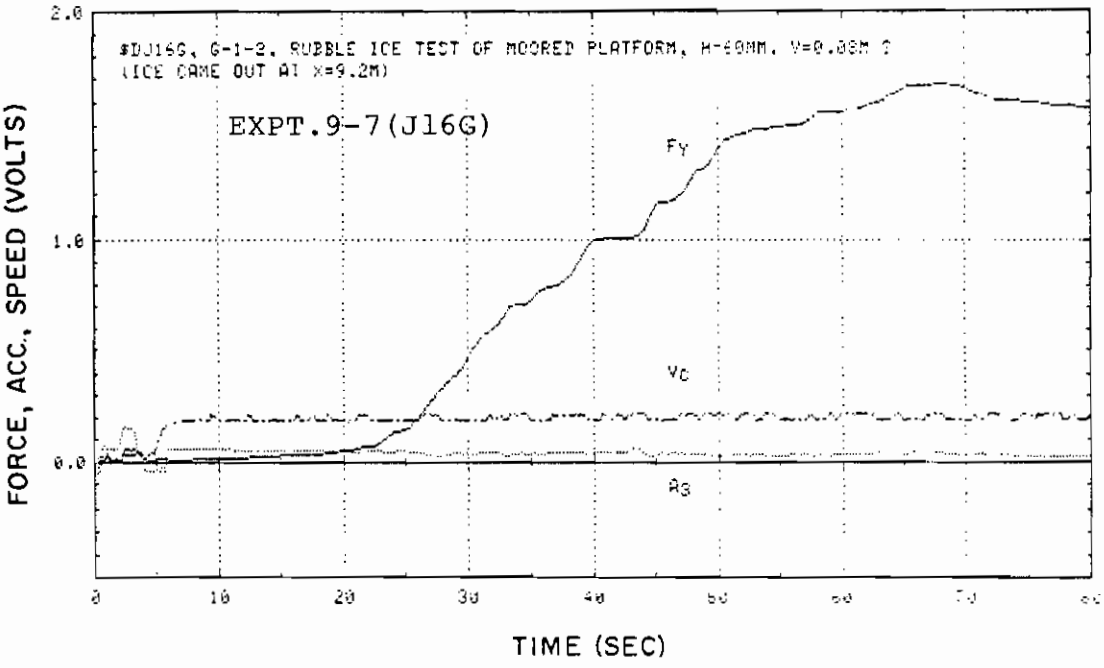

Fig. A-2-39

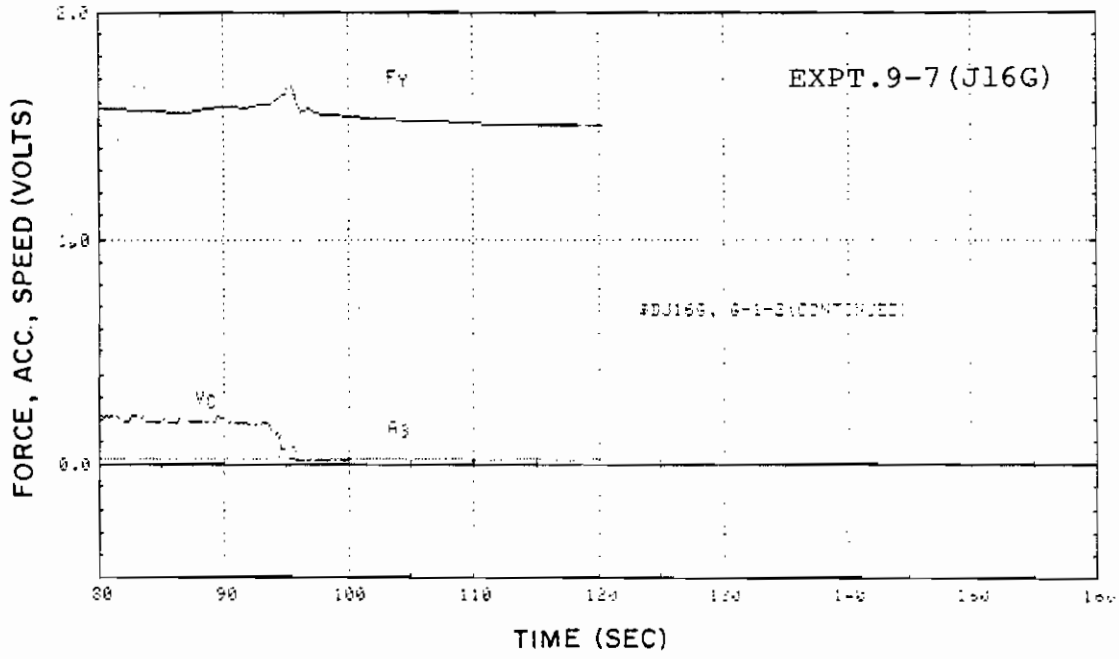

Fig. A-2-40

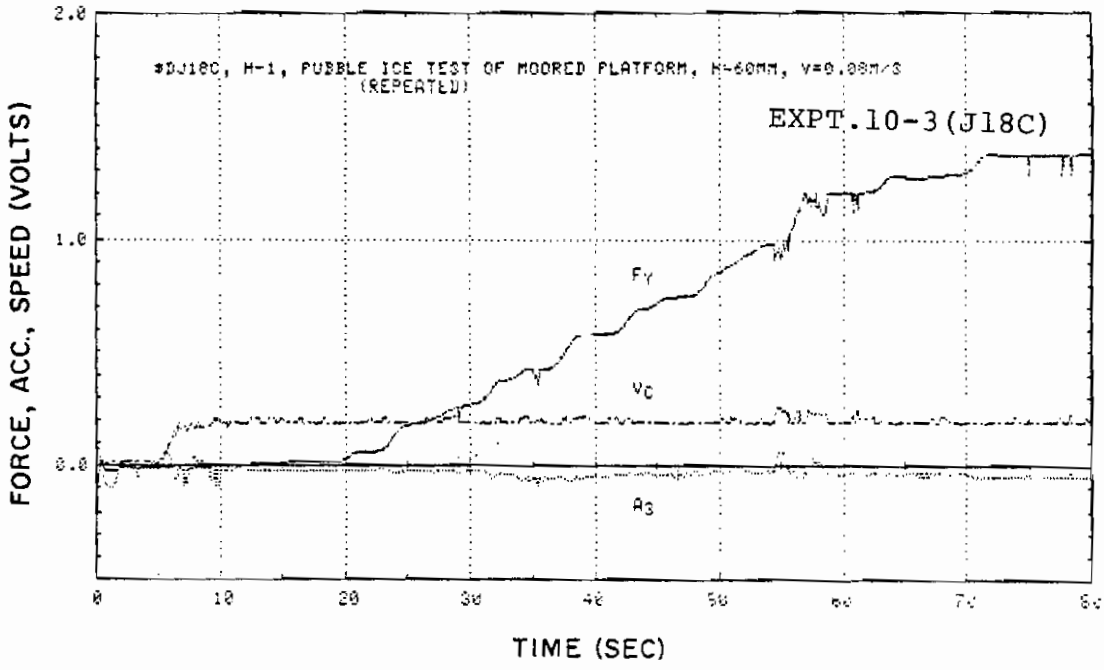

Fig. A-2-41

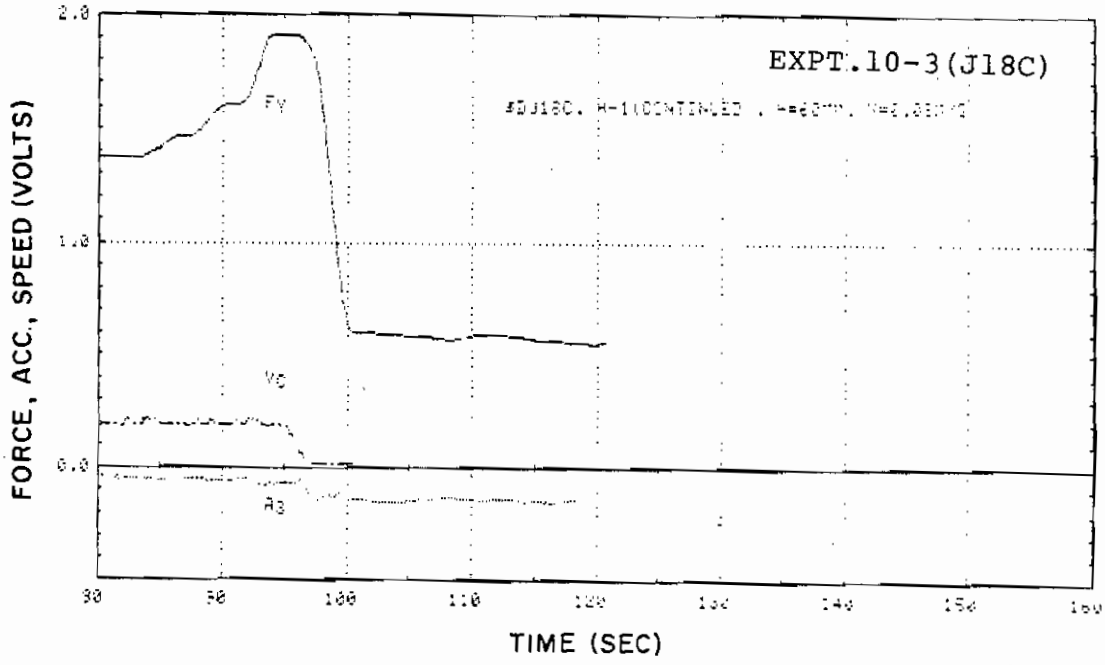

Fig. A-2-42

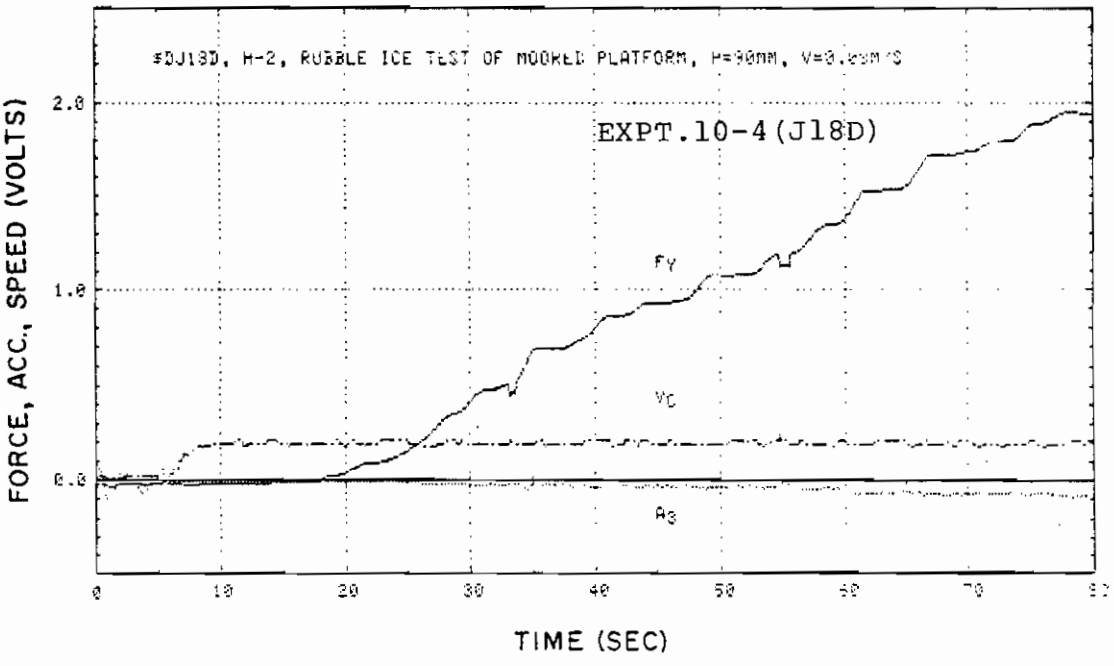

Fig. A_2-43

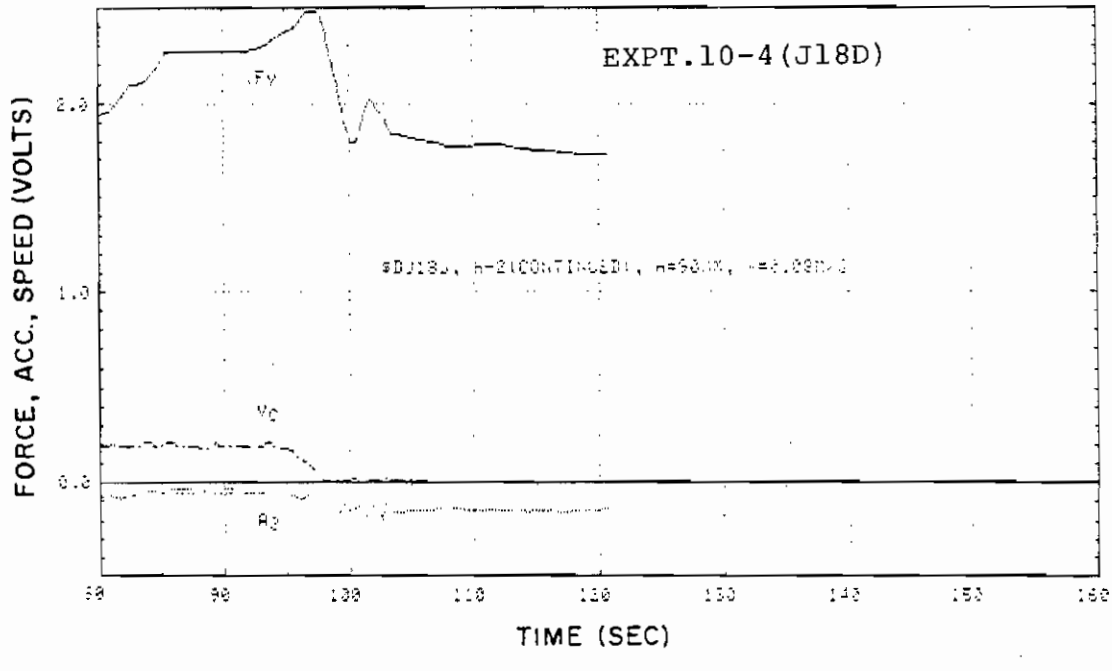

Fig. A-2-44

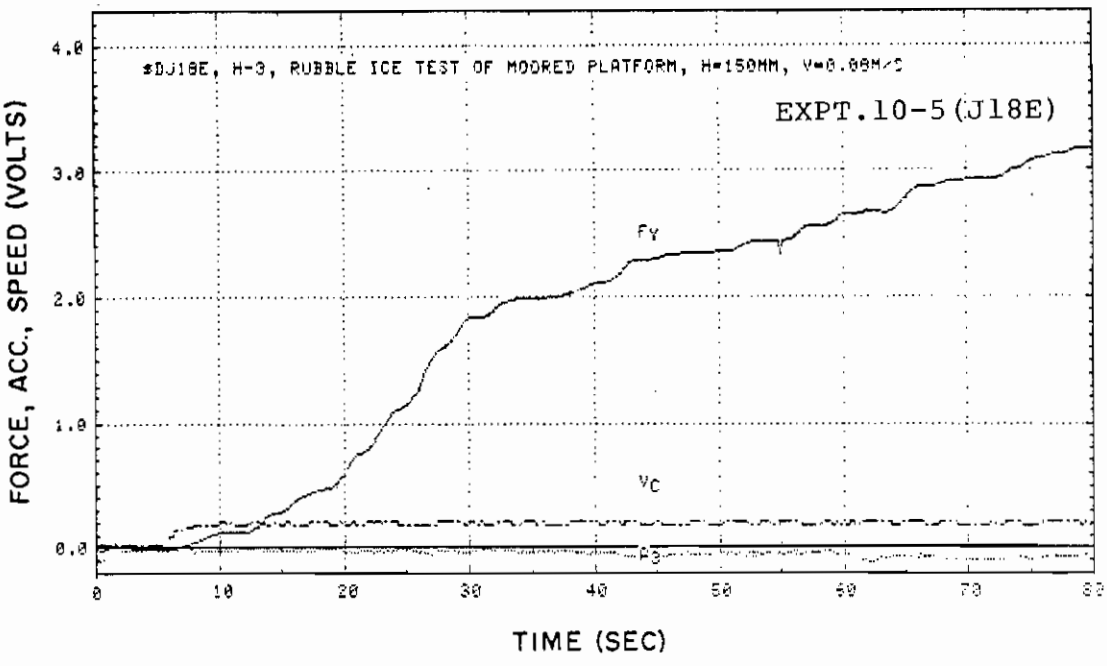

Fig. A-2-45

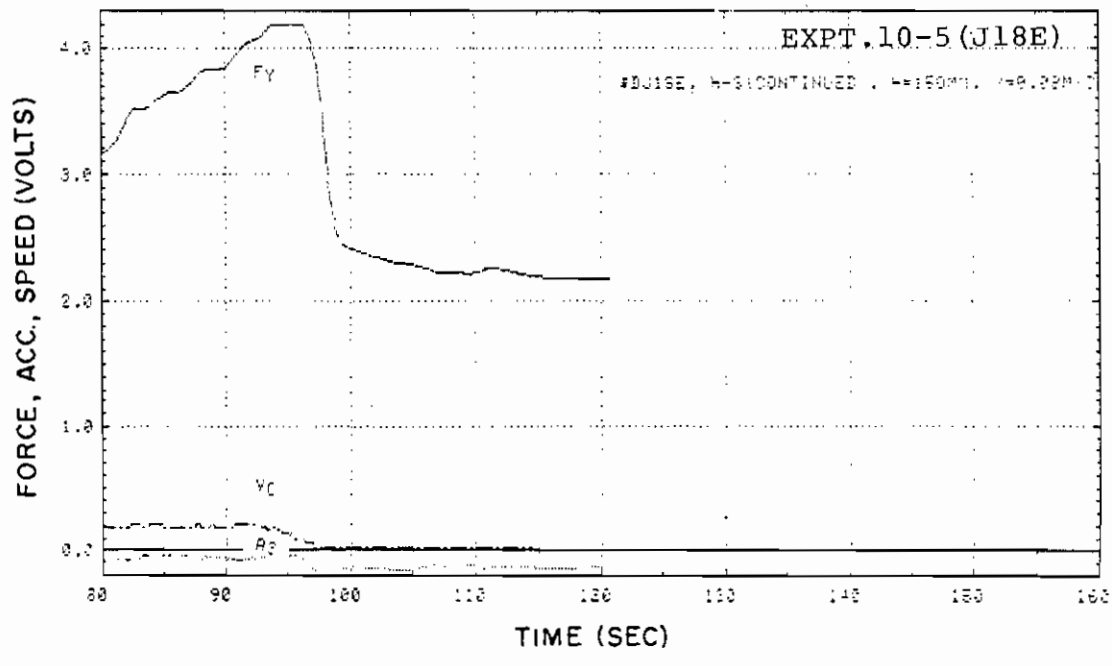

Fig. A-2-46

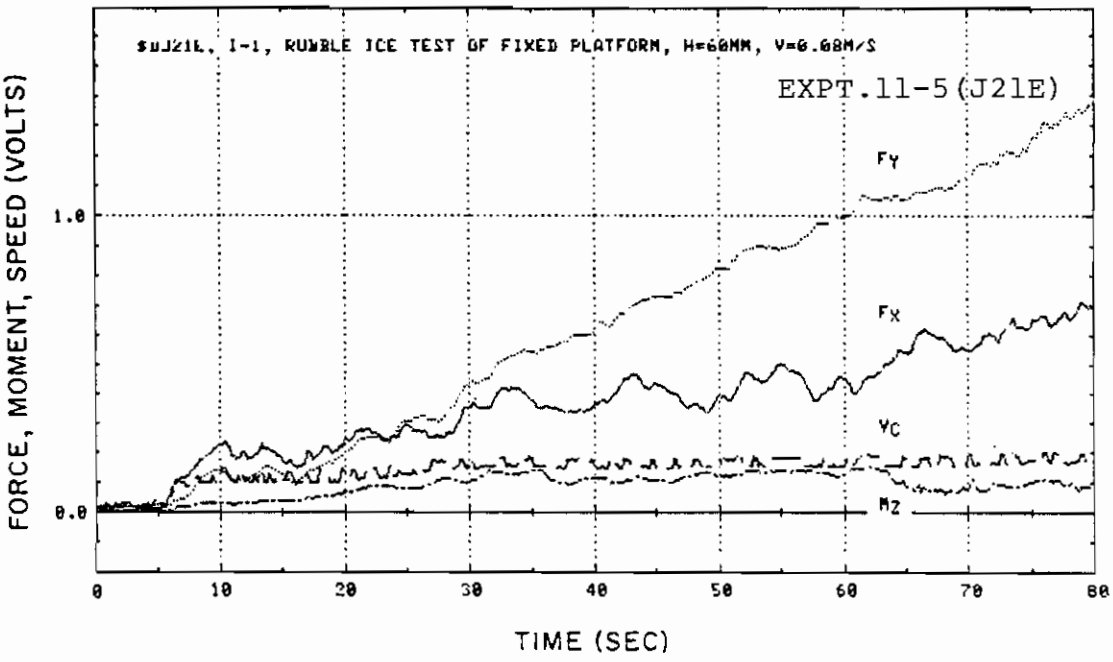

Fig. A-2-47

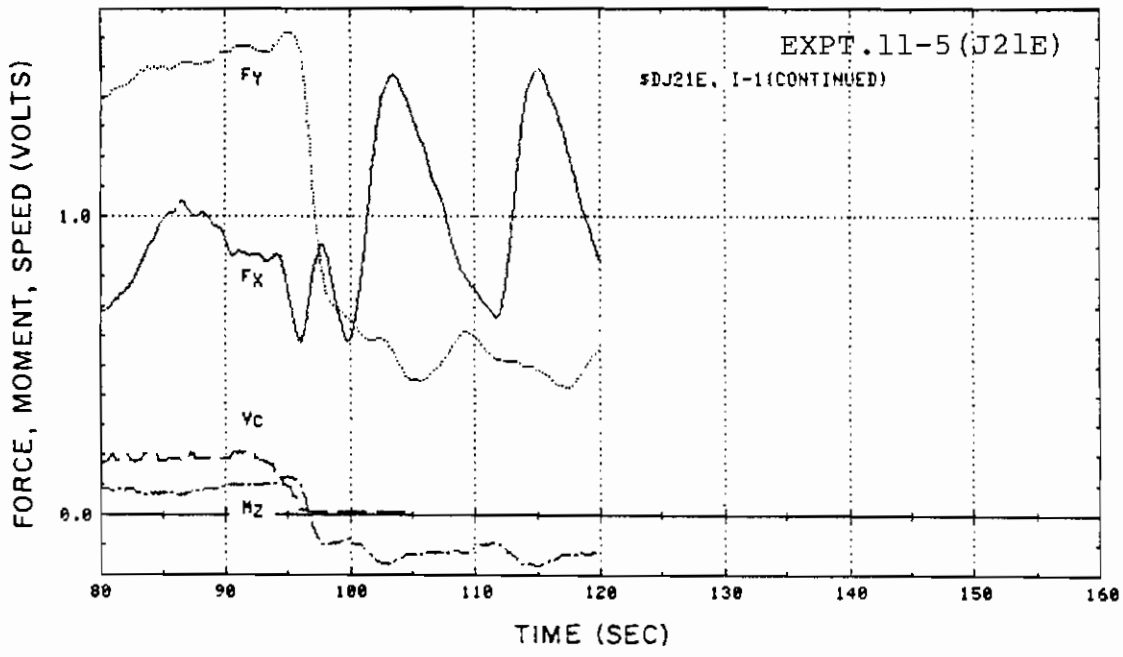

Fig. A-2-48

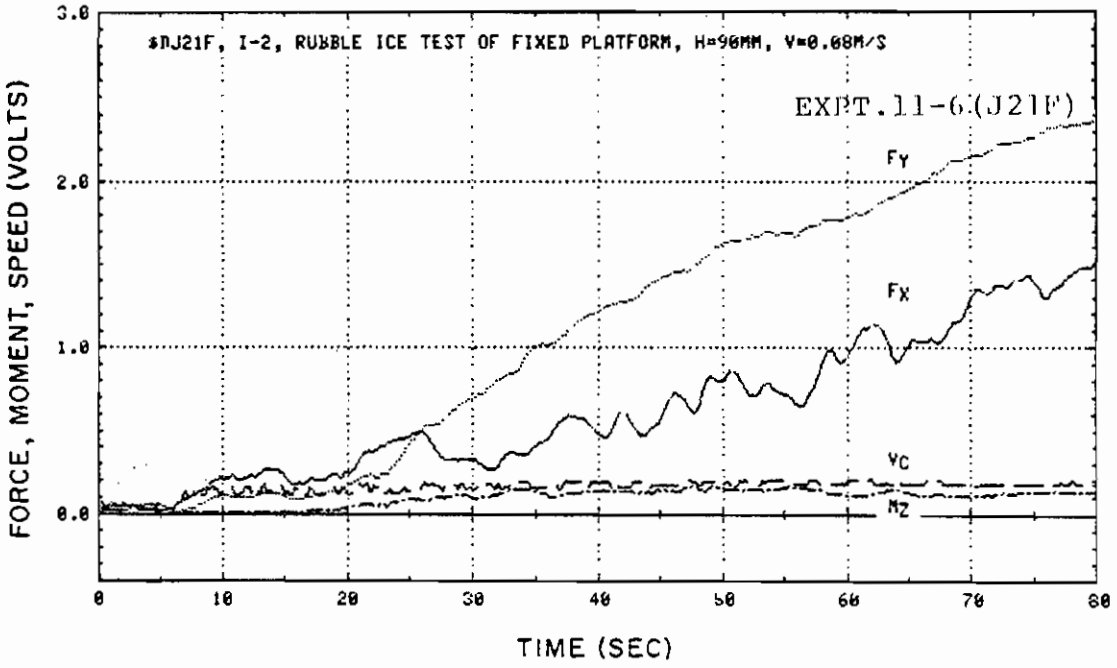

Fig. A-2-49

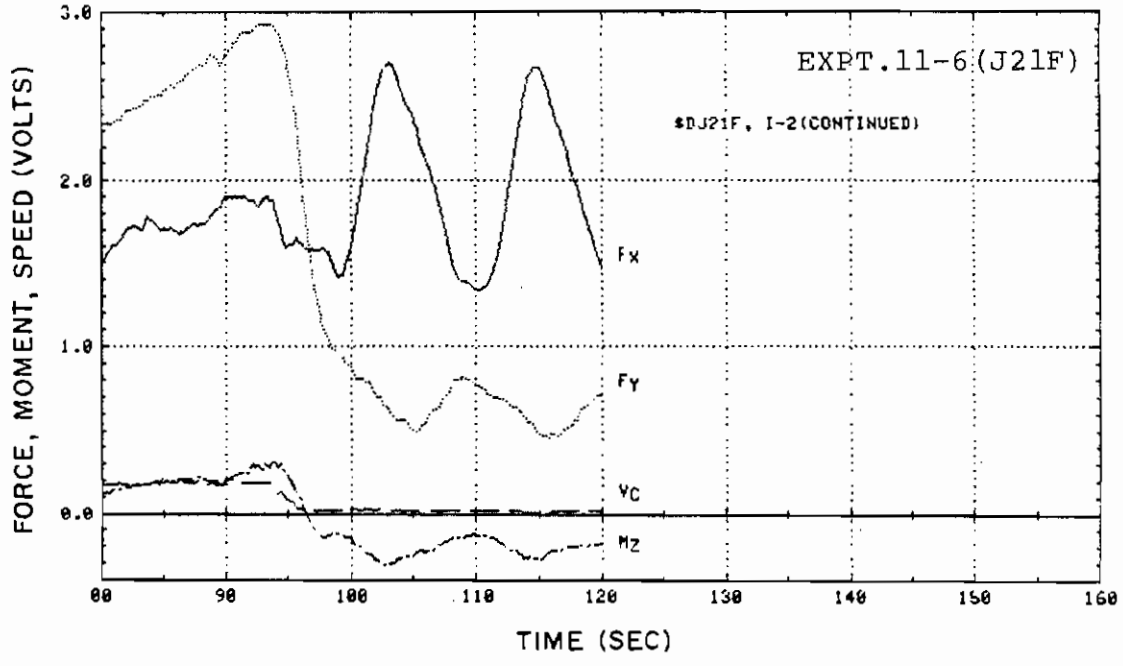

Fig. A-2-50

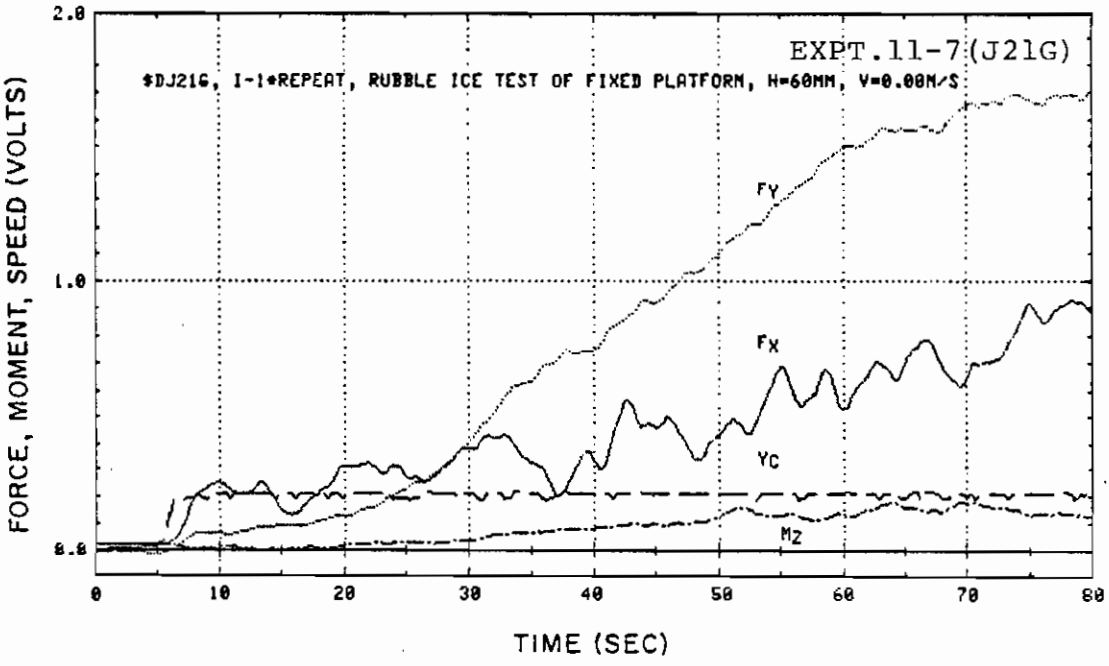

Fig. A-2-51

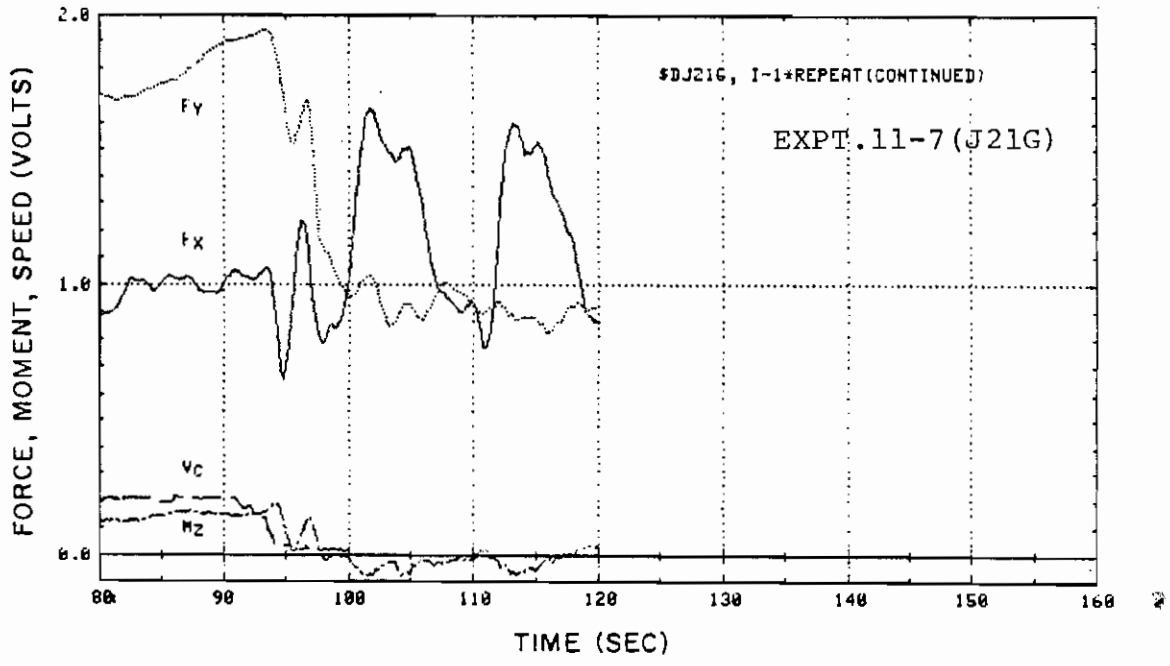

Fig. A-2-52

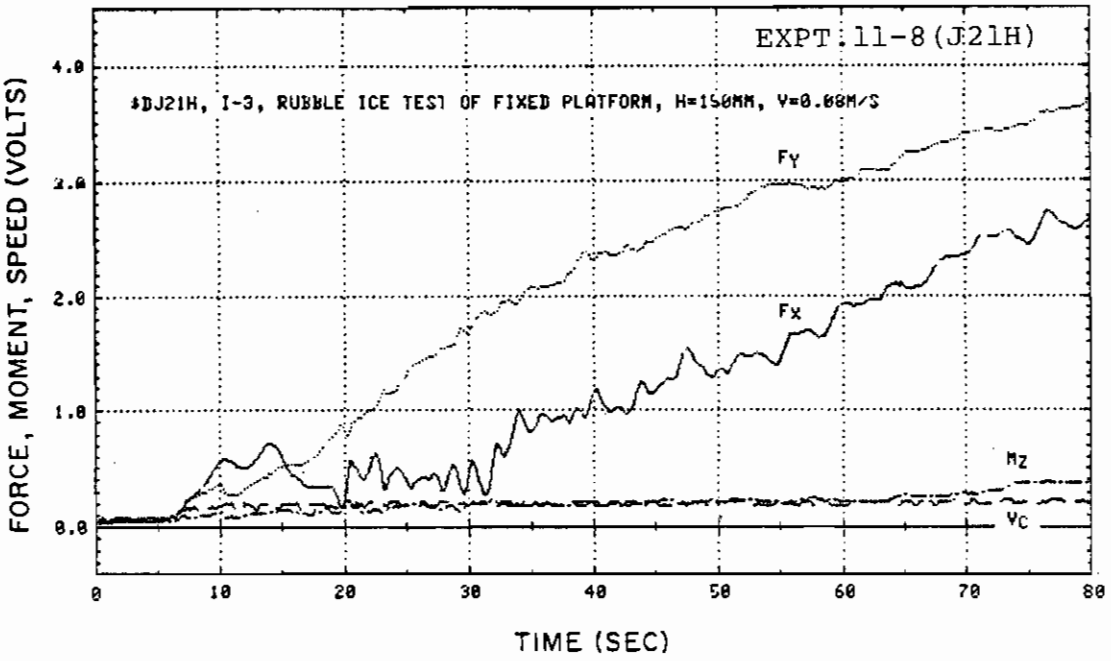

Fig. A-2-53

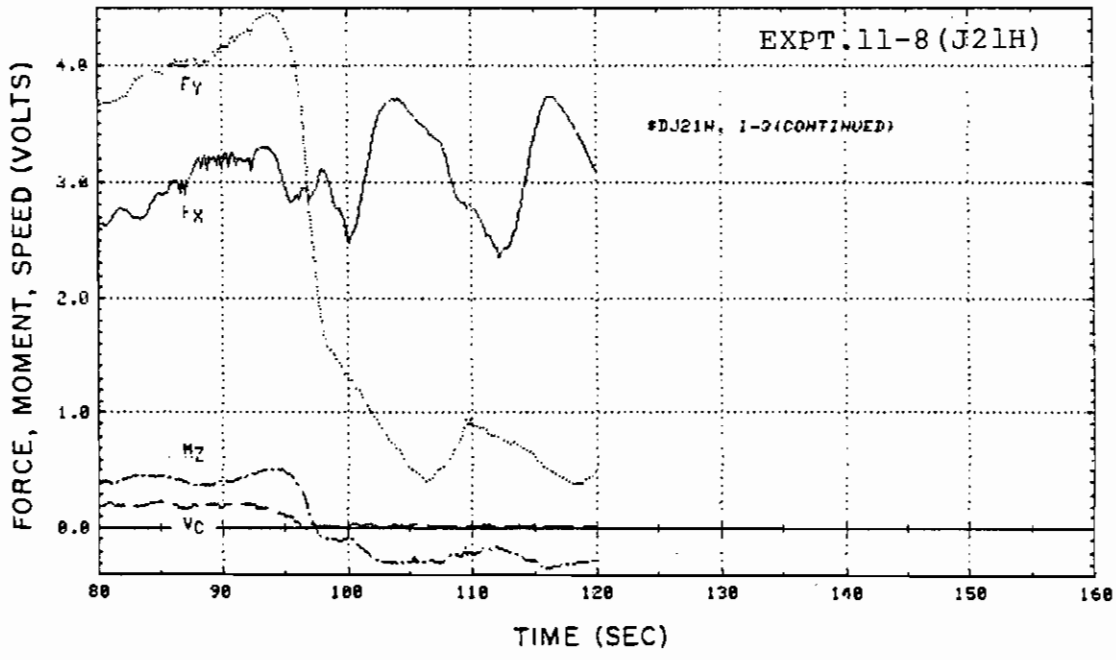

Fig. A-2-54

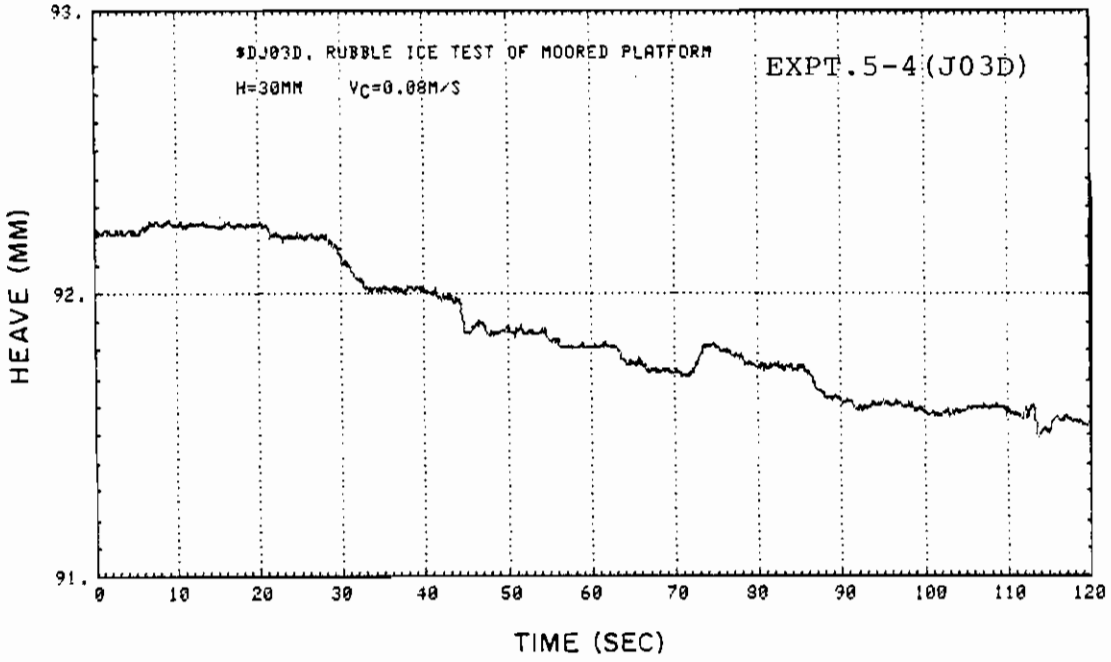

Fig. A-2-55

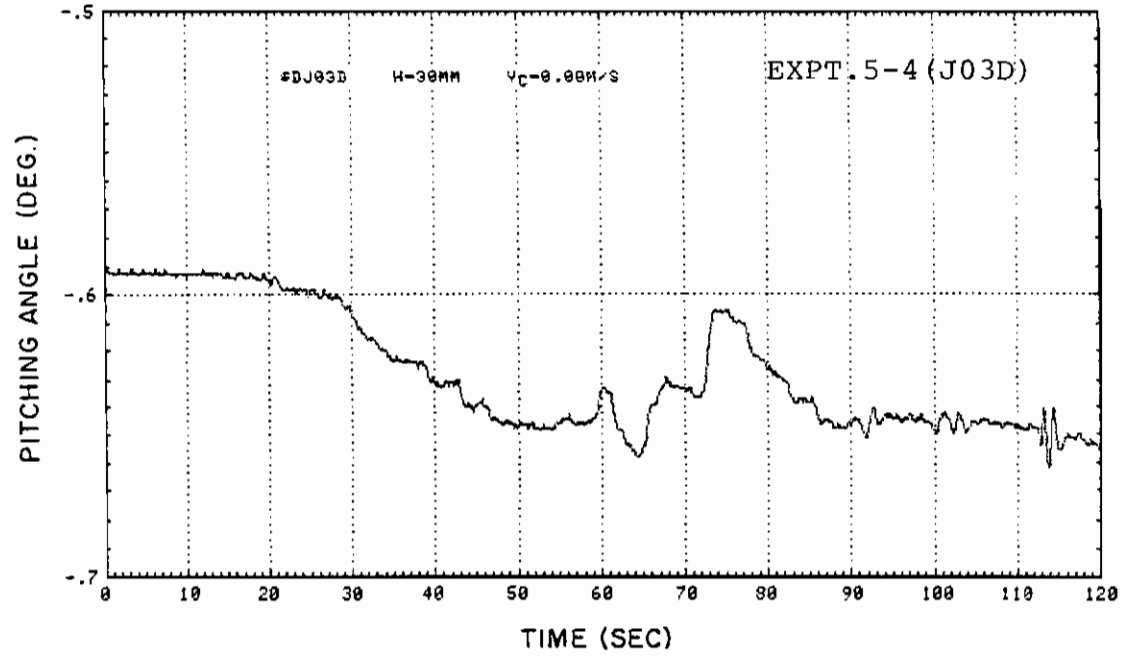

Fig. A-2-56

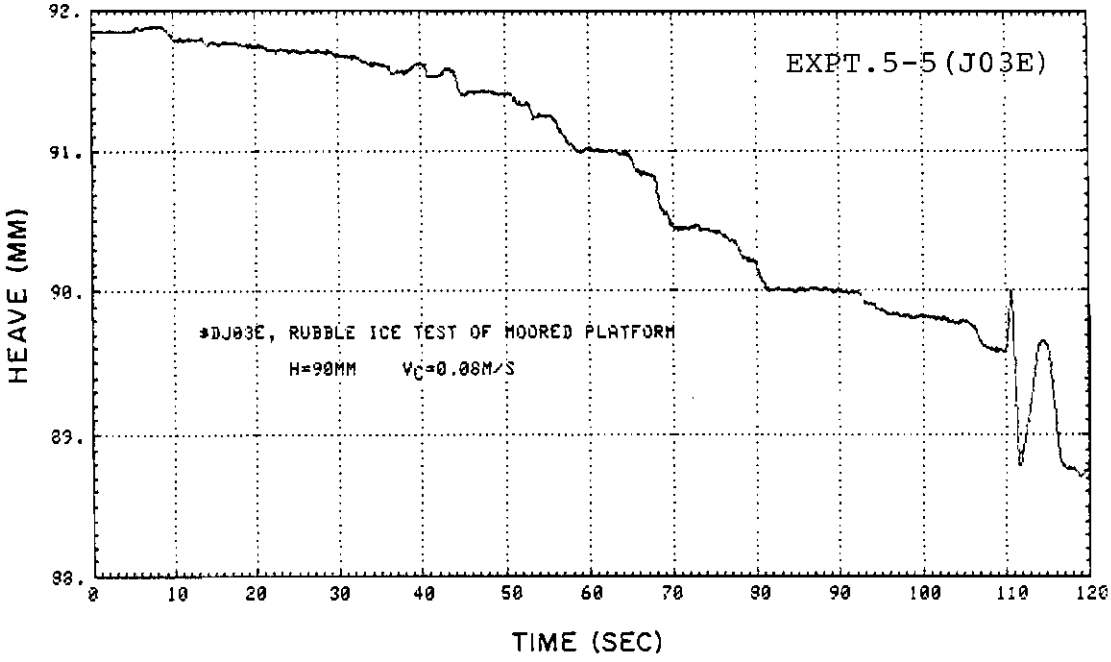

Fig. A-2-57

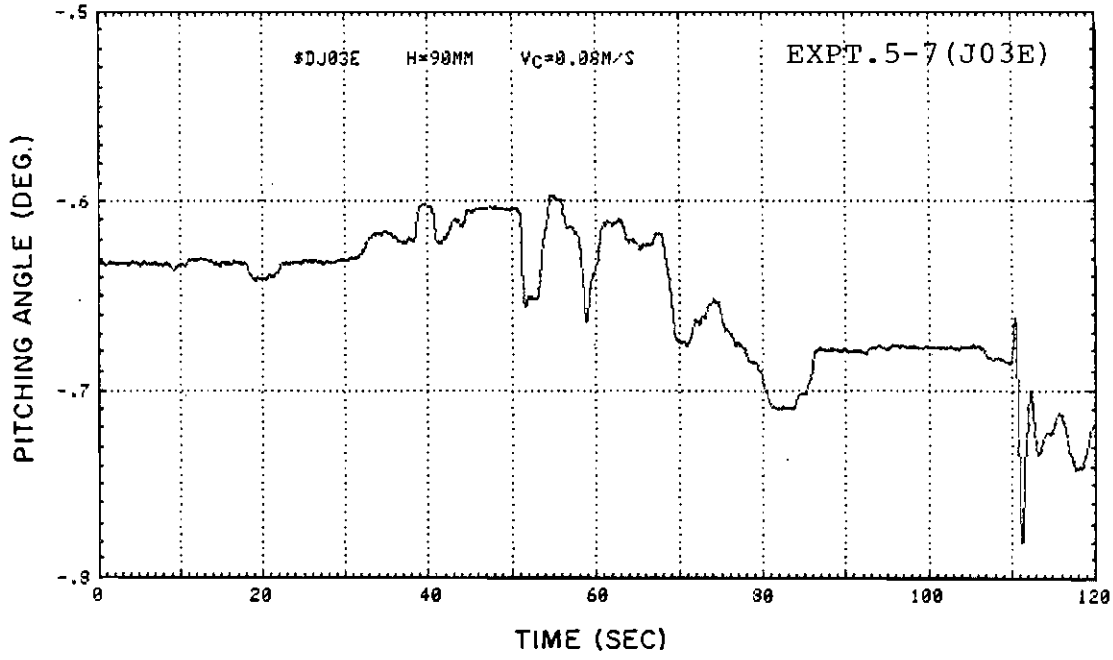

Fig. A-2-58

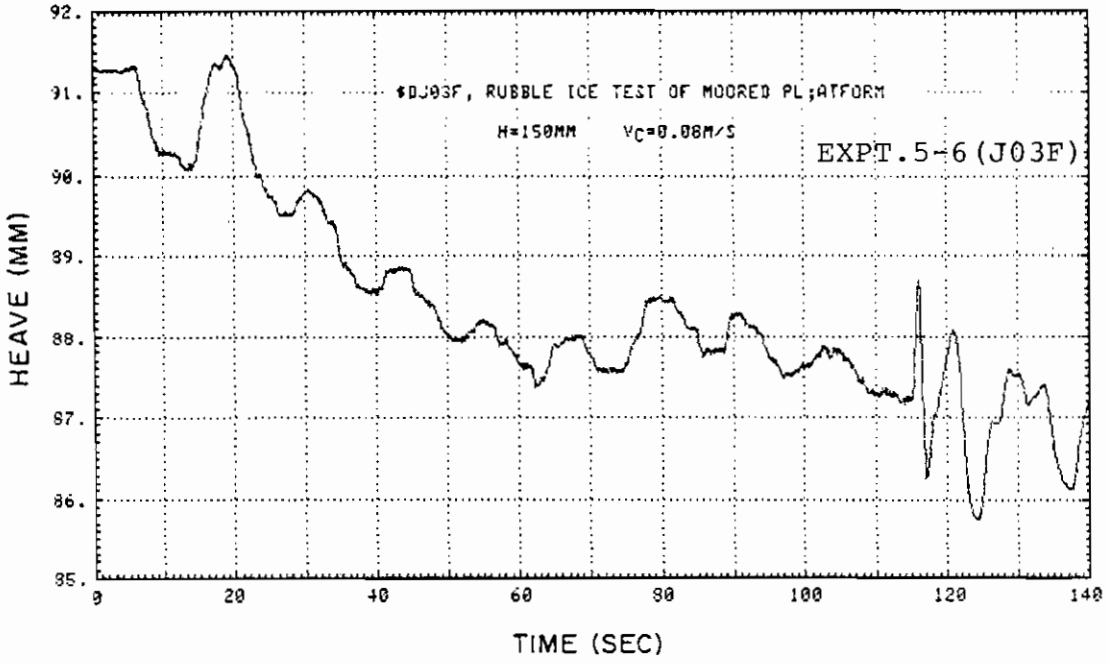

Fig. A-2-59

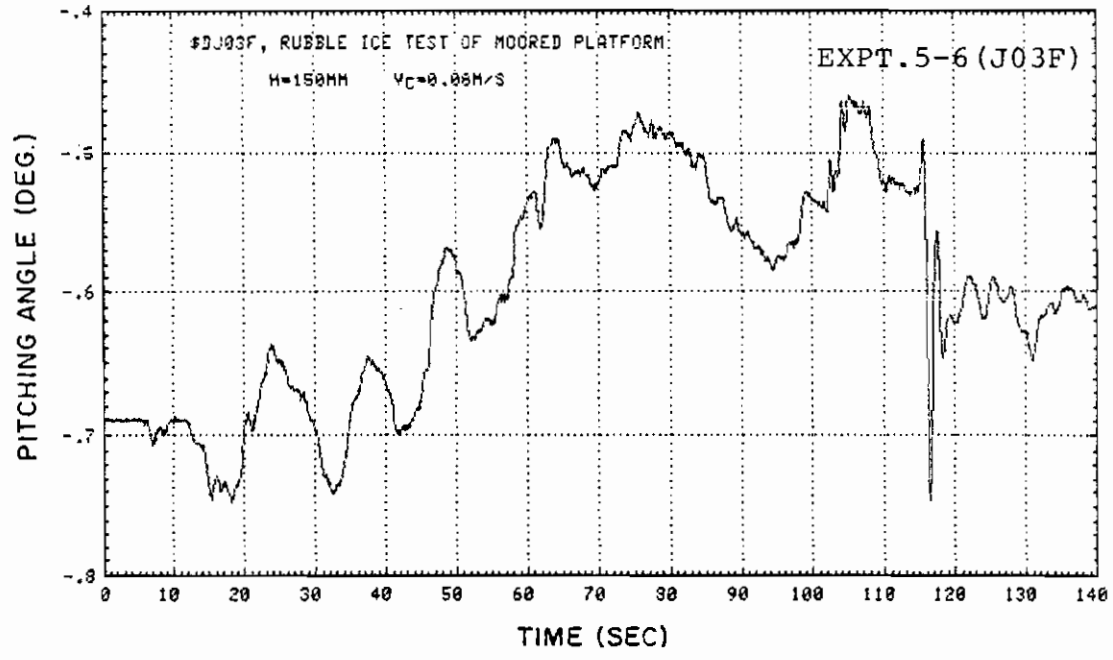

Fig. A-2-60

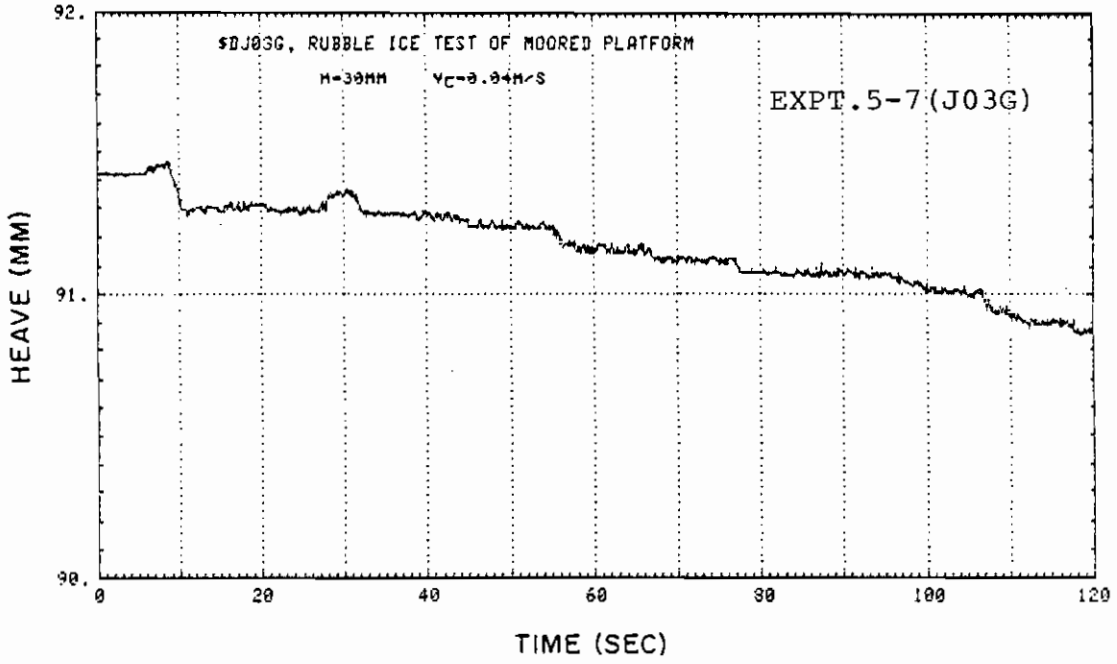

Fig. A-2-61

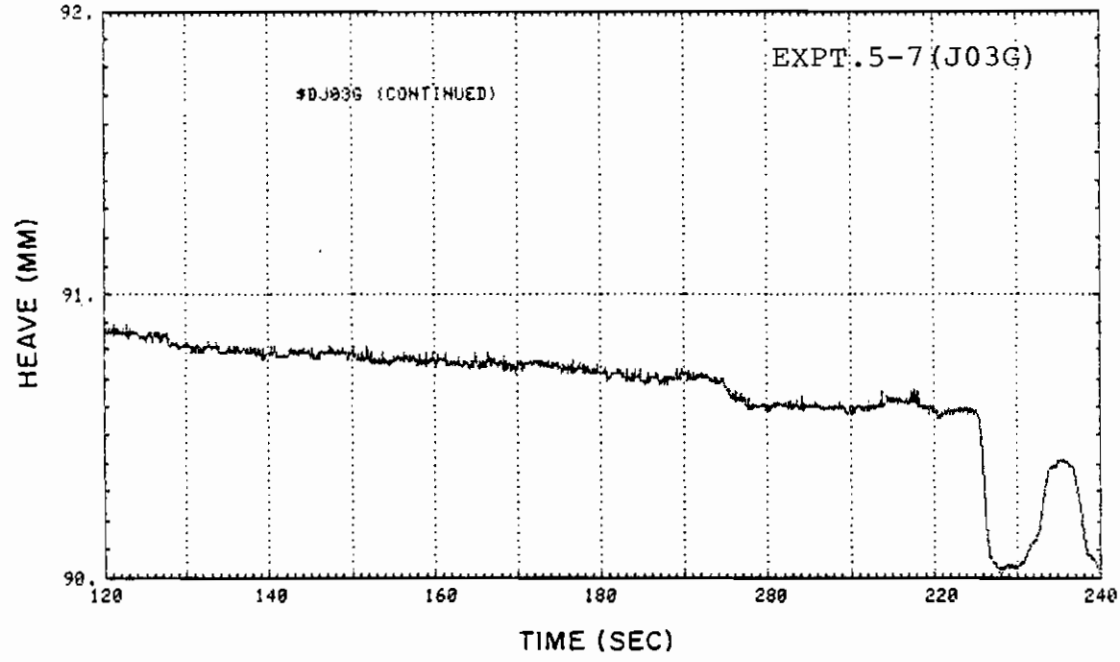

Fig. A-2-62

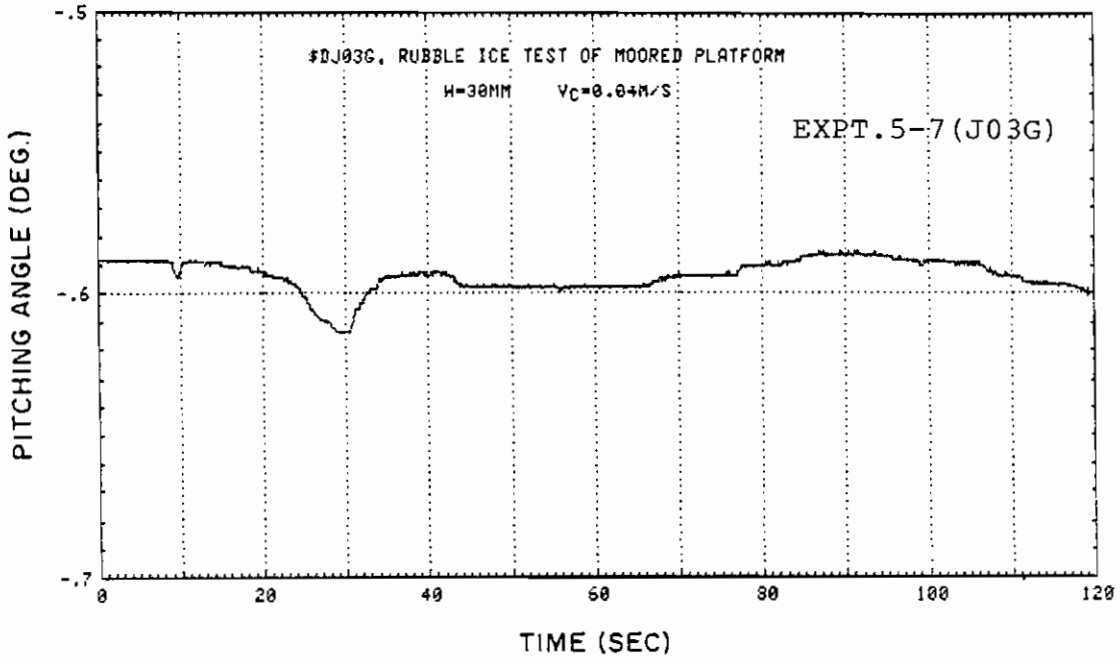

Fig. A-2-63

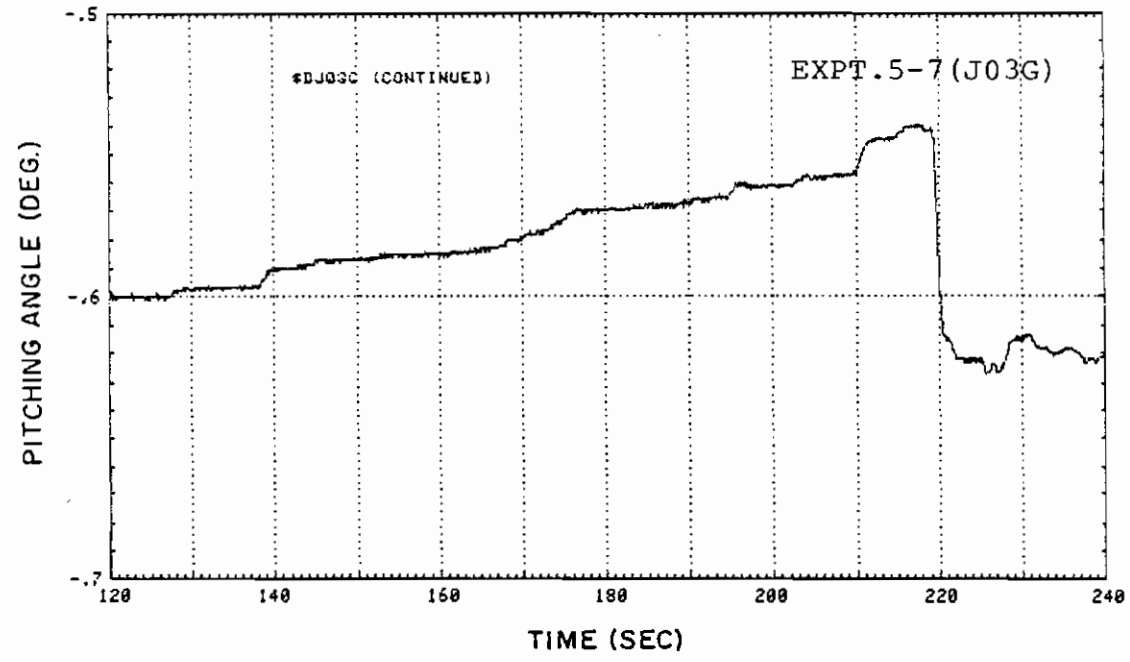

Fig. A-2-64

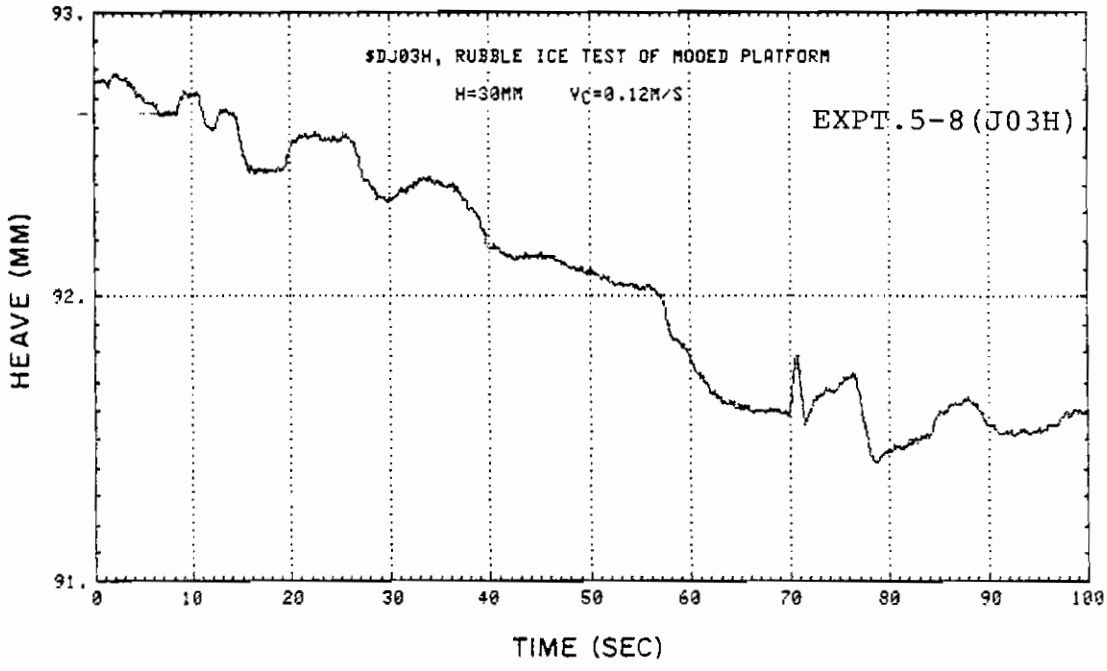

Fig. A-2-65

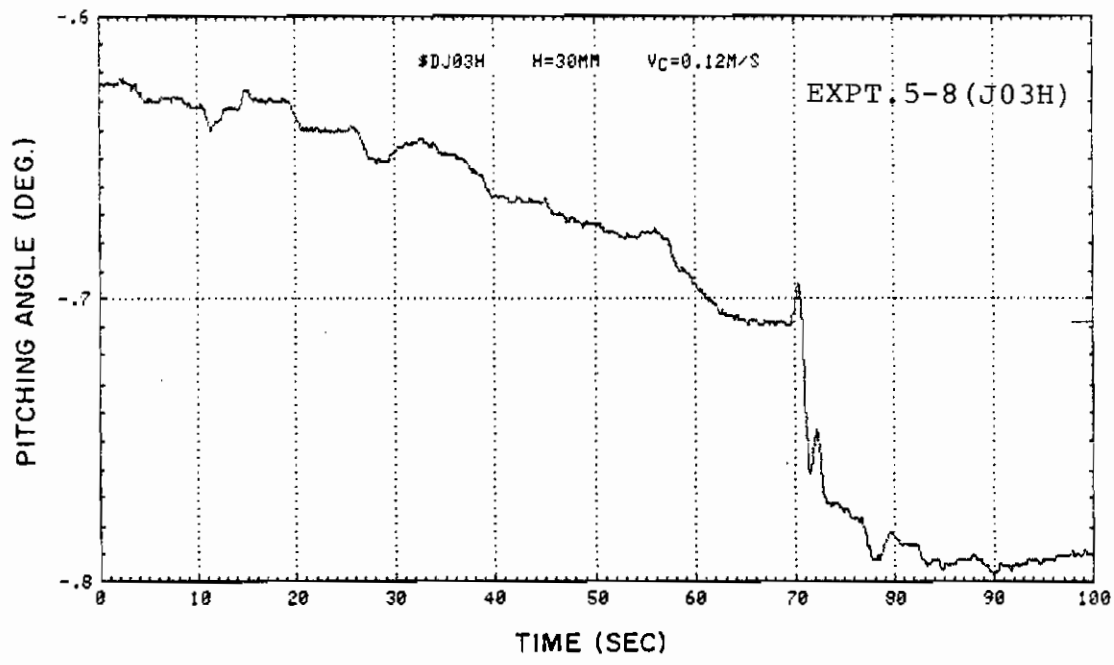

Fig. A-2-66

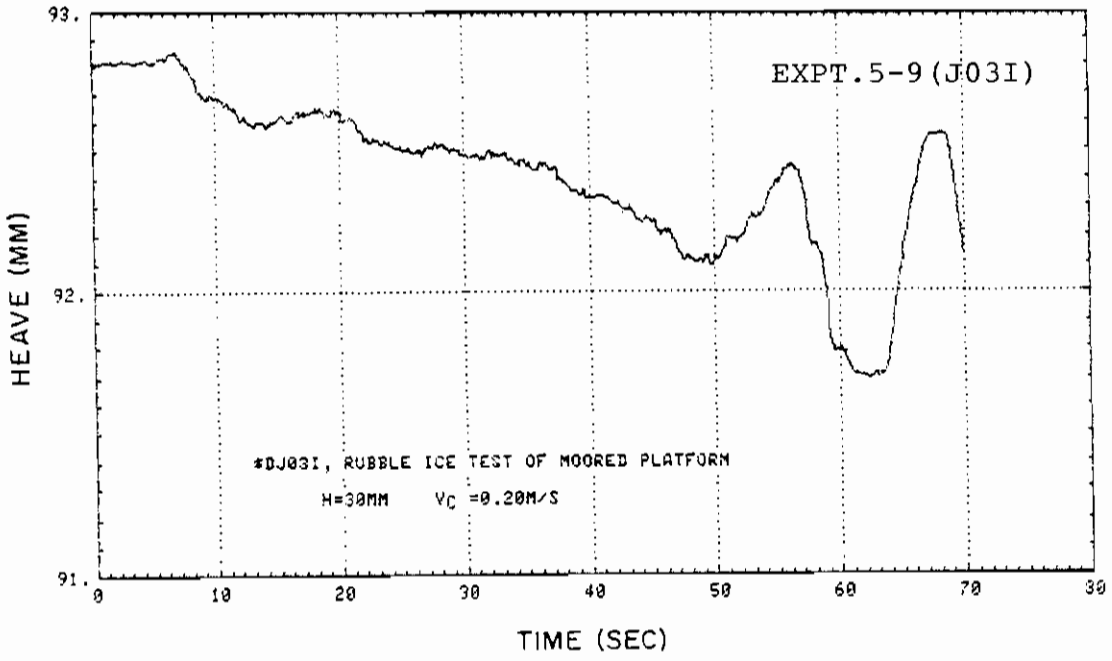

Fig. A-2-67

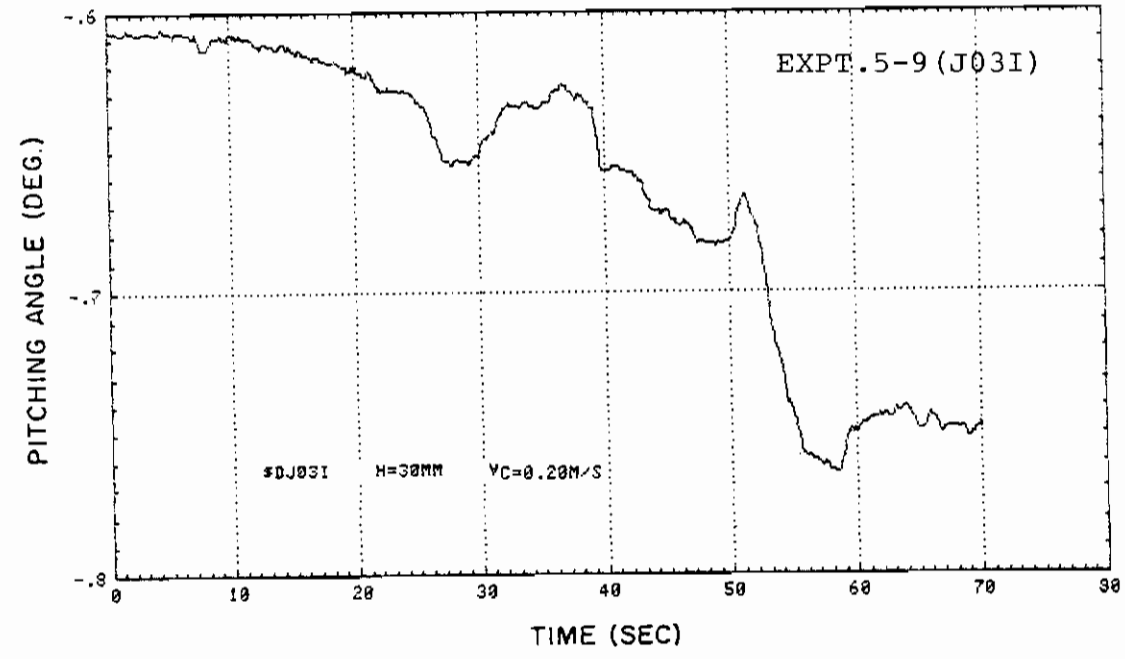

Fig. A-2-68

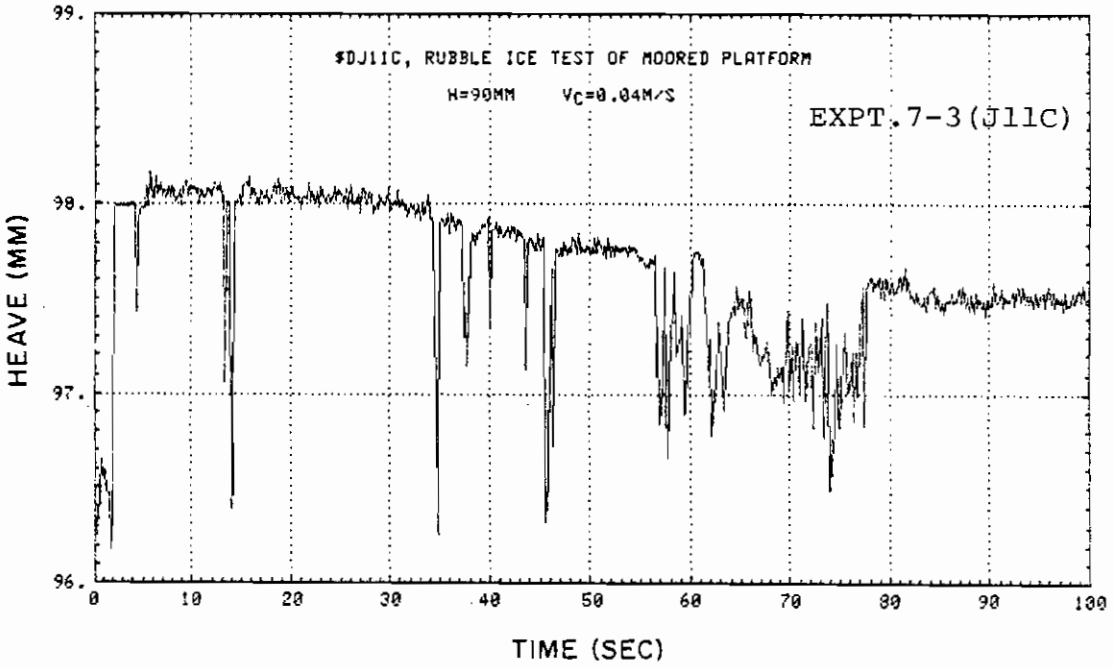

Fig. A-2-69

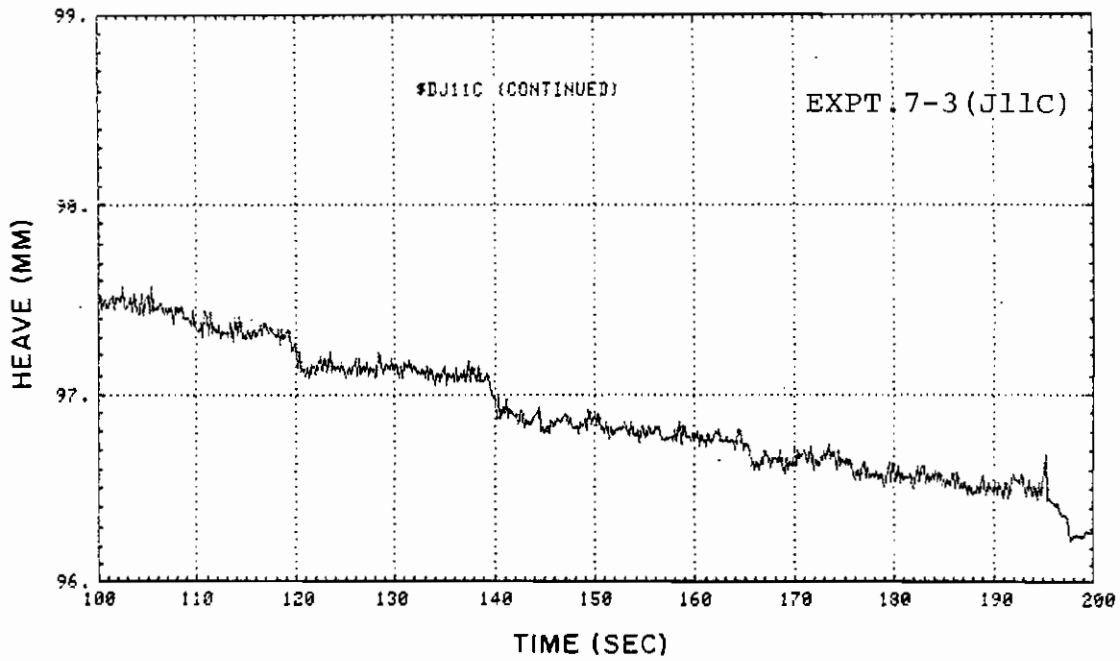

Fig. A-2-70

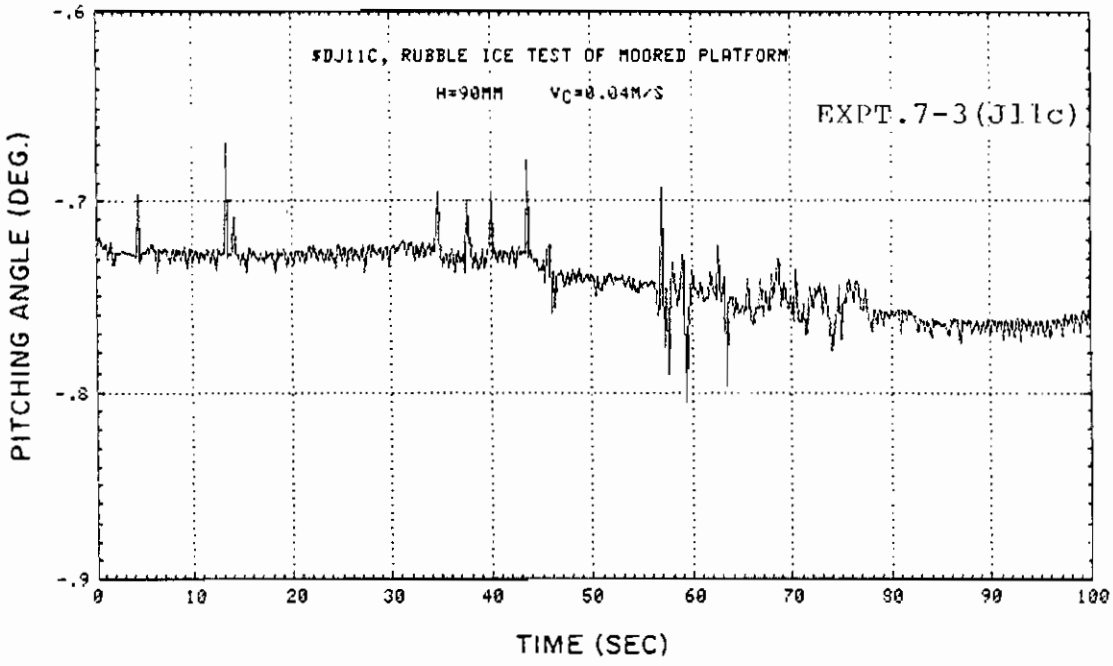

Fig. A-2-71

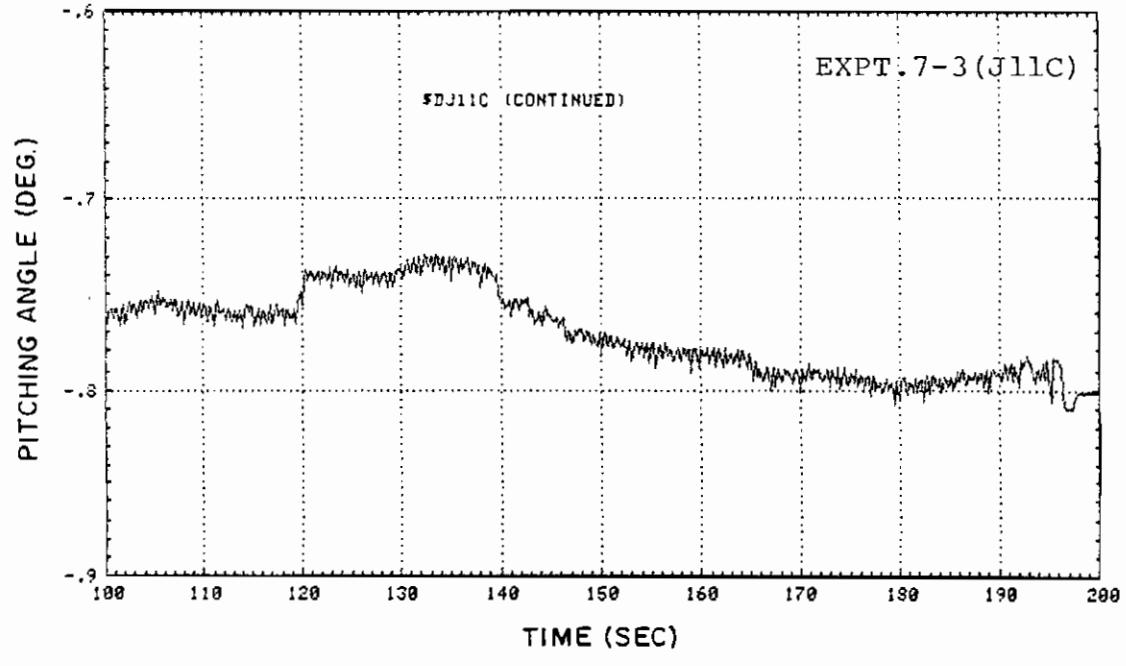

Fig. A-2-72

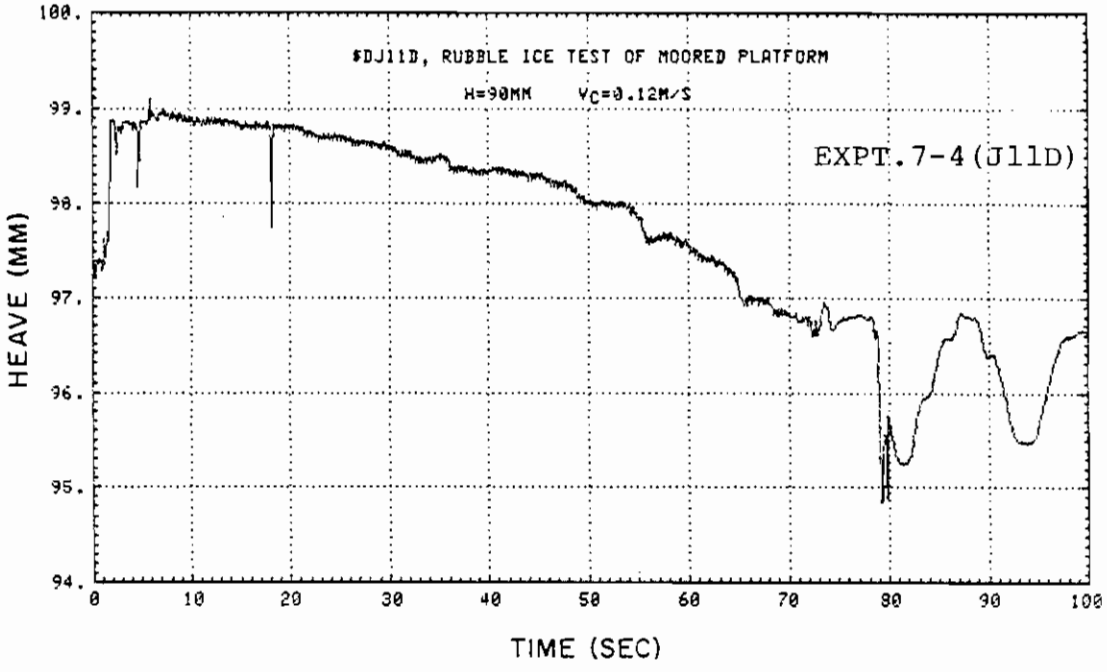

Fig. A-2-73

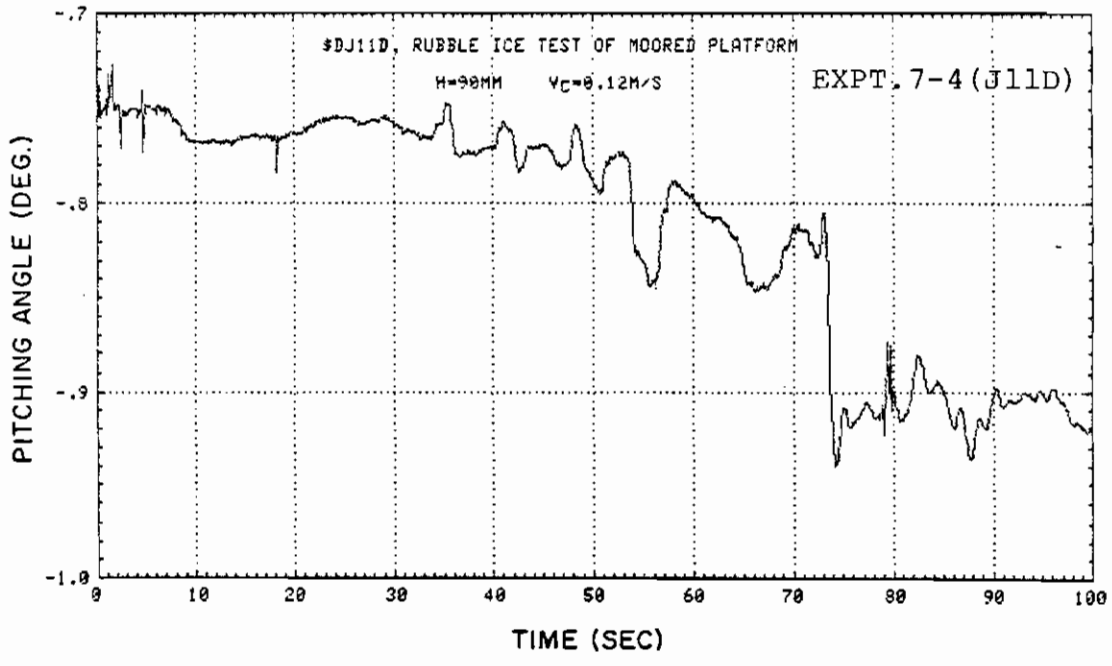

Fig. A-2-74

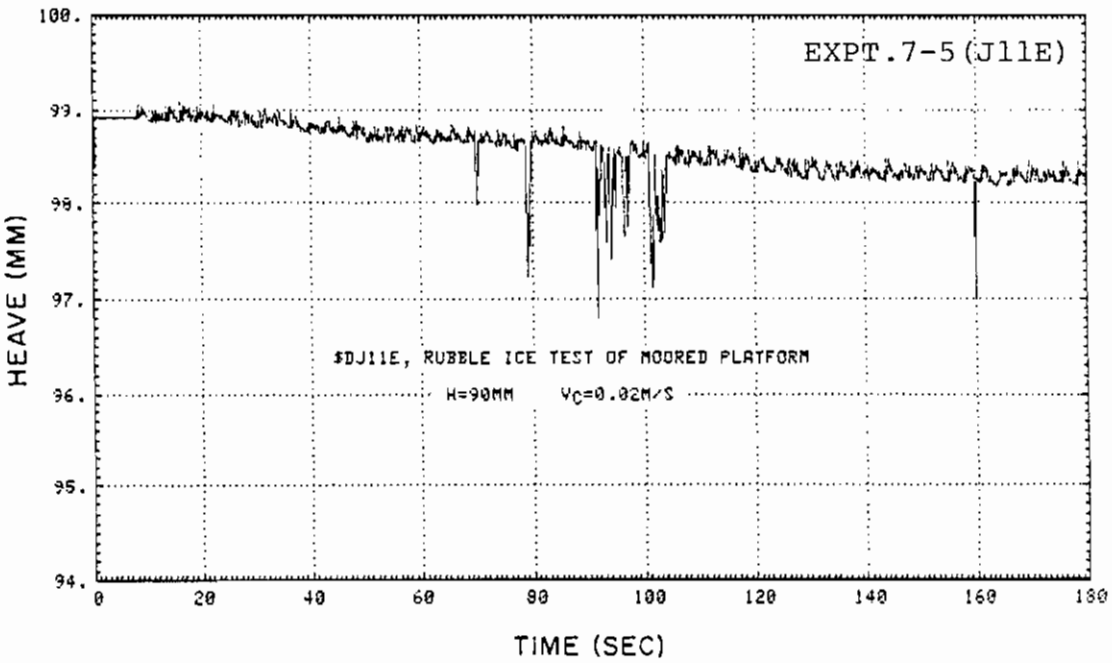

Fig. A-2-75

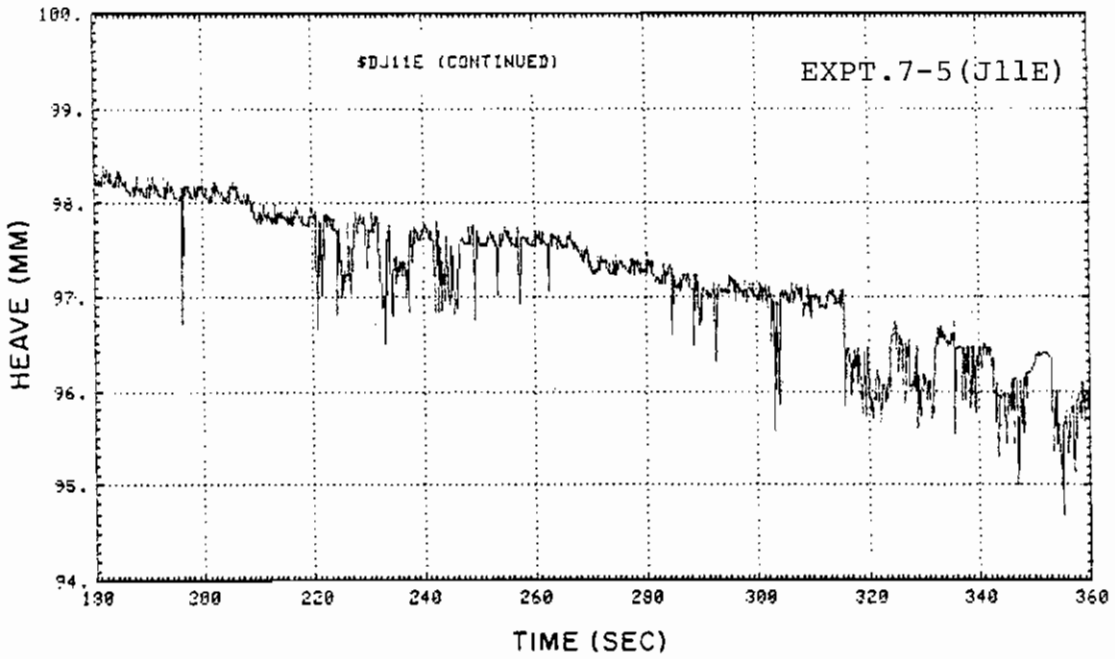

Fig. A-2-76

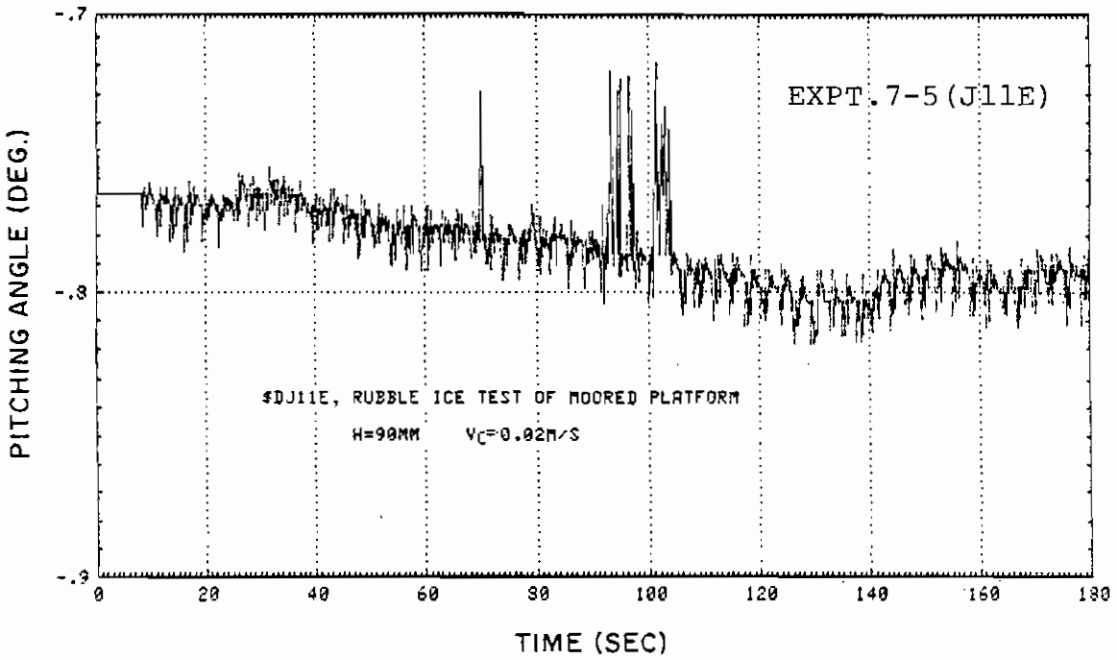

Fig. A-2-77

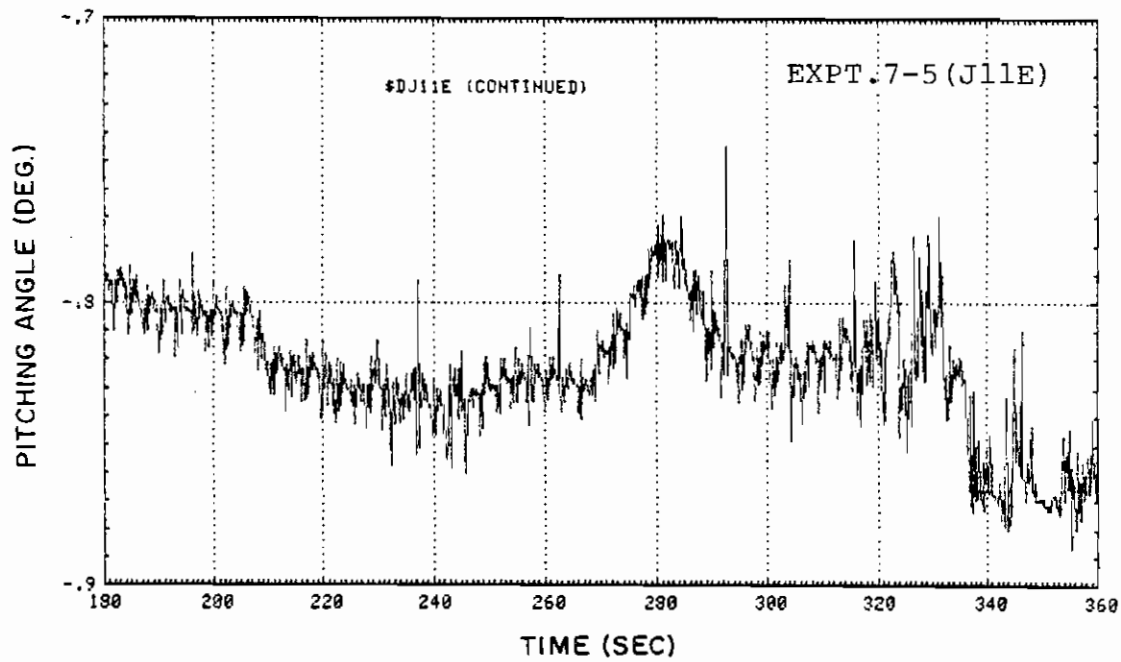

Fig. A-2-78

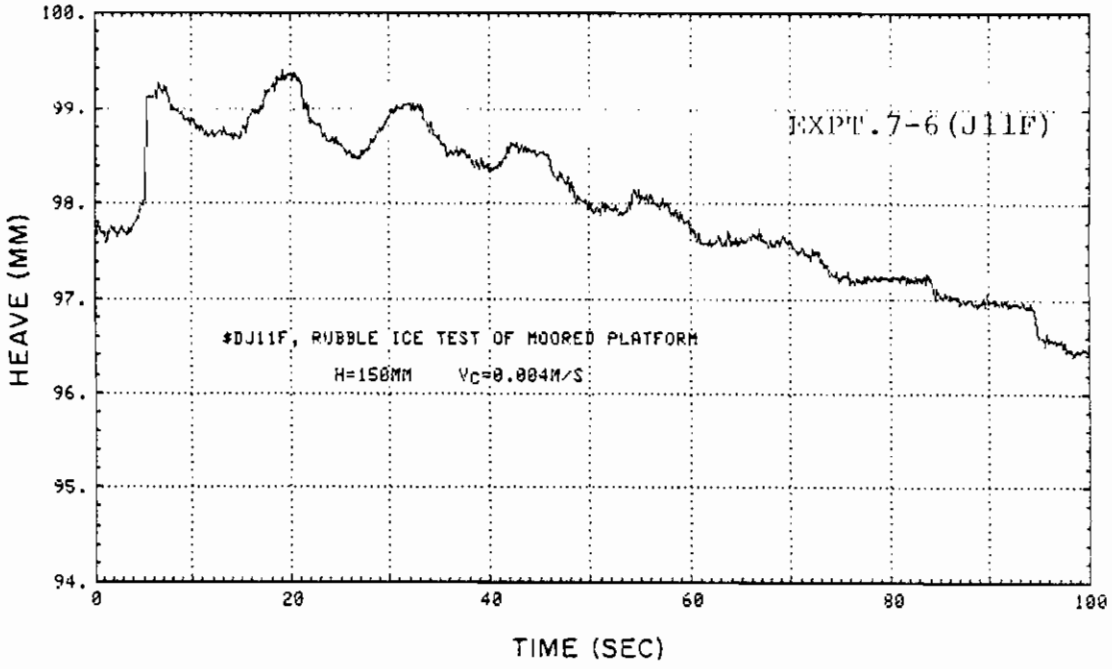

Fig. A-2-79

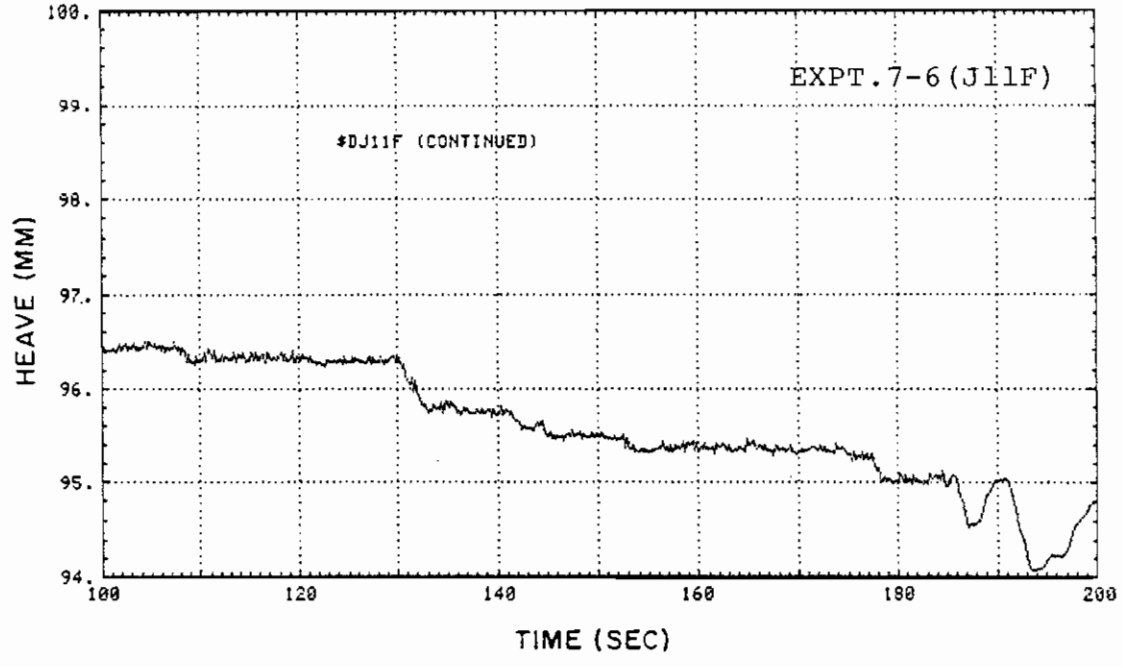

Fig. A-2-80

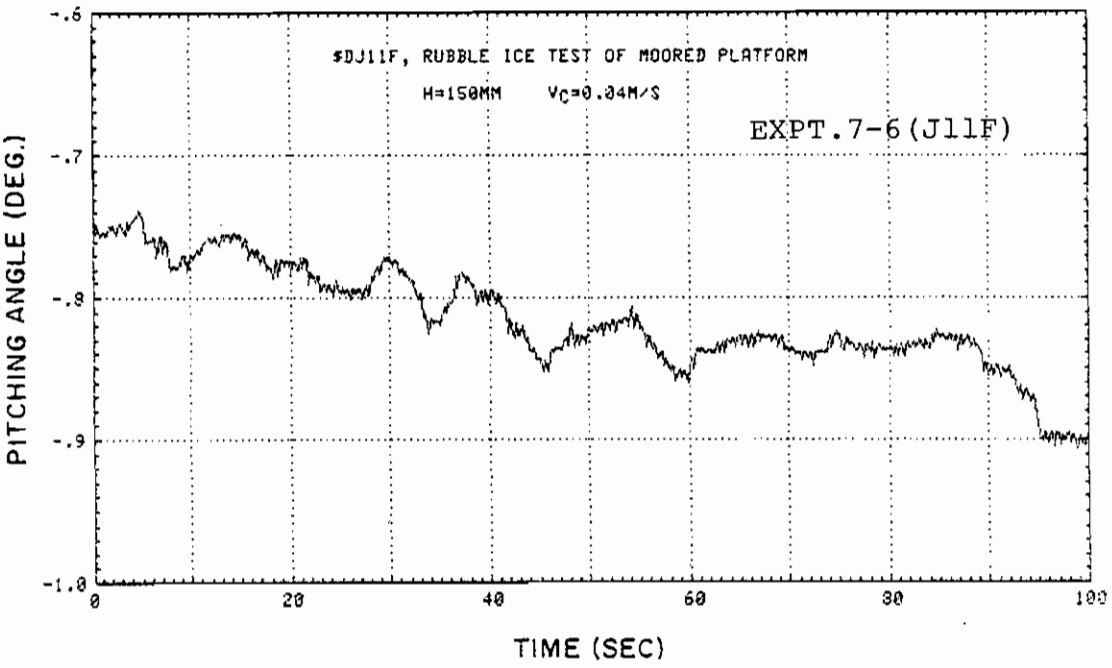

Fig. A-2-81

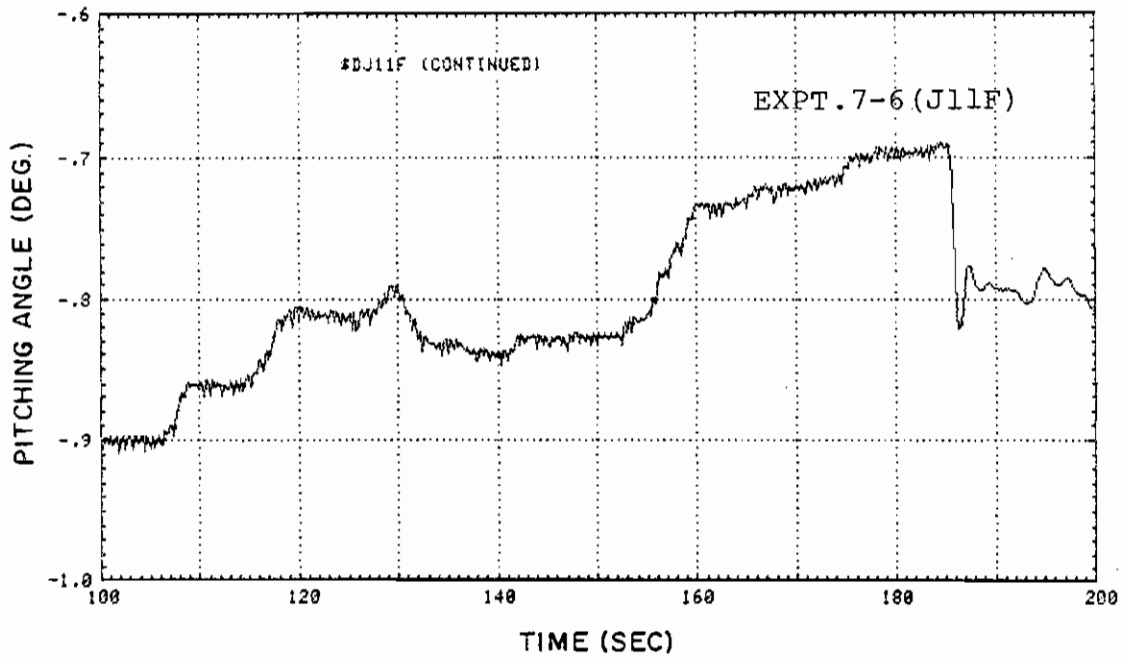

Fig. a-2-82

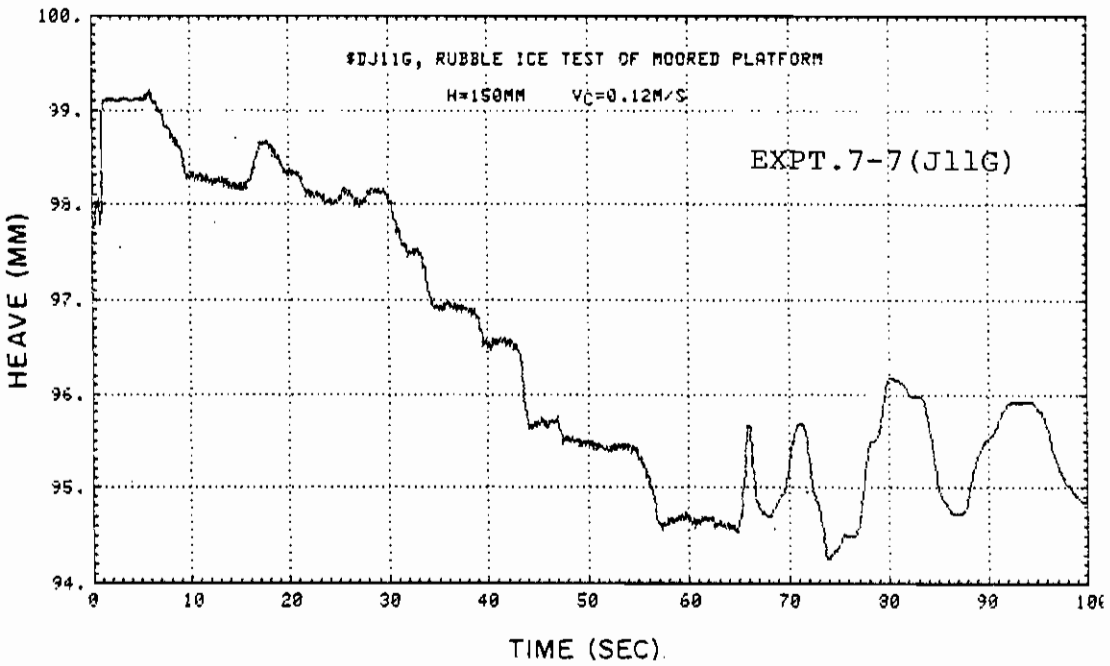

Fig. A-2-83

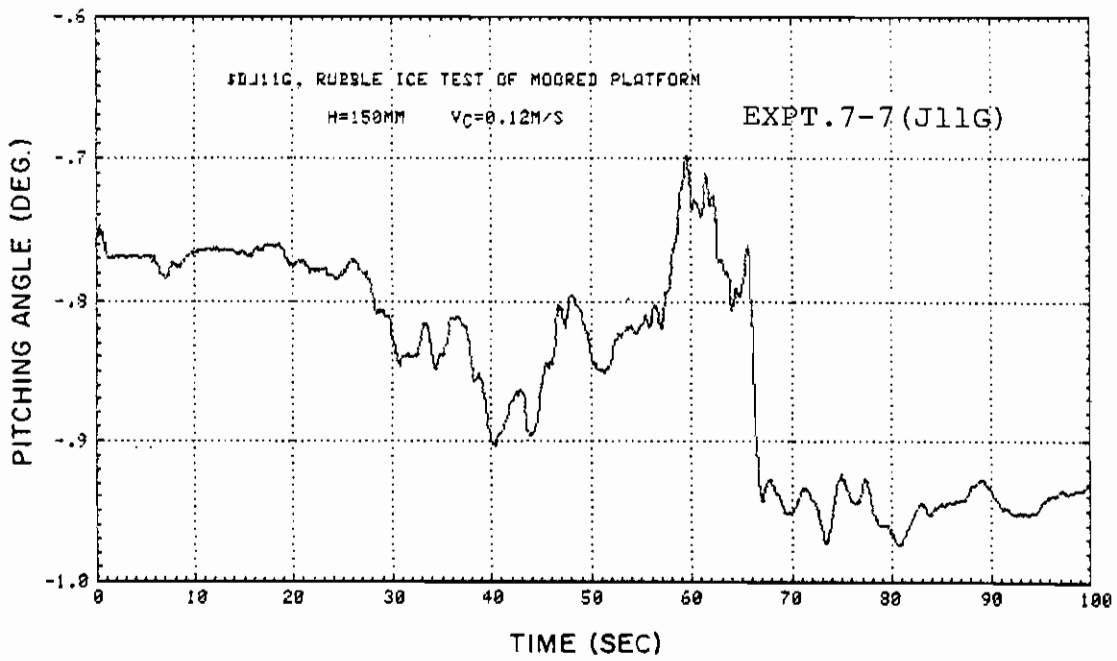

Fig. A-2-84

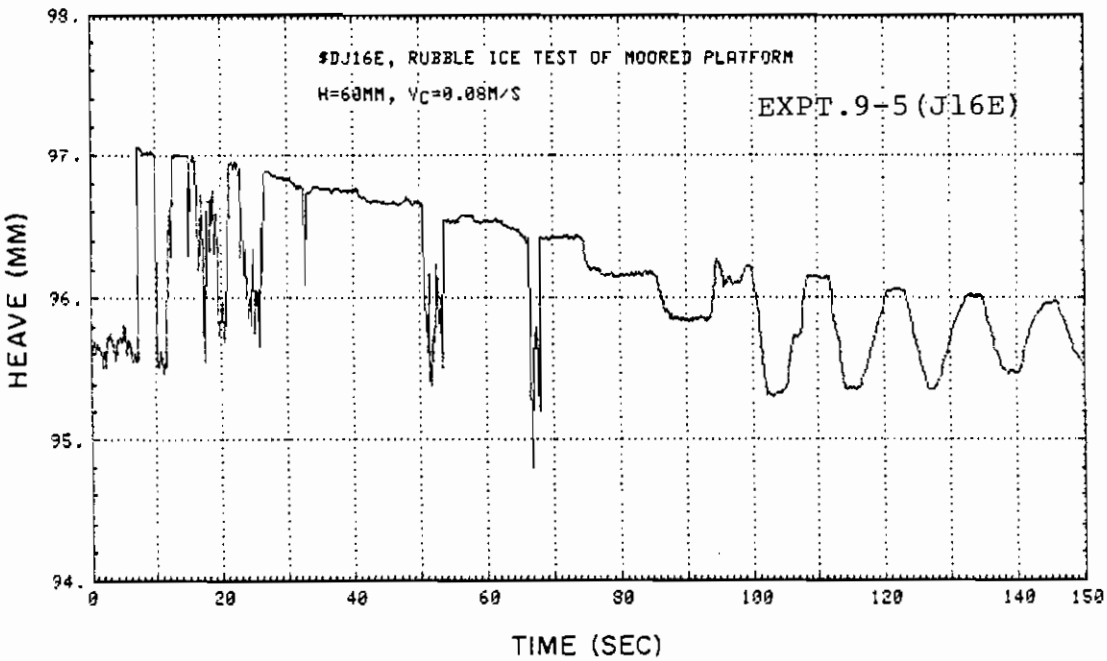

Fig. A-2-85

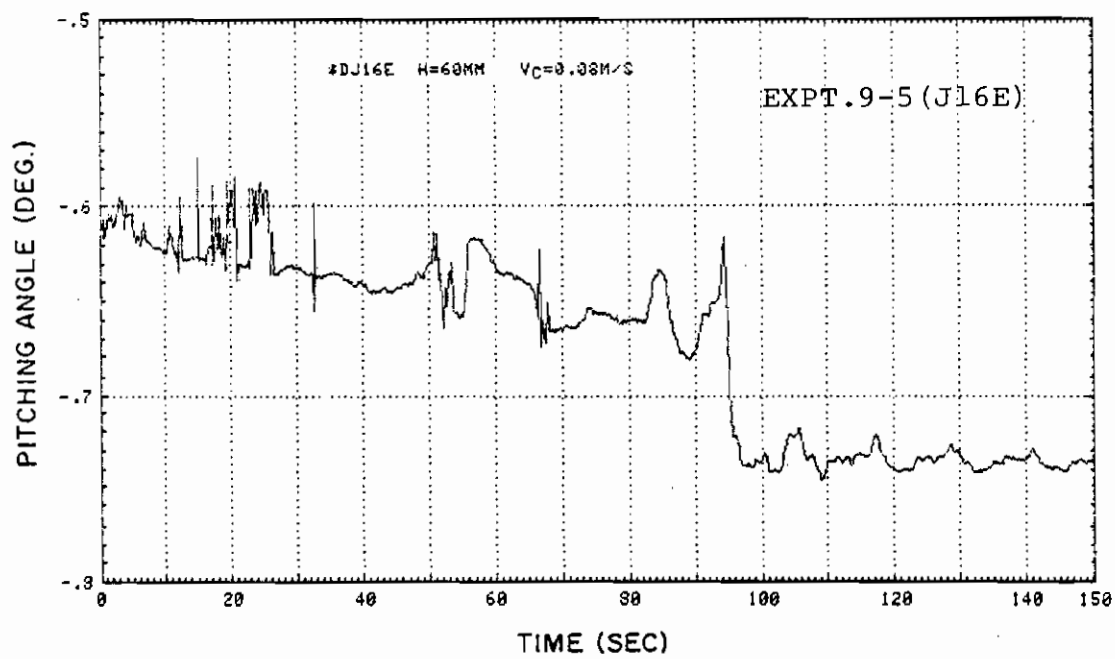

Fig. A-2-86

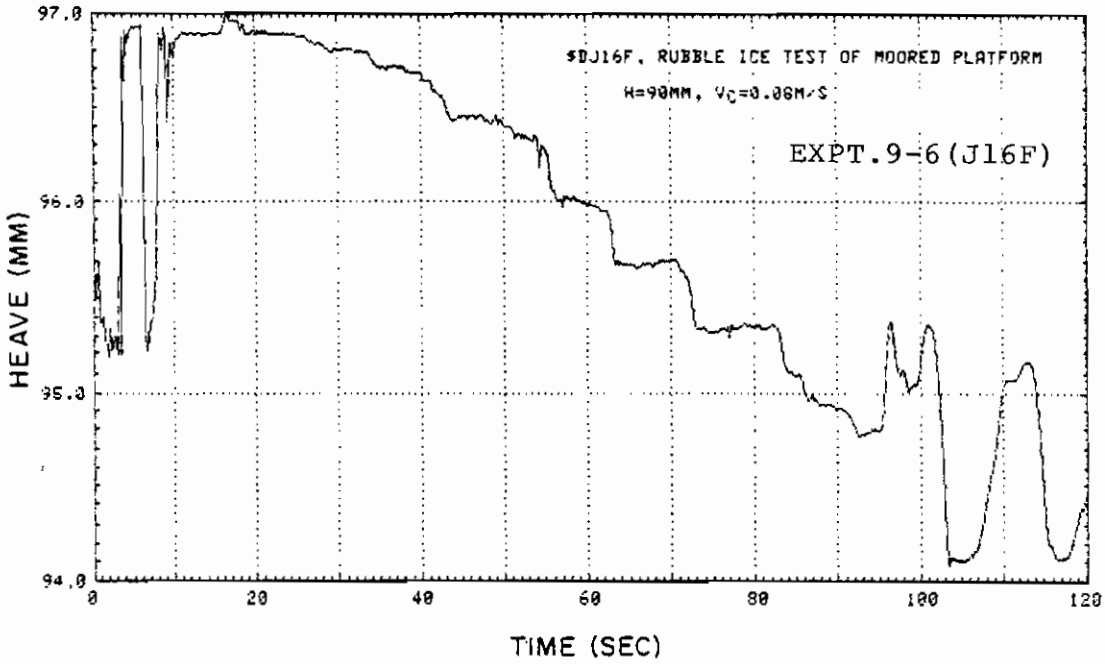

Fig. A-2-87

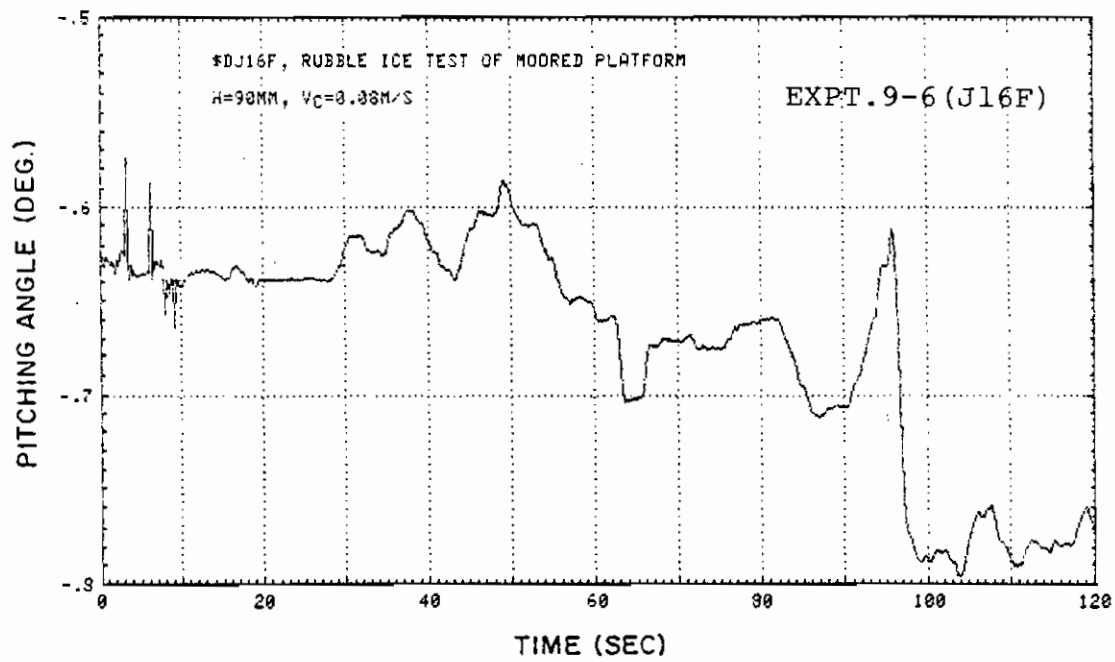

Fig. A-2-88

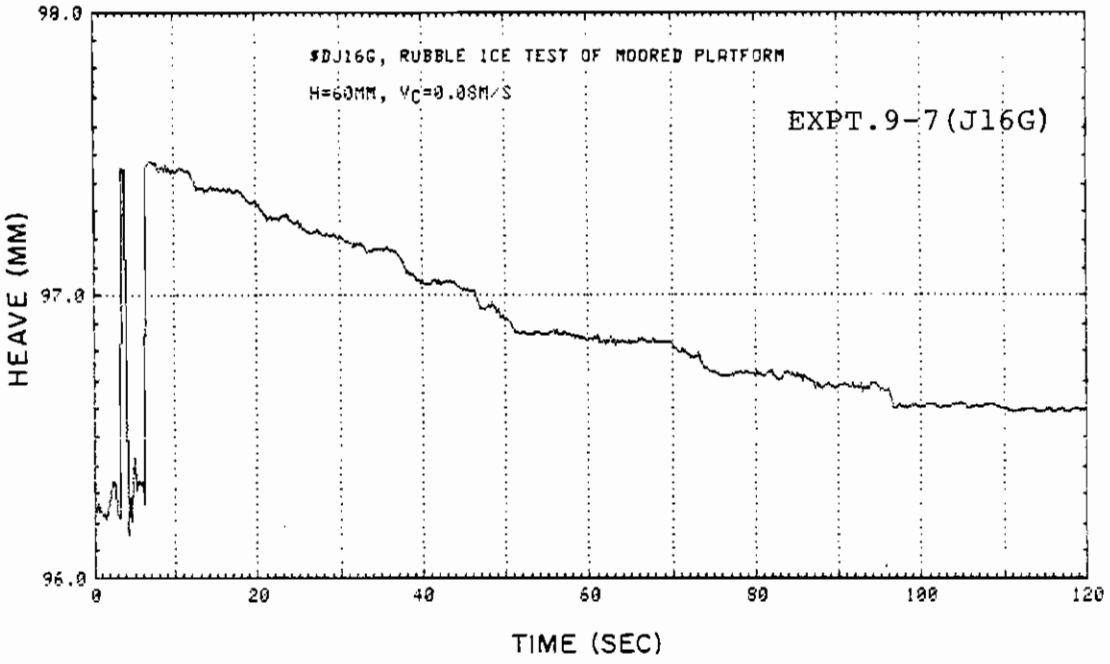

Fig. A-2-89

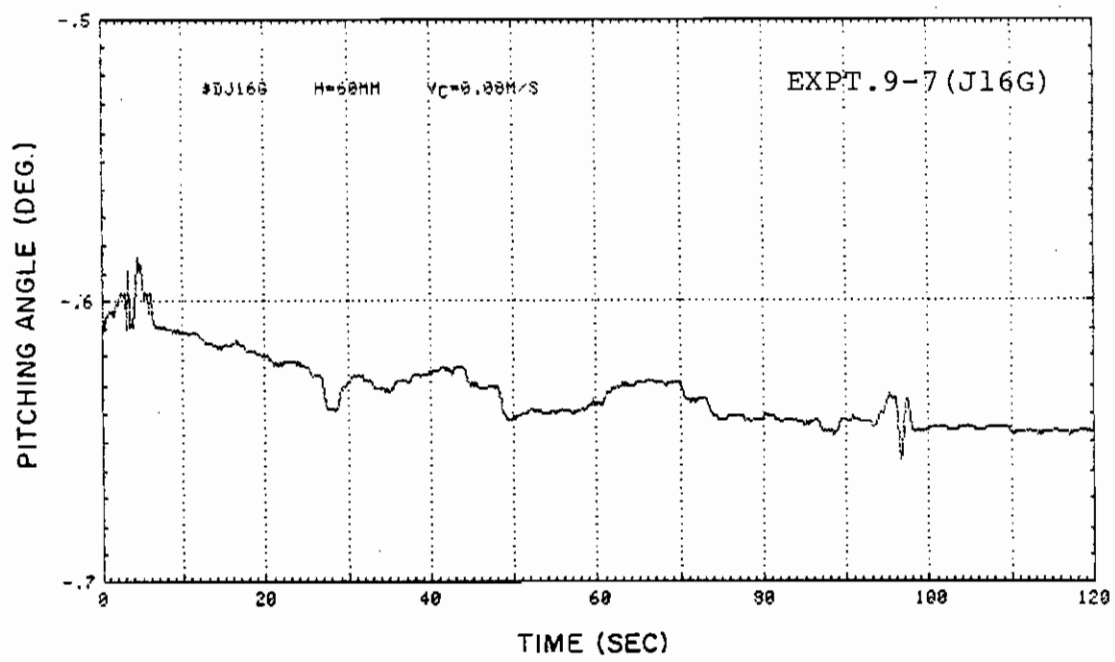

Fig. A-2-90

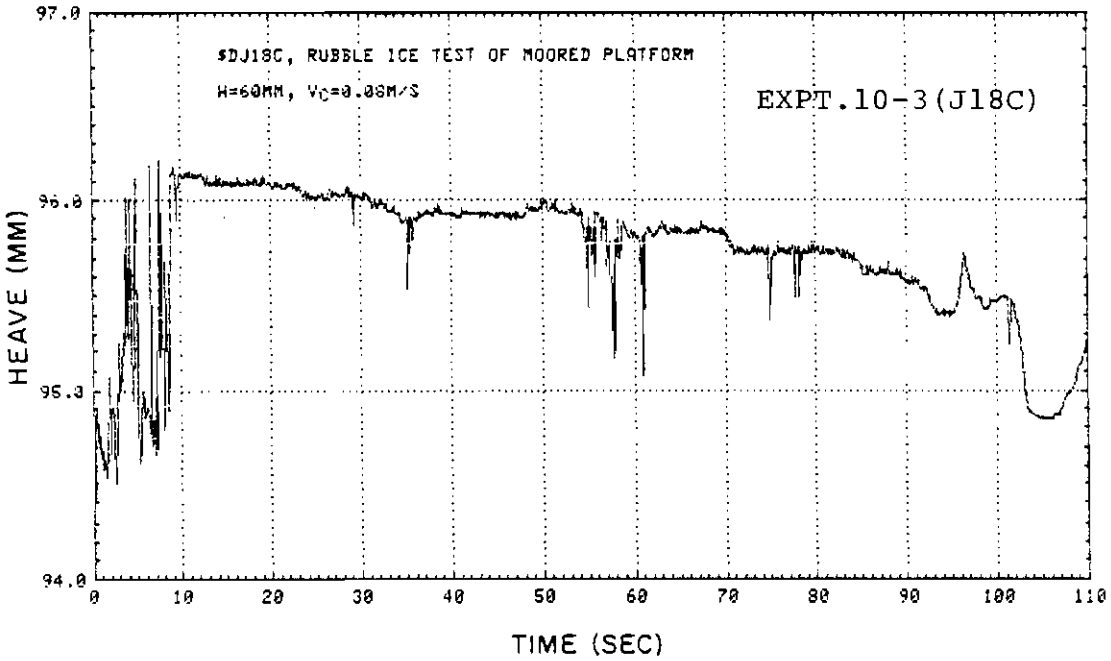

Fig. A-2-91

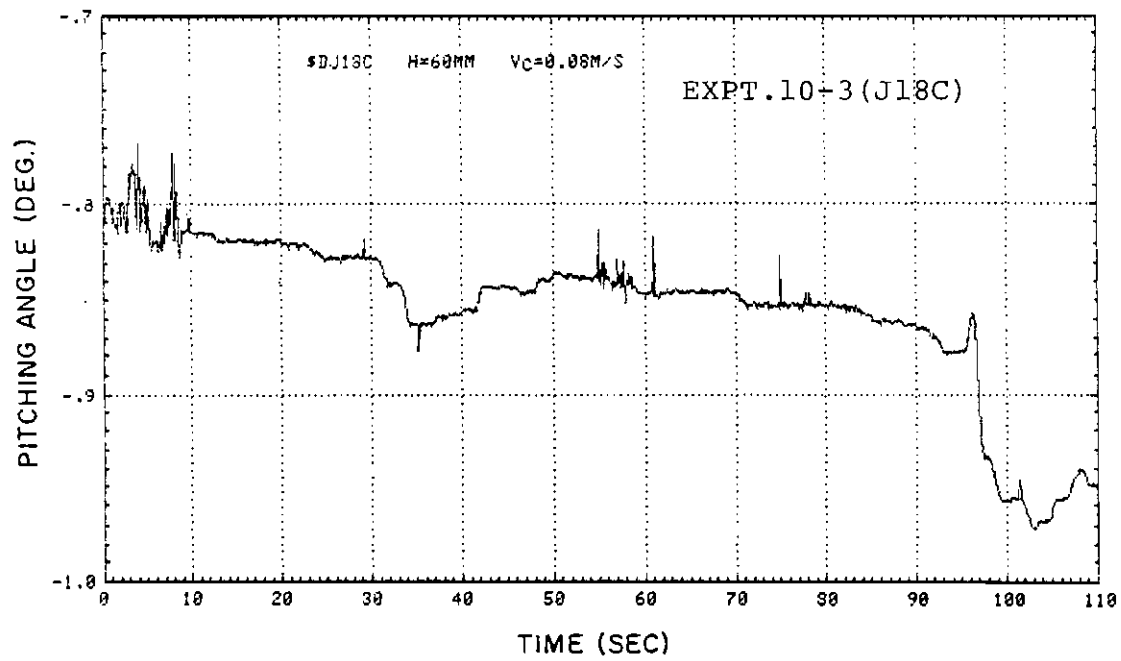

Fig. A-2-92

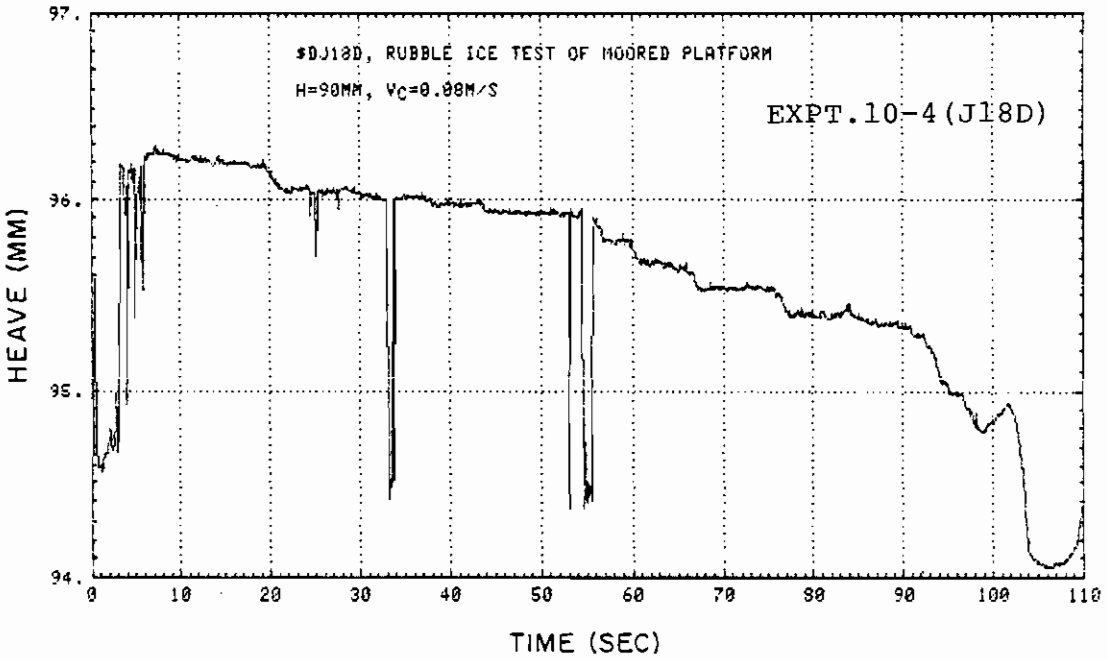

Fig. A-2-93

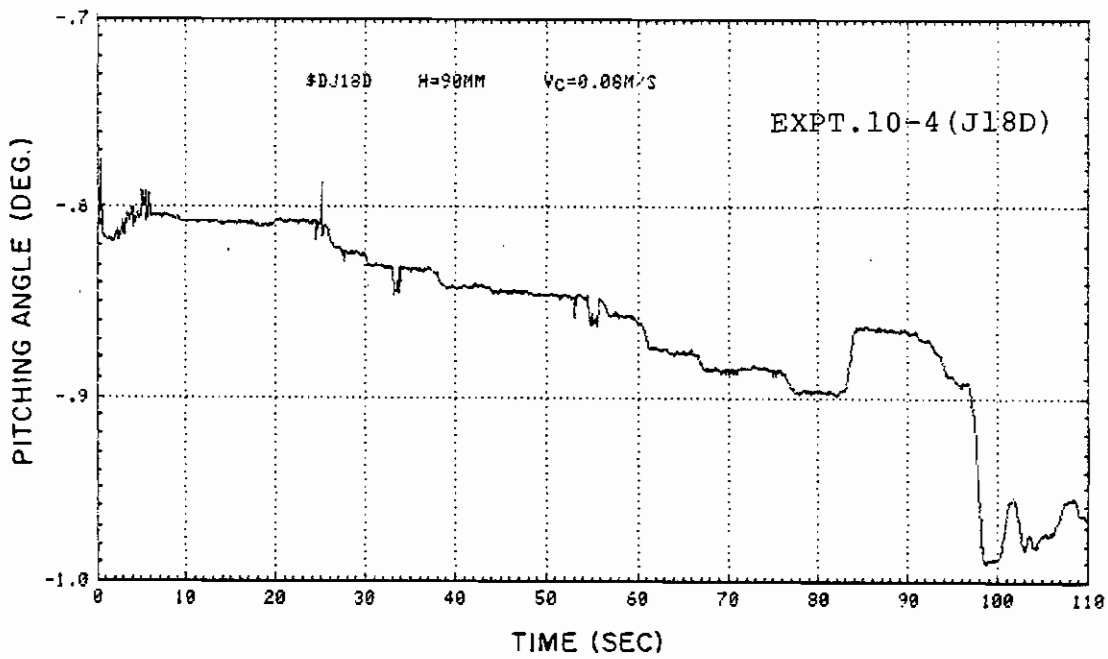

Fig. A-2-94

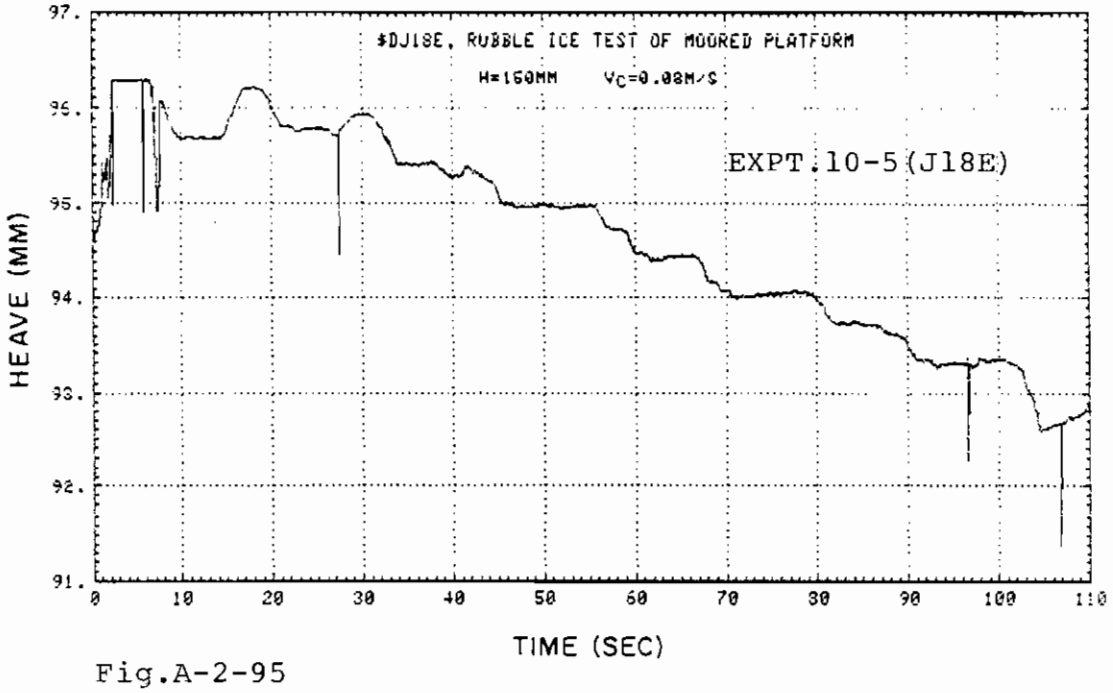

Fig.A-2-95

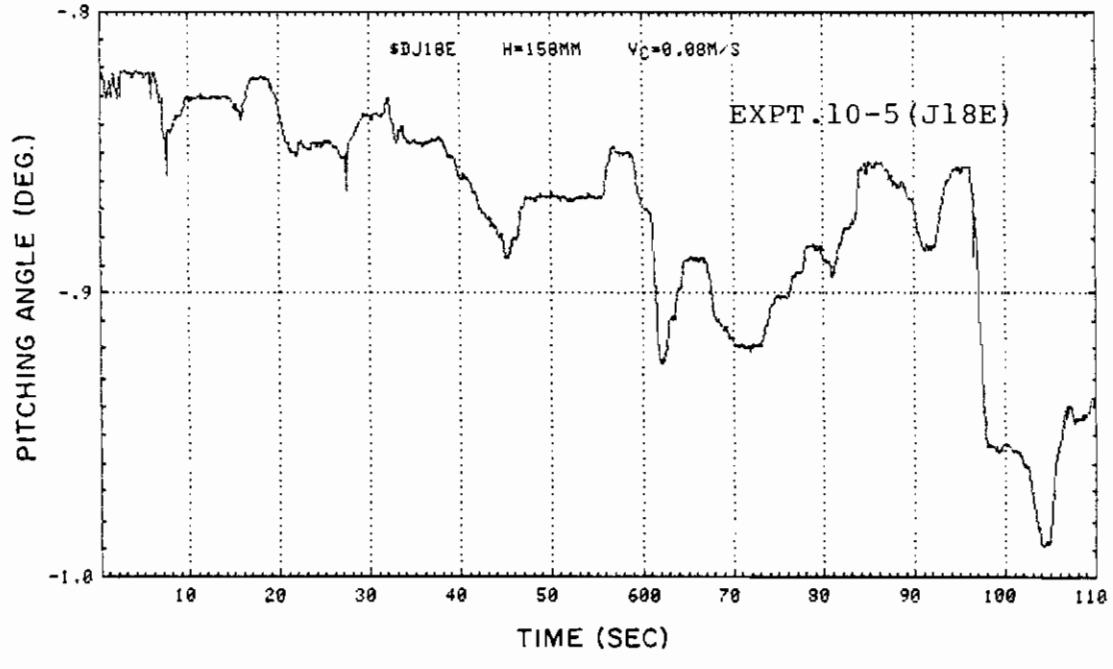

Fig.A-2-96

APPENDIX 3: Ice Accumulation around the Platform

Note:

(i) Thickness measurements are in centimeters

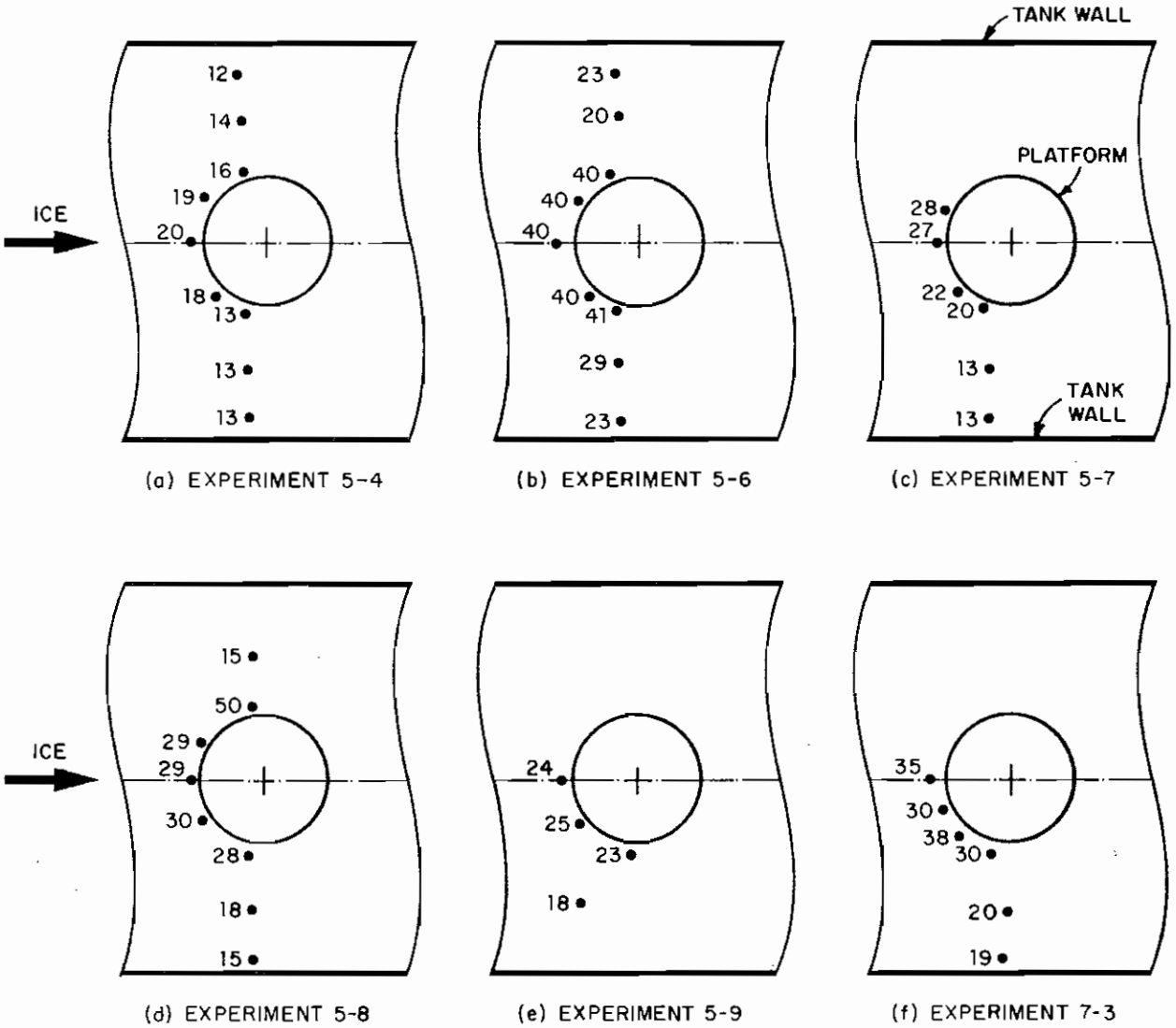
ICE
12
14
16
19
20
18
13
13
13
(a) EXPERIMENT 5-4
23
20
40
40
40
40
41
29
23
(b) EXPERIMENT 5-6
TANK WALL
PLATFORM
28
27
22
20
13
13
TANK WALL
(c) EXPERIMENT 5-7
ICE
15
50
29
29
30
28
18
15
(d) EXPERIMENT 5-8
24
25
23
18
(e) EXPERIMENT 5-9
35
30
38
30
20
19
(f) EXPERIMENT 7-3

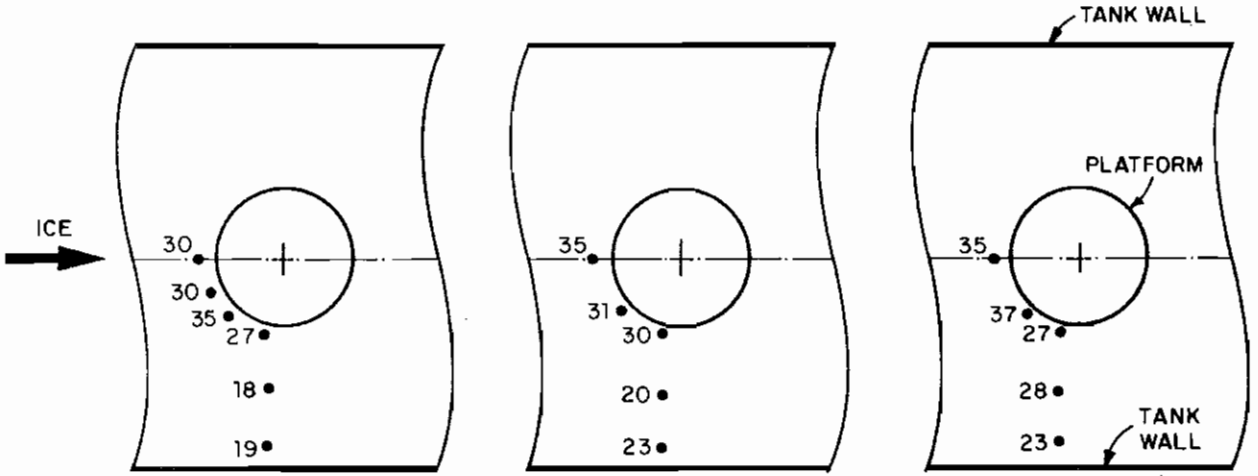

(g) EXPERIMENT 7-4 (h) EXPERIMENT 7-5 (i) EXPERIMENT 7-6

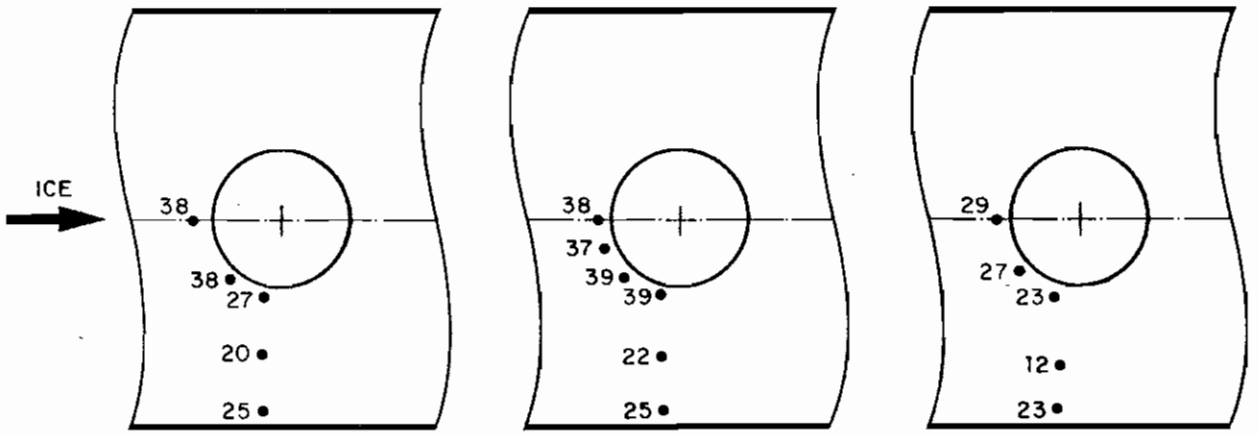

(j) EXPERIMENT 7-7 (k) EXPERIMENT 7-8 (l) EXPERIMENT 7-9

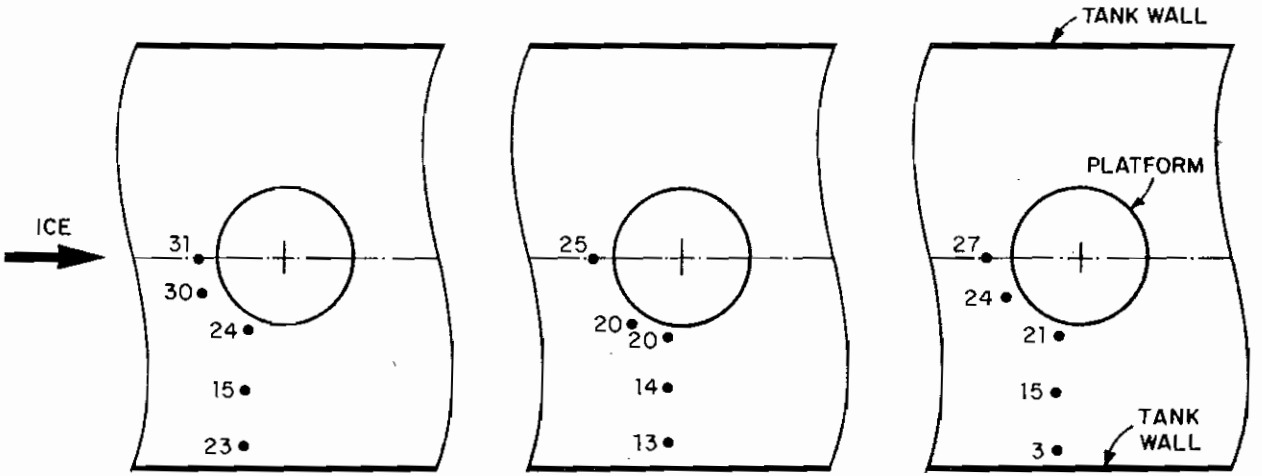

(m) EXPERIMENT 9-6 (n) EXPERIMENT 9-7 (o) EXPERIMENT 10-3

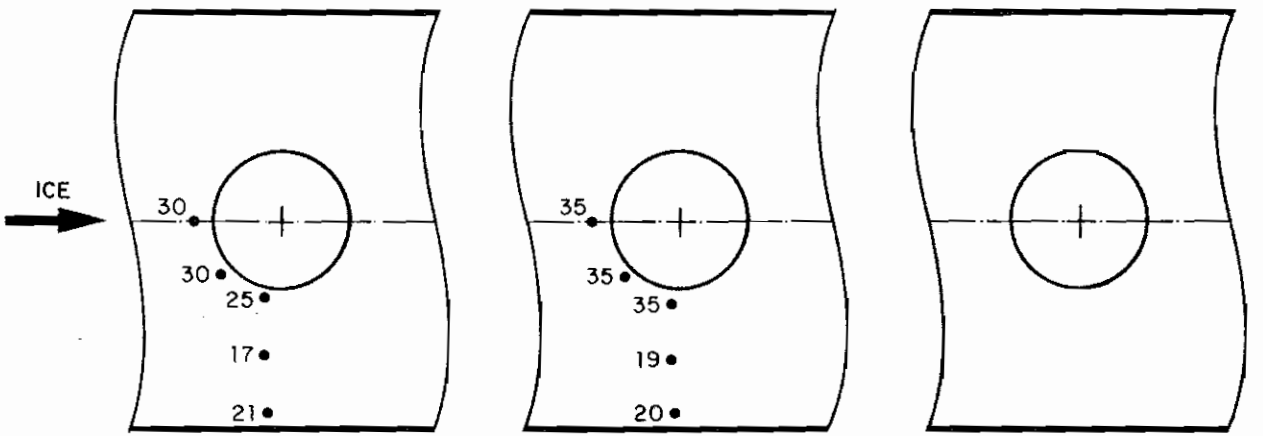

(p) EXPERIMENT 10-4 (q) EXPERIMENT 10-5

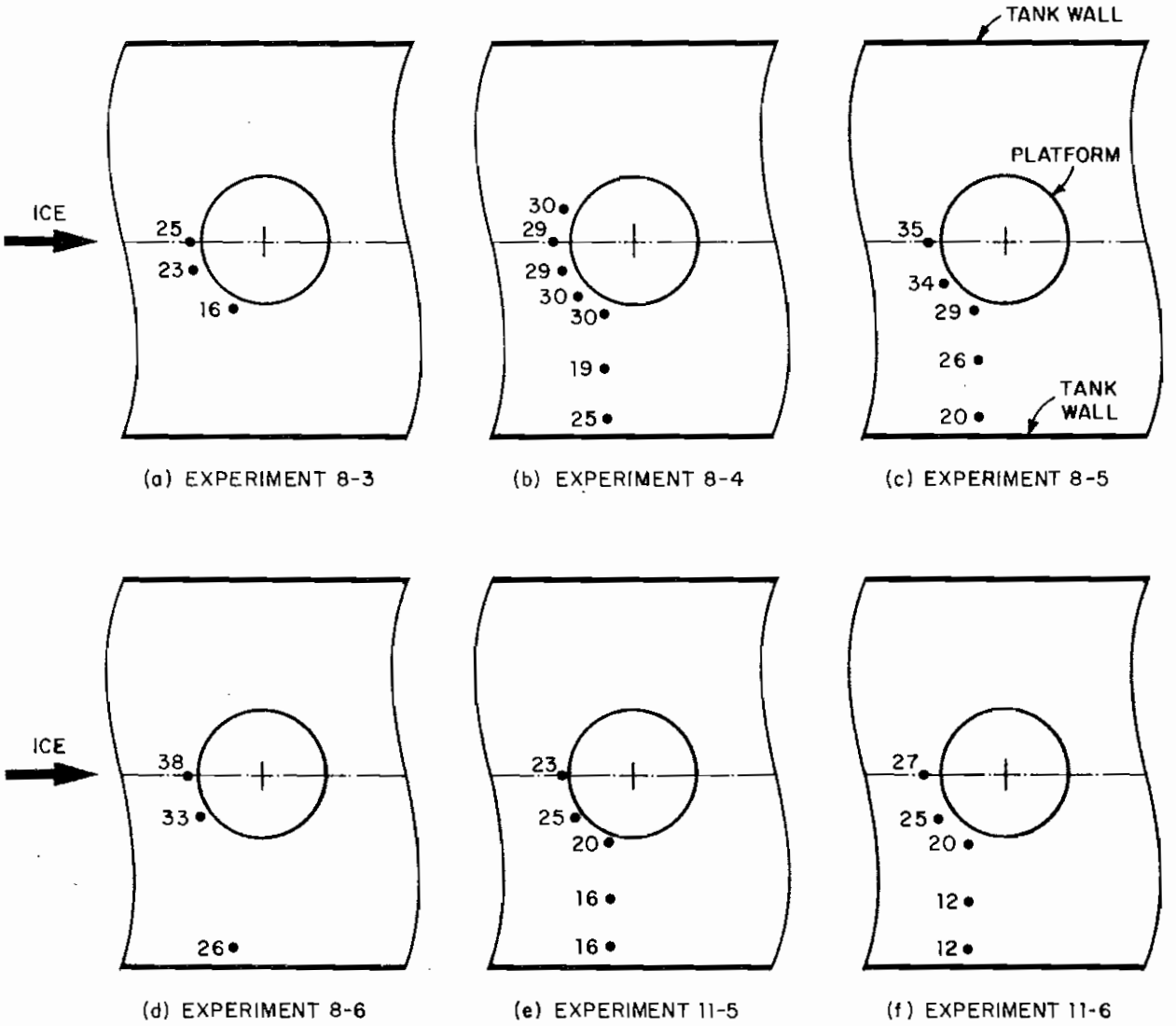

(a) EXPERIMENT 8-3 (b) EXPERIMENT 8-4 (c) EXPERIMENT 8-5

(d) EXPERIMENT 8-6 (e) EXPERIMENT 11-5 (f) EXPERIMENT 11-6